

NONLINEAR DYNAMICS AND SYSTEMS THEORY

An International Journal of Research and Surveys

Volume 20

Number 4

2020

CONTENTS

Fixed Point Regions, Unified Construction of Fixed Point Mappings for Integral, Quadratic, and Fractional Equations.....347
T. A. Burton and I. K. Purnaras

An Enhanced Bi-Directional Chaotic Optimization Algorithm.....365
F. Derouiche and T. Hamaizia

Speed Sensorless Direct Torque Control Strategy of a Doubly Fed Induction Motor Using an ANN and an EKF374
T. Djellouli, S. Moulahoum, A. Moualdia, M.S. Bouchrit and P. Wira

Solving Laplace Equation within Local Fractional Operators by Using Local Fractional Differential Transform and Laplace Variational Iteration Methods.....388
H. K. Jassim, J. Vahidi and V. M. Ariyan

Solution to the Critical Burgers Equation for Small Data in a Bounded Domain397
M. B. Kania

Application of the Direct Power Control Strategy in a Shunt Active Filter by Exploiting the Solar Photovoltaic Energy as a Continuous Source.....410
A. Morsli, A. Tlemçani, A. Krama, A. Abbadi, L. Zellouma and H. Nouri

Uniqueness of Solution to the von Karman Equations with Free Boundary Conditions.....425
J. Oudaani, A. El Mouatasim and B. El-Aqqad

Stability of the Artificial Equilibrium Points in the Low-Thrust Restricted Three-Body Problem when the Smaller Primary is an Oblate Spheroid439
Md. Sanam Suraj, Amit Mittal, Krishan Pal and Deepak Mittal

General Simplex Method for Fully Fuzzy Linear Programming with the Piecewise Linear Fuzzy Numbe.....451
M. Z. Tuffaha and M. H. Alrefaei

Contents of Volume 20, 2020461

NONLINEAR DYNAMICS & SYSTEMS THEORY

Volume 20, No. 4, 2020

Nonlinear Dynamics and Systems Theory

An International Journal of Research and Surveys

EDITOR-IN-CHIEF A.A.MARTYNYUK

*S.P.Timoshenko Institute of Mechanics
National Academy of Sciences of Ukraine, Kiev, Ukraine*

MANAGING EDITOR I.P.STAVROULAKIS

Department of Mathematics, University of Ioannina, Greece

REGIONAL EDITORS

P.BORNE, Lille, France
 M.FABRIZIO, Bologna, Italy
Europe

M.BOHNER, Rolla, USA
 HAO WANG, Edmonton, Canada
USA and Canada

T.A.BURTON, Port Angeles, USA
 C.CRUZ-HERNANDEZ, Ensenada, Mexico
USA and Latin America

M.ALQURAN, Irbid, Jordan
Jordan and Middle East

K.L.TEO, Perth, Australia
Australia and New Zealand

Nonlinear Dynamics and Systems Theory

An International Journal of Research and Surveys

EDITOR-IN-CHIEF A.A.MARTYNYUK

The S.P.Timoshenko Institute of Mechanics, National Academy of Sciences of Ukraine,
Nesterov Str. 3, 03680 MSP, Kiev-57, UKRAINE / e-mail: journalndst@gmail.com

MANAGING EDITOR I.P.STAVROULAKIS

Department of Mathematics, University of Ioannina
451 10 Ioannina, HELLAS (GREECE) / e-mail: ipstav@cc.uoi.gr

ADVISORY EDITOR A.G.MAZKO

Institute of Mathematics of NAS of Ukraine, Kiev (Ukraine)
e-mail: mazko@imath.kiev.ua

REGIONAL EDITORS

M.ALQURAN (Jordan), e-mail: marwan04@just.edu.jo
P.BORNE (France), e-mail: Pierre.Borne@ec-lille.fr
M.BOHNER (USA), e-mail: bohner@mst.edu
T.A.BURTON (USA), e-mail: taburton@olympen.com
C. CRUZ-HERNANDEZ (Mexico), e-mail: ccruz@cicese.mx
M.FABRIZIO (Italy), e-mail: mauro.fabrizio@unibo.it
HAO WANG (Canada), e-mail: hao8@ualberta.ca
K.L.TEO (Australia), e-mail: K.L.Teo@curtin.edu.au

EDITORIAL BOARD

| | |
|-----------------------------|-------------------------------------|
| Aleksandrov, A.Yu. (Russia) | Jafari, H. (South African Republic) |
| Artstein, Z. (Israel) | Khusainov, D.Ya. (Ukraine) |
| Awrejcewicz, J. (Poland) | Kloedon, P. (Germany) |
| Benrejeb, M. (Tunisia) | Kokologiannaki, C. (Greece) |
| Braiek, N.B. (Tunisia) | Krishnan, E.V. (Oman) |
| Chen Ye-Hwa (USA) | Limarchenko, O.S. (Ukraine) |
| D'Anna, A. (Italy) | Nguang Sing Kiong (New Zealand) |
| De Angelis, M. (Italy) | Okninski, A. (Poland) |
| Denton, Z. (USA) | Peterson, A. (USA) |
| Vasundhara Devi, J. (India) | Radziszewski, B. (Poland) |
| Djemai, M. (France) | Shi Yan (Japan) |
| Dshalalow, J.H. (USA) | Sivasundaram, S. (USA) |
| Eke, F.O. (USA) | Sree Hari Rao, V. (India) |
| Gajic Z. (USA) | Staicu V. (Portugal) |
| Georgiou, G. (Cyprus) | Stavarakakis, N.M. (Greece) |
| Herlambang T. (Indonesia) | Vatsala, A. (USA) |
| Honglei Xu (Australia) | Zuyev, A.L. (Germany) |
| Izobov, N.A. (Belarussia) | |

ADVISORY COMPUTER SCIENCE EDITORS

A.N.CHERNIENKO and A.S.KHOROSHUN, Kiev, Ukraine

ADVISORY LINGUISTIC EDITOR

S.N.RASSHYVALOVA, Kiev, Ukraine

INSTRUCTIONS FOR CONTRIBUTORS

(1) General. Nonlinear Dynamics and Systems Theory (ND&ST) is an international journal devoted to publishing peer-refereed, high quality, original papers, brief notes and review articles focusing on nonlinear dynamics and systems theory and their practical applications in engineering, physical and life sciences. Submission of a manuscript is a representation that the submission has been approved by all of the authors and by the institution where the work was carried out. It also represents that the manuscript has not been previously published, has not been copyrighted, is not being submitted for publication elsewhere, and that the authors have agreed that the copyright in the article shall be assigned exclusively to InforMath Publishing Group by signing a transfer of copyright form. Before submission, the authors should visit the website:

<http://www.e-ndst.kiev.ua>

for information on the preparation of accepted manuscripts. Please download the archive Sample_NDST.zip containing example of article file (you can edit only the file Samplefilename.tex).

(2) Manuscript and Correspondence. Manuscripts should be in English and must meet common standards of usage and grammar. To submit a paper, send by e-mail a file in PDF format directly to

Professor A.A. Martynyuk, Institute of Mechanics,
Nesterov str.3, 03057, MSP 680, Kiev-57, Ukraine
e-mail: journalndst@gmail.com

or to one of the Regional Editors or to a member of the Editorial Board. Final version of the manuscript must typeset using LaTeX program which is prepared in accordance with the style file of the Journal. Manuscript texts should contain the title of the article, name(s) of the author(s) and complete affiliations. Each article requires an abstract not exceeding 150 words. Formulas and citations should not be included in the abstract. AMS subject classifications and key words must be included in all accepted papers. Each article requires a running head (abbreviated form of the title) of no more than 30 characters. The sizes for regular papers, survey articles, brief notes, letters to editors and book reviews are: (i) 10-14 pages for regular papers, (ii) up to 24 pages for survey articles, and (iii) 2-3 pages for brief notes, letters to the editor and book reviews.

(3) Tables, Graphs and Illustrations. Each figure must be of a quality suitable for direct reproduction and must include a caption. Drawings should include all relevant details and should be drawn professionally in black ink on plain white drawing paper. In addition to a hard copy of the artwork, it is necessary to attach the electronic file of the artwork (preferably in PCX format).

(4) References. Each entry must be cited in the text by author(s) and number or by number alone. All references should be listed in their alphabetic order. Use please the following style:

Journal: [1] H. Poincare, Title of the article. *Title of the Journal* **volume**
(issue) (year) pages. [Language]

Book: [2] A.M. Lyapunov, *Title of the Book*. Name of the Publishers, Town, year.

Proceeding: [3] R. Bellman, Title of the article. In: *Title of the Book*. (Eds.).
Name of the Publishers, Town, year, pages. [Language]

(5) Proofs and Sample Copy. Proofs sent to authors should be returned to the Editorial Office with corrections within three days after receipt. The corresponding author will receive a sample copy of the issue of the Journal for which his/her paper is published.

(6) Editorial Policy. Every submission will undergo a stringent peer review process. An editor will be assigned to handle the review process of the paper. He/she will secure at least two reviewers' reports. The decision on acceptance, rejection or acceptance subject to revision will be made based on these reviewers' reports and the editor's own reading of the paper.

NONLINEAR DYNAMICS AND SYSTEMS THEORY

An International Journal of Research and Surveys
Published by InforMath Publishing Group since 2001

Volume 20

Number 4

2020

CONTENTS

| | |
|---|-----|
| Fixed Point Regions, Unified Construction of Fixed Point Mappings for Integral, Quadratic, and Fractional Equations | 347 |
| <i>T. A. Burton and I. K. Purnaras</i> | |
| An Enhanced Bi-Directional Chaotic Optimization Algorithm | 365 |
| <i>F. Derouiche and T. Hamaizia</i> | |
| Speed Sensorless Direct Torque Control Strategy of a Doubly Fed Induction Motor Using an ANN and an EKF | 374 |
| <i>T. Djellouli, S. Moulahoum, A. Moualdia, M.S. Bouchrit and P. Wira</i> | |
| Solving Laplace Equation within Local Fractional Operators by Using Local Fractional Differential Transform and Laplace Variational Iteration Methods | 388 |
| <i>H. K. Jassim, J. Vahidi and V. M. Ariyan</i> | |
| Solution to the Critical Burgers Equation for Small Data in a Bounded Domain ... | 397 |
| <i>M. B. Kania</i> | |
| Application of the Direct Power Control Strategy in a Shunt Active Filter by Exploiting the Solar Photovoltaic Energy as a Continuous Source | 410 |
| <i>A. Morsli, A. Tlemçani, A. Krama, A. Abbadi, L. Zellouma and H. Nouri</i> | |
| Uniqueness of Solution to the von Karman Equations with Free Boundary Conditions | 425 |
| <i>J. Oudaani, A. El Mouatasim and B. El-Aqqad</i> | |
| Stability of the Artificial Equilibrium Points in the Low-Thrust Restricted Three-Body Problem when the Smaller Primary is an Oblate Spheroid | 439 |
| <i>Md. Sanam Suraj, Amit Mittal, Krishan Pal and Deepak Mittal</i> | |
| General Simplex Method for Fully Fuzzy Linear Programming with the Piecewise Linear Fuzzy Number | 451 |
| <i>M. Z. Tuffaha and M. H. Alrefaei</i> | |
| Contents of Volume 20, 2020 | 461 |

Founded by A.A. Martynyuk in 2001.

Registered in Ukraine Number: KB 5267 / 04.07.2001.

NONLINEAR DYNAMICS AND SYSTEMS THEORY

An International Journal of Research and Surveys

Impact Factor from SCOPUS for 2018: 0.870, SJR – 0.292, and h-index – 15.

Nonlinear Dynamics and Systems Theory (ISSN 1562–8353 (Print), ISSN 1813–7385 (Online)) is an international journal published under the auspices of the S.P. Timoshenko Institute of Mechanics of National Academy of Sciences of Ukraine and Curtin University of Technology (Perth, Australia). It aims to publish high quality original scientific papers and surveys in areas of nonlinear dynamics and systems theory and their real world applications.

AIMS AND SCOPE

Nonlinear Dynamics and Systems Theory is a multidisciplinary journal. It publishes papers focusing on proofs of important theorems as well as papers presenting new ideas and new theory, conjectures, numerical algorithms and physical experiments in areas related to nonlinear dynamics and systems theory. Papers that deal with theoretical aspects of nonlinear dynamics and/or systems theory should contain significant mathematical results with an indication of their possible applications. Papers that emphasize applications should contain new mathematical models of real world phenomena and/or description of engineering problems. They should include rigorous analysis of data used and results obtained. Papers that integrate and interrelate ideas and methods of nonlinear dynamics and systems theory will be particularly welcomed. This journal and the individual contributions published therein are protected under the copyright by International InforMath Publishing Group.

PUBLICATION AND SUBSCRIPTION INFORMATION

Nonlinear Dynamics and Systems Theory will have 4 issues in 2021, printed in hard copy (ISSN 1562–8353) and available online (ISSN 1813–7385), by InforMath Publishing Group, Nesterov str., 3, Institute of Mechanics, Kiev, MSP 680, Ukraine, 03057. Subscription prices are available upon request from the Publisher, EBSCO Information Services (<mailto:journals@ebSCO.com>), or website of the Journal: <http://e-ndst.kiev.ua>. Subscriptions are accepted on a calendar year basis. Issues are sent by airmail to all countries of the world. Claims for missing issues should be made within six months of the date of dispatch.

ABSTRACTING AND INDEXING SERVICES

Papers published in this journal are indexed or abstracted in: Mathematical Reviews / MathSciNet, Zentralblatt MATH / Mathematics Abstracts, PASCAL database (INIST–CNRS) and SCOPUS.



Fixed Point Regions, Unified Construction of Fixed Point Mappings for Integral, Quadratic, and Fractional Equations

T. A. Burton^{1*} and I. K. Purnaras²

¹ Northwest Research Institute, 732 Caroline St., Port Angeles, WA 98362, U.S.A.

² Department of Mathematics, University of Ioannina, P. O. Box 1186, 451 10, Ioannina, Greece

Received: February 29, 2020; Revised: May 27, 2020

Abstract: This paper is a study of integral equations by means of mapping a closed bounded convex nonempty set G into its interior. This tells us that all possible fixed points reside in G which we then call a fixed point region. The study is restricted to convolution kernels $A(t-s)$ for which there is a transformation yielding an equivalent equation. We then devise a method whereby we can often find the above mentioned set G . This leads us to globally stable fixed points. The term which makes the equation of quadratic type is added in after the transformation, whereas existing theory along these lines adds it in directly to the Volterra equation. That method produces difficulties with compactness of the mapping. In our work compactness is never an issue.

Keywords: *fixed point regions; integral equations; quadratic equations; fractional equations; fixed points; transformations.*

Mathematics Subject Classification (2010): 34A08, 34A12, 45D05, 45G05, 47H10.

1 Introduction

This paper was motivated by the fact that many fixed point theorems begin with an integral equation and the preemptive assumption that there is a closed convex nonempty bounded set G in a Banach or normed space of bounded continuous functions $\phi : [0, \infty) \rightarrow \mathfrak{R}$ with the supremum norm, together with a continuous mapping of $G \rightarrow G$. Often the first mapping which comes to mind is the natural one defined by the integral equation.

* Corresponding author: <mailto:taburton@olypen.com>

Then there are several additional conditions which would then yield a fixed point being a solution of the integral equation.

First, if we say that G is bounded and the mapping maps G into itself, then we are requiring that

The mapping maps bounded sets into bounded sets.

Accordingly, the first task of this paper is to give a coherent method for transforming an integral equation of the type under consideration here into one which maps bounded sets into bounded sets. In fact, we have long worked with exactly that transformation.

Second, there is such a wide class of integral equations that a paper of finite length needs to have a way of driving diverse equations into a single flexible type whether we start with a heat equation, a fractional differential equation of either Riemann-Liouville or Caputo type, or a quadratic integral equation.

In fact, we do exactly that and the final form into which all can fit after several known transformations is

$$x(t) = a(t) + g(t, x(t)) \int_0^t R(t-s)x(s) \left[1 - \frac{f(s, x(s))}{J} \right] ds.$$

Here, $R > 0$ is the resolvent of a kernel and $\int_0^\infty R(t)dt = 1$. It is this property which assures us that the natural mapping

maps bounded sets into bounded sets.

Third, many fixed point theorems require mappings with compactness or contraction conditions. This is known to fail for products $g(t, x(t)) \int_0^t R(t-s)f(s, x(s))ds$. We are not bothered by this because we never mention either compactness or contractions.

Fourth, we continue with the idea raised in several earlier papers that there is a conclusion which is competitive with the conclusion that there is a fixed point. Our conclusion is always that there is a closed bounded convex nonempty set G of such a nature that any fixed point which exists will reside entirely in G .

2 A Roadmap to Unification

We will begin with several very different kinds of equations. Through a series of transformations each will be brought down to the common Volterra integral equation of the form

$$x(t) = a(t) - \int_0^t A(t-s)f(s, x(s))ds \tag{1}$$

although the functions will change for each of them. But all of the functions are continuous and $A(t) > 0$ and often

$$\int_0^\infty A(s)ds = \infty.$$

Clearly, something must be done because it cannot map bounded sets into bounded sets.

Next, through a variation of parameters formula and substantial theory going back to Friedman in 1963 and organized by Miller in 1971, every one of those equations will now pass through (1) and become

$$x(t) = b(t) + \int_0^t R(t-s) \left[x(s) - \frac{f(s, x(s))}{J} \right] ds, \tag{2}$$

where

$$b(t) = a(t) - \int_0^t R(t-s)a(s)ds$$

and R will vary from one equation to the next being the resolvent of A and depending on the choice of J which can be any positive number. Regardless of the differences between various A and J it will always be true that R is continuous on $(0, \infty)$, $R(t) > 0$ and

$$\int_0^\infty R(t)dt \leq 1.$$

That condition will give our primary victory in having (2) map bounded sets into bounded sets.

At this point we reach back in history to 1950 when Chandrasekhar [9] offered the equation

$$x(t) = 1 + x(t) \int_0^1 \phi(s)x(s)ds$$

to describe radiation transfer which jolted fixed point theory investigators into a cottage industry called “quadratic integral equations”. They knew that

$$\int_0^t A(t-s)f(s, x(s))ds$$

was often a compact map (see [8] for example), as required in many fixed point theorems, but a product

$$g(t, x(t)) \int_0^t A(t-s)f(s, x(s))ds$$

is not compact even with g and f continuous. By simply Googling “quadratic integral equations”, we find a myriad of publications including many in pdf format freely available for download. Our bibliography contains several.

To take all of this into account we return to (2) and perturb it with $g(t, x)$ obtaining our final product as

$$x(t) = b(t) + g(t, x(t)) \int_0^t R(t-s) \left[x(s) - \frac{f(s, x(s))}{J} \right] ds \tag{3}$$

with the assumption that $g(t, x)$ is continuous and

$$|g(t, x)| \leq 1. \tag{4}$$

Thus, if $g(t, x)$ is missing in an equation of interest, then it is simply replaced by 1. In spite of all the equations which we are going to describe here, it is only (3) that we must treat.

This is the unity.

But we will take it one step further. We will offer a result concerning a closed bounded convex nonempty set G which will contain any possible fixed point of the natural mapping defined by (3). It will be a single theorem encompassing all the problems treated.

3 Some Related Problems

It is not at all necessary for the reader to be acquainted with fractional equations to get the point that in each case we start with one type of equation, but always transform it into one specific class. We will start with a fractional differential equation of Riemann-Liouville type and continue down to its relationship with very common Volterra equations. In preparation for that we offer some references. A modern introduction to fractional differential equations is found in Diethelm [12]. A very readable history of the theory up to 1974 is found in Chapter 1 of Oldham and Spanier [16] and a continuation up to the present time is found in Abbas, Benchohra, Graef, and Henderson [1]. However, we quickly see in the work below that the fractional calculus is immediately left behind and it is translated into an integral equation of common type going back almost 100 years. We start with the fractional differential equation, translate it into an integral equation with more than one singularity, introduce a shift of length T , and then transform it into a classical integral equation. The reader may wish to simply start with that final translation and follow the chain down from there. The next equation will be a fractional differential equation of Caputo type which was introduced because the Riemann-Liouville equation has a troublesome initial condition. In one step we translate it into a common Volterra integral equation. From there on we are all on familiar ground and the reader will need no guidance as we descend the chain.

We will see $R(t)$ throughout this list. It is the resolvent of the kernel. For fractional and some other kinds of equations it is the continuous resolvent of the kernel $(t-s)^{q-1}$ satisfying

$$0 < R(t), \int_0^\infty R(s)ds = 1$$

and will be discussed in detail later. It is found in Miller [15, pp. 212-213]. It has the most useful property found in fixed point theory, namely, it enables us to show that the natural mapping defined by the integral equation maps bounded sets into bounded sets. We frequently find that we need a closed bounded convex nonempty set G and a continuous mapping of G into G .

(i) We begin with the Riemann-Liouville fractional differential equation

$$D^q x(t) = f(t, x(t)), \lim_{t \rightarrow 0^+} t^{1-q} x(t) = x^0 \neq 0, \quad q \in (0, 1).$$

It is inverted as

$$x(t) = x^0 t^{q-1} + \frac{1}{\Gamma(q)} \int_0^t (t-s)^{q-1} f(s, x(s)) ds$$

and transformed in two steps to

$$y(t) = F(t) + \int_0^t R(t-s) \left[y(s) + \frac{f(s+T, y(s))}{J} \right] ds,$$

where $J > 0$ is an arbitrary constant. Here, $T > 0$ is a constant arising in a local existence theorem and $y(t) = x(t+T)$. All of the details are found in [2, pp. 242-271] (see, especially, p. 252 and (4.4)). It is the recurring form of that last equation which enables us to find a closed bounded convex nonempty set G so that the natural mapping maps G into the interior of G and contains all possible fixed points.

(ii) Close to (i) is the fractional differential equation of Caputo type sought mainly for the more direct initial conditions. It is

$${}^cD^q x(t) = f(t) - g(t, x(t)), \quad x(0) \in \mathfrak{R}, \quad 0 < q < 1,$$

with f and g continuous, which inverts as

$$x(t) = x(0) - \frac{1}{\Gamma(q)} \int_0^t (t-s)^{q-1} [g(s, x(s)) - f(s)] ds.$$

One more transformation brings it in line with (i) and the property that bounded sets are mapped into bounded sets owing again to the function R . The final form is

$$x(t) = x(0) \left[1 - \int_0^t R(s) ds \right] + \int_0^t R(t-s) \left[x(s) - \frac{g(s, x(s)) - f(s)}{J\Gamma(q)} \right] ds.$$

Details may be found in [3], pp. 442-456. See, especially, Example 5.6, p. 450.

(iii) The next equation is the one which made this entire project possible by generating the resolvent R which is used in each of the transformations. We begin with a heat equation found in Miller [15, p. 209]

$$y(t) = -(\pi K)^{-1/2} \int_0^t (t-s)^{-1/2} g(s, y(s)) ds,$$

where K is thermal conductivity of the medium. The construction of this equation can be traced back to pp. 356-361 of the book by Weinberger [21]. Miller [15, p. 209] picks it up and this is the beginning of his presentation which will lead us to the construction of that all important transformation and the introduction of the resolvent R . We will return to this and the construction of R later. In order to make the text consistent, we will write this equation as

$$x(t) = - \int_0^t (t-s)^{-1/2} f(s, x(s)) ds.$$

Our transformation will yield

$$x(t) = \int_0^t R(t-s) \left[x(s) - \frac{f(s, x(s))}{J} \right] ds$$

and we will refer to it as our heat equation.

There can now be gathered into this a large and basic theory of heat equations generated near 1950 and published by Padmavally [17], Mann and Wolf [18], and Roberts and Mann [19]. We will not detail it here.

This will conclude the discussion of problems which can be put in the form of

$$x(t) = a(t) + \int_0^t R(t-s)x(s) \left[1 - \frac{f(s, x(s))}{Jx(s)} \right] ds.$$

When we consider that either of the fractional problems represent a theory about which entire books have been written, it is clear that we are dealing with a substantial fraction of problems from applied mathematics.

But there is one more type which does not fit snugly in this set of problems which has generated an enormous literature. That is the so-called quadratic theory of integral equations. Interest in the problem was sparked by a paper written in 1950 by Chandrasekhar [9] in the study of radiative transfer governed by

$$x(t) = 1 + x(t) \int_0^1 \phi(s)x(s)ds$$

in which ϕ is a second order polynomial presumably giving rise to the name “quadratic” integral equations. We discussed aspects of it with (3). Many applications of off shoots may be found in Darwish [10] and Darwish and Henderson [11], for example, but the form of the equation with that product with the integral has been the driving force for a great many investigations in fixed point theory. At this time the area of study is so active that one can get an idea of the amount of work done in it by asking “google” for “quadratic integral or integro-differential equations”.

4 Transformations

In 1963, Friedman [13] isolated a wide and important set of kernels and the entire process is well formulated by Miller [15, pp. 207-213] with refinements continuing to p. 224 and with more recent refinements given by Gripenberg [14]. It is required that $A(t)$ satisfy the following three conditions (A1)–(A3) which are present in many important problems in heat conduction and throughout fractional differential equations.

It is to be noted that if A satisfies (A1)–(A3) and $\int_0^\infty A(s)ds = \infty$ and if g and f are bounded by the real numbers $\|g\|$ and $\|f\|$, then in the equation

$$x(t) = a(t) - \frac{g(t, x(t))}{\|g\|} \int_0^t \|g\| A(t-s)f(s, x(s))ds$$

the kernel will still satisfy (A1)–(A3) and it will still be the same equation if $\|g\|$ is a fixed positive number, being the supremum on $[0, \infty)$. We are going to assume that f and g are bounded because the entire focus here will be on a natural mapping which maps bounded sets into bounded sets and we are interested in solutions on $[0, \infty)$.

Conditions (A1)–(A3) are defined as follows:

(A1) $A(t) \in C(0, \infty) \cap L^1(0, 1)$.

(A2) $A(t)$ is positive and non-increasing for $t > 0$.

(A3) For each $T > 0$ the function $A(t)/A(t+T)$ is non-increasing in t for $0 < t < \infty$.

In those references above it is shown that the resolvent equation is

$$R(t) = A(t) - \int_0^t A(t-s)R(s)ds \quad (5)$$

and that its solution R is continuous on $(0, \infty)$ and

$$0 < R(t) \leq A(t), \quad \int_0^\infty R(t)dt = 1 \quad (6)$$

when the integral of A is infinite. When the integral of A is finite, then the integral of R is less than one.

Notice that if J is a positive constant, then $JA(t)$ still satisfies (A1)–(A3). We have noted just now that $\int_0^t A(t-s)f(s, x(s))ds$ may map bounded sets into unbounded sets. If

we could possibly exchange $R(t)$ for $A(t)$, then we could map bounded sets into bounded sets. That is exactly what we do and the transformation can be reversed so that the transformed equation has the same solutions as the original equation.

In a sequence of papers we showed the advantages of transforming the standard integral equation

$$x(t) = a(t) - \int_0^t A(t-s)f(s, x(s))ds \tag{7}$$

using a variation of parameters formula of Miller [15, pp. 191-192] into

$$x(t) = z(t) + \int_0^t R(t-s) \left[x(s) - \frac{f(s, x(s))}{J} \right] ds, \tag{8}$$

with

$$z(t) = a(t) - \int_0^t R(t-s)a(s)ds. \tag{9}$$

Here are the steps. Start with (7) and $a(t)$ continuous on $[0, \infty)$ while A satisfies (A1)–(A3) and J is an arbitrary positive constant at this point, but later is chosen precisely as previously discussed. We then have

$$\begin{aligned} x(t) &= a(t) - \int_0^t A(t-s)[Jx(s) - Jx(s) + f(s, x(s))]ds \\ &= a(t) - \int_0^t JA(t-s)x(s)ds + \int_0^t JA(t-s) \left[x(s) - \frac{f(s, x(s))}{J} \right] ds. \end{aligned}$$

The linear part is

$$z(t) = a(t) - \int_0^t JA(t-s)z(s)ds \tag{10}$$

and the resolvent equation is

$$R(t) = JA(t) - \int_0^t JA(t-s)R(s)ds \tag{11}$$

so that by the linear variation-of-parameters formula we have

$$z(t) = a(t) - \int_0^t R(t-s)a(s)ds \tag{12}$$

and by the non-linear variation of parameters formula [15, pp. 191-193]

$$x(t) = z(t) + \int_0^t R(t-s) \left[x(s) - \frac{f(s, x(s))}{J} \right] ds.$$

We will always write this as

$$x(t) = a(t) - \int_0^t R(t-s)a(s)ds + \int_0^t R(t-s) \left[x(s) - \frac{f(s, x(s))}{J} \right] ds \tag{13}$$

which has a reversible mapping into (7).

The transformation from (7) to (13) was first given in [4] for a Caputo equation in which case there are few difficulties. Further discussion of the transformation is found in [2] which allows $a(t)$ to be singular. In that reference the reader can follow from (2) on p. 249 to its transformed form on p. 263.

We cannot overemphasize the role of J , as we will see later.

5 Fixed Point Regions

The compactness required in so many fixed point theorems eludes us and we stop for a moment of thought. If we just work a bit harder we may let the mapping map G into G° , the interior of G . Perhaps that will be enough to provide for us some usable information. This is where we pick up from earlier papers ([5, p. 297], [6, p. 344], [7, p. 7]) in which we showed that under our specified mapping condition the set G can be shown to

contain entirely every possible fixed point of (1).

Instead of fixed point theory, we are now studying what can be derived from **fixed point regions G** . Our next task is to show how this concept relates to standard fixed point theory and for this we begin with Schauder's and Schaefer's fixed point theorems. We will find that the new concept is a simple counterpart of the combination of both of those theorems. Here is the statement as given in [7].

Theorem 5.1 *Let $T > 0$ and $(\mathcal{B}, \|\cdot\|)$ be the Banach space of continuous functions $\phi : [0, T] \rightarrow \mathfrak{R}$ with the supremum norm and let P be a Volterra operator mapping $\mathcal{B} \rightarrow \mathcal{B}$ which is continuous. Let $r > 0$ and G be the closed ball of center zero and radius r in \mathcal{B} :*

$$G := \{\phi \in \mathcal{B} : \|\phi\| \leq r\}.$$

Suppose that $P : G \rightarrow G^\circ$ and that P has the property that if $\phi \in \mathcal{B}$ and if $(P\phi)(0) = \phi(0)$, then $|\phi(0)| < r$. If $\phi \in \mathcal{B}$ is a fixed point of P , then ϕ resides in G° .

Here is a typical example of quadratic type.

Example 5.1 Consider the scalar equation

$$x(t) = a(t) + \lambda(\text{Arctan}x(t)) \int_0^t R(t-s)[x(s) - \sin x(s)]ds.$$

Choose

$$0 < \lambda < 1/\pi, \|a\| \leq \pi/4, \quad G = \{\phi : [0, \infty) \rightarrow \mathfrak{R}, \|\phi\| \leq \pi/2\}.$$

Note that for $\|x\| \leq \pi/2$ then $\left|1 - \frac{\sin x}{x}\right| \leq 1$.

Under these conditions the natural mapping P satisfies

$$\begin{aligned} |(P\phi)(t)| &\leq \|a\| + (\lambda\pi/2) \int_0^t R(t-s)|\phi(s)| \left|1 - \frac{\sin \phi(s)}{\phi(s)}\right| ds \\ &\leq \|a\| + \lambda(\pi/2)(\pi/2) \int_0^t R(t-s)ds \\ &< \pi/4 + \lambda(\pi^2/4), \end{aligned}$$

so

$$\|P\phi\| \leq \pi/4 + \lambda(\pi^2/4) < (\pi/4) + (\pi/4) = \pi/2.$$

Hence $P : G \rightarrow G^\circ$.

Now, we may go through the proof and see that all is unchanged if $\lambda \text{Arctan}x(t)$ is replaced by $\lambda\pi/2$.

Theorem 5.2 (Schauder [20, p. 25]) *Let G be a non-empty convex subset of a normed space \mathcal{B} . Let P be a continuous mapping of G into a compact set $K \subset G$. Then P has a fixed point.*

Schauder’s theorem fails in our problem here because the map generated by our equation is not compact. Schauder’s theorem fails us in another way also. Even if there is a fixed point in G his theorem offers us no way to tell if there are other fixed points outside of G . This can be a disaster. Generally, we select G for two reasons. First, we find through trial and error that we can show that P maps G into G . But there is a far more serious reason. In a given real-world problem there are points in the space which are favorable to our project and so we select G to contain them. On the other hand there may be points which are a total disaster for our project and we cannot move forward with the project until we know that they cannot be selected. Here, our method helps in two ways. Even if Schauder’s theorem applies we are well advised to proceed with the mapping and be sure that G contains all possible fixed points. We can make choices to put all fixed points in a predetermined ball.

Theorem 5.3 (Schaefer [20, p. 29]) *Let \mathcal{B} be a normed space, P , a continuous mapping of $\mathcal{B} \rightarrow \mathcal{B}$ which is compact on each bounded subset K of \mathcal{B} . Then either*

- (i) *the equation $x = \lambda Px$ has a solution for $\lambda = 1$, or*
- (ii) *the set of all such solutions x (if any), for $0 < \lambda < 1$, is unbounded.*

Not only is this theorem replete with demands for compactness, but there is not a hint of where the fixed point might lie or how many there might be. Our method seems to offer no help for Schaefer’s, but it does cast a light to show a somewhat equal worth. In principle, would we prefer to know where all possible solutions lie, or would we prefer to know that there is at least one lying somewhere? We are arguing that both conclusions can be targets of equally high value.

6 Mapping Bounded Sets into Bounded Sets

The perfect choice of J

So many fixed point theorems begin with the assumption that there is a closed bounded convex nonempty set G and a mapping of G into G . That part is stated so smoothly that it is reasonable to get the impression that it is a simple condition and that the real challenge consists of all the added conditions needed to ensure the existence of a fixed point. Several decades of study reveal the very opposite for many of us. We feel that the upcoming work which shows a simple way of getting the required G in this context is, perhaps, the main contribution of this paper.

In the transformation of (7) to (13) we will see that J has entered and we would have no idea how to select it. It will play a major role in our work. In case $f(t, x)$ depends only on x , there is a definite path to finding G so that the natural mapping, P , of $G \rightarrow G^o$ will contain the smallest possible fixed point region. It is successful if

$$\lim_{|x| \downarrow 0} \frac{f(x)}{x} = J \tag{14}$$

exists as a finite positive number. To explain the working here, we are asking that $xf(x) \geq 0$ so that

$$\frac{xf(x)}{x^2} \geq 0$$

which implies that if the limit exists, then it is ≥ 0 . In particular, then the limit as $|x| \downarrow 0$ satisfies

$$\lim_{|x| \downarrow 0} \frac{f(x)}{Jx} = 1. \quad (15)$$

From this we see that the limit as $|x| \downarrow 0$ satisfies

$$\lim_{|x| \downarrow 0} \left[1 - \frac{f(x)}{Jx} \right] = 0 \quad (16)$$

and that is the perfect choice for J . It will allow the integrand to completely control the magnitude of the natural mapping P of G into G , making the fixed point region as small as possible. The only magnitude it cannot control is $\|a\|$ since by Theorem 5.1 $a(t)$ is always part of the fixed point region. In other words:

Remark 6.1 Equation (16) is exactly the property which helps us to find G and to make G map into G^o when f and g are bounded, f is independent of t , and (14) holds.

7 The Shrinking Functions

We have mentioned earlier that investigators started with the standard Volterra equation

$$x(t) = a(t) - \int_0^t A(t-s)f(s, x(s))ds$$

and studied the problems raised by addition of the term $g(t, x(t))$ in

$$x(t) = a(t) - g(t, x(t)) \int_0^t A(t-s)f(s, x(s))ds,$$

which was actually an arbitrary choice. (Remember that J is chosen by (15) if possible.)

We choose instead to start with the equivalent transformed equation (13) and add in the $g(t, x(t))$ to it obtaining

$$x(t) = a(t) - \int_0^t R(t-s)a(s)ds + g(t, x(t)) \int_0^t R(t-s) \left[x(s) - \frac{f(s, x(s))}{J} \right] ds \quad (17)$$

and noticing that $a(t) - \int_0^t R(t-s)a(s)ds$ is the forcing function. Refer back to Chandrasekhar's equation

$$x(t) = 1 + x(t) \int_0^t \phi(s)x(s)ds$$

and notice that $g(t, x) = x$ and that does not multiply the forcing function, namely 1. It multiplies the integral.

In Example 5.1 there appeared an example of

$$S(x) =: x - f(x),$$

namely,

$$x - \sin x,$$

from which we obtained

$$|x| \left| 1 - \frac{\sin x}{x} \right|$$

with

$$0 \leq \frac{\sin x}{x} < 1, \quad x \neq 0,$$

when we take

$$G = \{ \phi : [0, \infty) \rightarrow \mathfrak{R}, \|\phi\| \leq \pi/2 \}, \quad \|a\| \leq \pi/4.$$

Let us review Example 5.1 and the first line of the mapping P in the proof. We have

$$\begin{aligned} |(P\phi)(t)| &\leq \|a\| + (\lambda\pi/2) \int_0^t R(t-s)|\phi(s)| \left| 1 - \frac{\sin \phi(s)}{\phi(s)} \right| ds \\ &\leq \|a\| + \lambda(\pi/2)(\pi/2) \int_0^t R(t-s) ds \\ &< \pi/4 + \lambda(\pi/2)(\pi/2), \end{aligned}$$

so for $\lambda < \frac{1}{\pi}$

$$\|P\phi\| \leq \pi/4 + \lambda(\pi/2)(\pi/2) < \pi/4 + (1/\pi)(\pi^2/4) = \pi/2.$$

In that first line we see that the last term shrinks the entire remainder of the mapping (excluding a) yielding $P : G \rightarrow G^\circ$. Thus, $1 - \frac{f(x)}{x}$ is shrinking $|x|$ which is exactly what it must do if the mapping is to map G into G° .

We will now work a problem to see how it unfolds, writing $a(t)$ instead of all of z . This will not distort the norms we later encounter. Before we start notice that if $xf(x) > 0$ for $x \neq 0$, then $f(0) = 0$ and if $f'(0)$ exists and it is positive, then by L'Hospital's rule

$$\lim_{x \rightarrow 0} \frac{f(x)}{x} = \frac{0}{0} = \frac{f'(0)}{1} > 0.$$

That is

$$\lim_{x \rightarrow 0} \frac{f(x)}{x} = J > 0$$

so

$$\lim_{x \rightarrow 0} \frac{f(x)}{Jx} = 1.$$

Example 7.1 Part I, f is not specified.

We begin with

$$x(t) = a(t) + g(t, x(t)) \int_0^t R(t-s)x(s) \left[1 - \frac{f(x(s))}{x(s)} \right] ds$$

and assume that

$$\lim_{|x| \downarrow 0} \frac{f(x)}{Jx} = 1$$

so that if we define the function h to be zero at zero and by

$$h(x) = 1 - \frac{f(x)}{Jx}$$

then it is continuous. For a given $\epsilon > 0$ there is a $D > 0$ such that $|x - 0| < D$ implies $|h(x) - h(0)| < \epsilon$. But $h(0) = 0$, so taking $\epsilon = 1/2$ we can find $D > 0$ so that $|x| < D$ implies

$$0 \leq \left| 1 - \frac{f(x)}{Jx} \right| < 1/2$$

which happens when $1/2 < f(x)/Jx < 3/2$. We cannot specify that in Part I because f is unknown. Assume again that $|g(t, x)| \leq 1$. We can now obtain G provided that

$$\|a\| < D/2.$$

Now, let

$$G = \{\phi : [0, \infty) \rightarrow \mathfrak{R}, \|\phi\| \leq D\}.$$

Then

$$\|P\phi\| \leq \|a\| + (1)(1)\|\phi\|(1/2) < (D/2) + (D/2) = D.$$

Thus $P : G \rightarrow G^0$.

In view of the continuity of g, ϕ (thus boundedness of ϕ), one may see that for any $\phi \in \mathcal{B}$ (the space of continuous functions on $[0, T]$ with $T > 0$ arbitrary), we have $|P(\phi)(0)| = |a(0)| < |D/2|$, thus by Theorem 5.1 every possible fixed point resides entirely in G .

Continuing, notice that the same argument can be given as $D \rightarrow 0$ with the result that when $a(t) = 0$, then by inspection $x = 0$ is a solution and it is unique. This concludes Part I of this example. We now turn to

Part II in which we specify

$$f(x) = \frac{x}{1+x^2}$$

which satisfies $xf(x) \geq 0$, f is bounded, and

$$\lim_{|x| \downarrow 0} \frac{f(x)}{x} = \lim_{|x| \downarrow 0} \frac{1}{1+x^2} = 1 = J.$$

Given $\epsilon = 1/2$, we must determine D so that $0 \leq |x| \leq D$ implies

$$0 < 1 - \frac{f(x)}{x} < 1/2.$$

Write that as

$$0 < 1 - \frac{1}{1+x^2} < 1/2.$$

Now $1 - \frac{1}{1+x^2}$ was zero at $x = 0$, so we let x increase to the value one making $\frac{1}{1+x^2} = 1/2$, telling us that $D = 1$ and

$$G = \{\phi : [0, \infty) \rightarrow \mathfrak{R} : \|\phi\| \leq 1\}.$$

This requires us to be able to choose $\|a\| < D/2 = 1/2$ since $\|\phi\| \leq 1$ implies that

$$\|P\phi\| \leq \|a\| + (1/2)D = \|a\| + (1/2) < 1$$

requires $\|a\| < 1/2$. This makes $P : G \rightarrow G^0$ and assures us that any fixed point lies entirely in G .

This concludes Part II and the example.

8 Another Perturbation

We are now concerned with a slightly different perturbation than the one studied in Section 7. Recall that we deal with the Volterra integral equation

$$x(t) = a(t) - \int_0^t A(t-s) f(s, x(s)) ds, \quad t \geq 0, \tag{18}$$

with a, f continuous and A continuous on $(0, \infty)$ with

$$\int_0^\infty A(s) ds = \infty,$$

and satisfying specific assumptions yielding that

$$\int_0^\infty R(u) du = 1.$$

Equation (18) is often perturbed by multiplying the integral by the factor $g(t, x)$, i.e, as

$$x(t) = a(t) - g(t, x(t)) \int_0^t A(t-s) f(s, x(s)) ds. \tag{19}$$

Considering a properly chosen $J > 0$ we, again, transform equation (18) into the (equivalent) equation

$$x(t) = a(t) + \int_0^t R(t-s) \left[x(s) - a(s) - \frac{f(s, x(s))}{J} \right] ds, \tag{20}$$

where R is the resolvent kernel of A satisfying the equation

$$R(t) = JA(t) - \int_0^t JA(t-u) R(u) du. \tag{21}$$

Now we choose to multiply the whole integral in (20) by the factor $g(t, x)$, i.e., we consider the equation

$$x(t) = a(t) - g(t, x(t)) \int_0^t R(t-s) \left[a(s) - \left(x(s) - \frac{f(s, x(s))}{J} \right) \right] ds,$$

which we write as

$$\begin{aligned} x(t) &= a(t) - g(t, x(t)) \int_0^t R(t-s) a(s) ds \\ &\quad + g(t, x(t)) \int_0^t R(t-s) \left[x(s) - \frac{f(s, x(s))}{J} \right] ds. \end{aligned} \tag{22}$$

Comparing to the perturbation in Section 7, here multiplication by $g(t, x)$ includes the part of the integral containing the function a . Our view now is that we leave $x - a$ untouched and perturb the integral part of the equation (20), just as it is done in equation (19). It should be mentioned that while equations (18) and (20) share solutions, the perturbations (19) and (22) do not.

As already mentioned, J may be any positive number, but the proper choice of $J > 0$ is crucial for our study. Any (arbitrary) choice of $J > 0$ leads to a unique kernel satisfying (21) as well as to the corresponding transformed equation (22) equivalent to the original equation (20). Clearly, there are so many equations to work with, and one may wonder which one might be a proper value of J that allows us to achieve our goal. In the two propositions that follow, we use different techniques to spot proper values of $J > 0$ allowing us to obtain the desired results.

We may now proceed to presenting conditions yielding fixed point regions for equation (22) when g, a are bounded. Note that f is not assumed to be bounded. Since we are interested in continuous solutions on $[0, \infty)$, due to the continuity of g one may see that for any continuous function ϕ , we have $|\mathcal{T}(\phi)(0)| = |a(0)|$ with \mathcal{T} being the natural mapping defined by the right-hand side of the equation (22). It turns out that in order to obtain a fixed point region for the equation (22) it is sufficient to find a suitable $D > 0$ (with $|a(0)| < D$) so that the corresponding ball in the space \mathcal{B} of bounded continuous functions with the usual sup-norm be mapped in its interior by \mathcal{T} . The Propositions below present sufficient conditions posed on g, a, f which yield the existence of such a D .

Proposition 8.1 *Let g, a be bounded by $\|g\|$ and $\|a\|$, respectively. Assume that there exist $m, M > 0$ with*

$$m \leq \frac{f(t, x)}{x} \leq M, \quad x \neq 0, \quad t \geq 0, \quad (23)$$

and such that

$$\|g\| \left(1 - \frac{m}{M}\right) = k < 1. \quad (24)$$

Then the set $G := \{x(t), t \geq 0 : \|x\| \leq D\}$ with $D > 0$ satisfying

$$\frac{\|a\| (1 + \|g\|)}{D} + k = k_0 < 1, \quad (25)$$

is a fixed point region for the equation (22) with $J = M$.

Proof. Firstly, note that by (23) we have

$$m \leq \frac{f(t, x)}{x} \leq M \implies 0 \leq 1 - \frac{f(t, x)}{Mx} \leq 1 - \frac{m}{M},$$

thus choosing $J = M$ it holds

$$0 \leq 1 - \frac{f(t, x)}{Jx} \leq 1 - \frac{m}{M}. \quad (26)$$

Then setting $\mathcal{T} : C([0, \infty), \mathbb{R}) \rightarrow C([0, \infty), \mathbb{R})$ with

$$\begin{aligned} \mathcal{T}x(t) & : = a(t) - g(t, x(t)) \int_0^t R(t-s) a(s) ds \\ & + g(t, x(t)) \int_0^t R(t-s) \left[x(s) - \frac{f(s, x(s))}{J} \right] ds, \end{aligned}$$

and choosing D by (25), in view of (24) and (26) we have for $t \geq 0, \|x\| \leq D$

$$\begin{aligned} |\mathcal{T}x(t)| &\leq \|a\| + |g(t, x(t))| \int_0^t R(t-s) |a(s)| ds \\ &\quad + |g(t, x(t))| \int_0^t R(t-s) \left| x(s) - \frac{f(s, x(s))}{J} \right| ds \\ &\leq \|a\| + \|g\| \|a\| \int_0^t R(s) ds \\ &\quad + \|g\| \int_0^t R(t-s) |x(s)| \left| 1 - \frac{f(s, x(s))}{Jx(s)} \right| ds \\ &< \|a\| + \|g\| \|a\| \cdot 1 + \|g\| \int_0^t R(t-s) \left(1 - \frac{m}{M} \right) \|x\| ds \\ &< \|a\| (1 + \|g\|) + kD \cdot 1 \\ &= D \left[\frac{\|a\| (1 + \|g\|)}{D} + k \right] = Dk_0, \end{aligned}$$

so $\|\mathcal{T}x\| \leq Dk_0 = D_0 < D$, and $\mathcal{T}(G) \subset G^\circ \subset B(0; D)$.

Clearly, if x is a fixed point of \mathcal{T} , then by continuity we will have $|x(0)| = |a(0)| < D$, so, due to $\mathcal{T}(G) \subset G^\circ$, the solution x cannot leave G .

In the same direction we consider the equation

$$x(t) = a(t) + \int_0^t A(t-s) f(s, x(s)) ds, \quad t \geq 0, \tag{27}$$

with f, a and A as before, but now we relax condition (23). Note that condition (23) includes the sign condition $xf(x) > 0, x \neq 0$. In fact, now we do not ask for any sign condition.

As before, we want to transform equation (27) using a properly chosen $J > 0$ and then perturb it to a quadratic equation by multiplying the integral by a bounded function $g(t, x)$. This time we assume that the bound of $|g|$ is less than 1 and choose $J > 0$ depending on the bound of g . It turns out that by asking that $\|g\| < 1$ we may avoid the left hand side assumption in (23) along with condition (24).

So we consider the perturbed transformed equation

$$\begin{aligned} x(t) &= a(t) - g(t, x(t)) \int_0^t R(t-s) a(s) ds \\ &\quad + g(t, x(t)) \int_0^t R(t-s) \left[x(s) + \frac{f(s, x(s))}{J} \right] ds, \end{aligned} \tag{28}$$

where $J > 0$ is some properly chosen constant depending on the bounds of g and a and the behavior of $\frac{f(t,x)}{x}$ on $[0, \infty) \times \{0\}$.

Proposition 8.2 *Let g and a be bounded by $\|g\| < 1$ and $\|a\|$, respectively, and assume that*

$$|f(t, x)| \leq \psi(x), \quad (t, x) \in [0, \infty) \times \mathbb{R},$$

for a continuous function $\psi : \mathbb{R} \rightarrow [0, \infty)$. If there exist $K, \delta > 0$ with

$$\left| \frac{\psi(x)}{x} \right| \leq K, \quad 0 < |x| \leq \delta, \tag{29}$$

then there exists a bounded set G which is a fixed point region for the equation (28) with J satisfying (32).

Proof. Since $\|g\| < 1$, we may consider a $D > 0$ such that

$$\frac{2\|a\|}{D} < 1 - \|g\|. \quad (30)$$

Due to continuity of $\frac{\psi(x)}{x}$, $|x| \geq \delta$ and (29), there exists an $M > 0$ with

$$\left| \frac{\psi(x)}{x} \right| \leq M, \quad |x| \leq D. \quad (31)$$

Now with this M in hand and in view of (30) and the assumption that $\|g\| < 1$ we may take a $J > 0$ such that

$$\frac{2\|a\|}{D} + \|g\| \left(1 + \frac{M}{J} \right) = k_1 < 1. \quad (32)$$

Taking into consideration (32) and (31) we have for $t \geq 0$, $\|x\| \leq D$

$$\begin{aligned} |\mathcal{T}x(t)| &\leq \|a\| + |g(t, x(t))| \int_0^t R(t-s) |a(s)| ds \\ &\quad + |g(t, x(t))| \int_0^t R(t-s) \left| x(s) + \frac{f(s, x(s))}{J} \right| ds \\ &\leq \|a\| + \|g\| \int_0^t R(s) \|a\| ds \\ &\quad + \|g\| \int_0^t R(t-s) |x(s)| \left[1 + \frac{|f(s, x(s))|}{J|x(s)|} \right] ds \\ &\leq \|a\| + \|g\| \int_0^t R(s) \|a\| ds \\ &\quad + \|g\| \int_0^t R(t-s) |x(s)| \left[1 + \frac{1}{J} \left| \frac{\psi(x(s))}{x(s)} \right| \right] ds \\ &< \|a\| + \|a\| \cdot 1 + \|g\| \int_0^t R(t-s) \left(1 + \frac{M}{J} \right) \|x\| ds \\ &< 2\|a\| + \|g\| \left(1 + \frac{M}{J} \right) D \\ &= D \left[\frac{2\|a\|}{D} + \|g\| \left(1 + \frac{M}{J} \right) \right] = k_1 D, \end{aligned}$$

so, for any $k_2 \in (k_1, 1)$ it holds $\|\mathcal{T}x\| < k_2 D := D_1 < D$, $\|x\| \leq D$, which implies that for $G := \{x \in C([0, +\infty)) : \|x\| \leq D\}$ we have $\mathcal{T}(G) \subset B(0; D_1) \subset G^\circ$.

Clearly, if x is a fixed point of \mathcal{T} , then by continuity of x, a and f we find

$$\begin{aligned} &\lim_{t \rightarrow 0^+} |g(t, x(t))| \int_0^t R(t-s) \left| x(s) + \frac{f(s, x(s))}{J} \right| ds \\ &\leq \left| 1 + \frac{M}{J} \right| \|g\| D \lim_{t \rightarrow 0^+} \int_0^t R(t-s) ds = 0, \end{aligned}$$

so

$$|x(0)| = \lim_{t \rightarrow 0^+} |\mathcal{T}x(t)| = \left| a(0) + \lim_{t \rightarrow 0^+} |g(t, x(t))| \int_0^t R(t-s) |a(s)| ds \right| = |a(0)| < \frac{D}{2}$$

and we may conclude that any fixed point x of \mathcal{T} is a function starting at $x(0)$ with $|x(0)| = |a(0)| < D$ and due to $\mathcal{T}(G) \subset G^\circ$ it cannot leave G .

When the function g is bounded by a bound which is greater than or equal to one, then multiplying our equation by g , i.e.,

$$x(t) = a(t) + g(t, x(t)) \int_0^t A(t-s) f(s, x(s)) ds$$

is equivalent to considering

$$x(t) = a(t) + \frac{g(t, x(t))}{\|g\| + 1} \int_0^t A(t-s) (\|g\| + 1) f(t, x(s)) ds$$

or

$$x(t) = a(t) + g_0(t, x(t)) \int_0^t A(t-s) f_0(s, x(s)) ds,$$

with $f_0(t, x) := (\|g\| + 1) f(t, x)$ and $g_0(t, x) := \frac{g(t, x)}{\|g\| + 1}$.

As the last equation may be seen as a perturbation (by $g_0(t, x(t))$) of the equation

$$x(t) = a(t) + \int_0^t A(t-s) f_0(s, x(s)) ds, \tag{33}$$

alternatively, one may choose to perturb the transformed equation of (33) by multiplying by $g_0(t, x(t))$, thus considering

$$\begin{aligned} x(t) &= a(t) + g_0(t, x(t)) \int_0^t R(t-s) a(s) ds \\ &\quad + g_0(t, x(t)) \int_0^t R(t-s) \left[x(s) + \frac{f_0(s, x(s))}{J} \right] ds. \end{aligned}$$

Clearly, if f satisfies (29), then so does f_0 (with $K_0 = K(\|g\| + 1)$), so the last Proposition is applicable and a fixed point region might be yielded.

Before closing the paper we cite three remarks. The first one concerns the assumptions on the kernel A which allow the kernel to have singularities as long as conditions (A1)-(A3) are satisfied. It is worth noticing that fractional kernels $(t-s)^q$ with $q \in (0, 1)$ do satisfy these conditions, so our results do apply in this case. The second remark concerns L^1 kernels. As it has already been mentioned, in such a case the integral of the resolvent kernel is less than one. With this in hand one may see that the results in both Propositions of this section still hold while conditions (24) and $\|g\| < 1$ may be relaxed to

$$\|g\| \left(1 - \frac{m}{M} \right) = k \leq 1 \tag{34}$$

and $\|g\| \leq 1$, respectively, yet m is allowed to be zero. As a final remark, we would like to emphasize on the fact that under the conditions of this study, not only the fixed point regions "trap" all bounded (continuous) solutions of the perturbed equation, but they also yield that there do not exist any unbounded ones.

References

- [1] S. Abbas, M. Benchohra, J. R. Graef and J. Henderson. *Implicit Fractional Differential and Integral Equations: Existence and Stability*. De Gruyter, Leipzig, Germany, 2018.
- [2] L. C. Becker, T. A. Burton and I. K. Purnaras. An inversion of a fractional differential equation and fixed points. *Nonlinear Dynamics and Systems Theory* **15** (3) (2015) 242–271.
- [3] L. C. Becker, T. A. Burton and I. K. Purnaras. Integral and fractional equations, positive solutions, and Schaefer’s fixed point theorem. *Opuscula Math.* **36** (4) (2016) 431–458.
- [4] T. A. Burton. Fractional differential equations and Lyapunov functionals. *Nonlinear Anal.:TMA* **4** (2011) 5648–5662.
- [5] T. A. Burton and I. K. Purnaras. Equivalence of differential, fractional differential, and integral equations: Fixed points by open mappings. *MESA* **8** (3) (2017) 293–305 (see p. 297).
- [6] T. A. Burton and I. K. Purnaras. Krasnoselskii’s theorem, integral equations, open mappings, and non-uniqueness. *Nonlinear Dynamics and Systems Theory* **18** (4) (2018) 342–358 (See p. 344).
- [7] T. A. Burton and I. K. Purnaras. Open mappings: The case for a new direction in fixed point theory, submitted.
- [8] T. A. Burton and B. Zhang. Fixed points and fractional differential equations: Examples. *Fixed Point Theory* **14** (2) (2013) 313–326.
- [9] S. Chandrasekhar. *Radiative Transfer*. Dover, New York, 1960.
- [10] M. A. Darwish. On a quadratic fractional integral equation with linear modification of the argument. *Can. Appl. Math. Q.* **16** (2008) 45–58.
- [11] M. A. Darwish and J. Henderson. Existence and asymptotic stability of solutions of a perturbed quadratic fractional integral equation. *Fract. Calc. Appl. Anal.* **12** (2009) 71–86.
- [12] K. Diethelm. *The Analysis of Fractional Differential Equations*. Springer, 2004.
- [13] A. Friedman. On integral equations of Volterra type. *J. d’Analyse Math.* **11** (1963) 381–413.
- [14] G. Gripenberg. On positive, nonincreasing resolvents of Volterra equations. *J. Differential Equations* **30** (1978) 380–390.
- [15] R. K. Miller. *Nonlinear Volterra Integral Equations*. Benjamin, Menlo Park, CA, 1971.
- [16] K. B. Oldham and J. Spanier. *The Fractional Calculus*. Academic Press, New York, 1974.
- [17] K. Padmavally. On a non-linear integral equation. *J. Math. and Mech.* **7** (4) 1958.
- [18] W. R. Mann and F. Wolf. Heat transfer between solids and gases under non-linear boundary conditions. *Quart. Appl. Math.* **9** (1950) 163–184.
- [19] J. H. Roberts and W. R. Mann. A nonlinear integral equation of Volterra type. *Pacific J. Math* **1** (1951) 431–445.
- [20] D. R. Smart. *Fixed Point Theorems*. Cambridge, 1980.
- [21] H. F. Weinberger. *A First Course in Partial Differential Equations with Complex Variables and Transform Methods*. Dover, Mineola, N. Y., 1995.



An Enhanced Bi-Directional Chaotic Optimization Algorithm

F. Derouiche ¹ and T. Hamaizia ^{2*}

¹ *Department of Mathematics, Faculty of Exact Sciences, University of Oum El-Bouaghi, Algeria*

² *Department of Mathematics, Faculty of Exact Sciences, University of Constantine 1, Algeria*

Received: June 20, 2020; Revised: October 5, 2020

Abstract: Based on the improved chaos searching strategy, an enhanced Bi-directional chaotic optimization algorithm (EBCOA) is proposed in this study. A Lozi chaos mapping is used as a chaos generator to produce a chaos variable. In the process of EBCOA, and in order to make the chaos search more efficient, a new sub-step local chaos optimization method is proposed and a global search is done to find the current optimal solution in a certain range, and then a fine search reduces the space of optimized variables. Compared with the algorithm of traditional chaos search, the proposed algorithm is more accurate and can respond quickly. Simulation and experimental results confirm the efficiency of the proposed algorithm.

Keywords: *chaos; global optimization; chaotic map; chaos optimization algorithm.*

Mathematics Subject Classification (2010): 34D45, 70K55.

1 Introduction

In the field of mathematics, physics and engineering science, it is well recognized that chaos theory can be applied as a very useful technique in practical application. Chaos is aperiodic behavior in a deterministic system which exhibits sensitive dependence on initial conditions, and thus provides great diversity based on the ergodic property of the chaos phase, which transits every state without repetition in certain ranges. Chaos is a term used to describe behavior that is seemingly random, but has an underlying mathematical order to it [1–5]. Chaos is very common in nature, but is often mistaken for random behavior. It is generated through a deterministic iteration formula. Due to

* Corresponding author: <mailto:el.tayyeb@umc.edu.dz>

these characteristics, chaos theory can be applied in the optimization algorithm [6, 7]. [9] proposed a chaotic differential evolution algorithm for multi-objective optimization. Many deterministic, stochastic methods for solving the global optimization problem have been proposed which, in turn, employed local moves or local exploitation, i.e., a new candidate point is generated in a neighborhood of the current one. For example, all Multistart-like algorithms generate candidate points in a neighborhood of the current one, Genetic Algorithms use mutation to generate a point in the neighborhood of a member of the current population, etc. The number of local minima is a critical issue for global optimization problems. It is well known that local moves alone are not enough to detect a global minimum because of getting trapped into a local minimum. Therefore, we need to employ other techniques to escape from local minima such random generation of starting points in Multistart-like algorithms; crossover in Genetic Algorithms, chaotic generation of starting points in two-phase algorithms (COA) [10–17].

In this study, an enhanced bi-directional chaos optimization algorithm (EBCOA) based on a new chaos search strategy is proposed in order to deal with premature convergence in later evolution. From the testing results of the benchmark functions, the results of EBCOA are obviously better than those of the standard bi-directional chaos optimization algorithm (BCOA). The rest of the paper is organized as follows. In Section 2, we describe the BCOA presented in the literature and we present a new approach, the EBCOA, based on the nested phases strategy and the use of 2-D chaotic sequences. In Section 3, simulation results are provided to validate the effectiveness of the proposed method. The paper ends with the conclusion as Section 4 followed by the references.

2 Chaos Search Strategy

Chaos occurs in many nonlinear systems, which is generated by deterministic equations. Chaotic systems with their interesting properties such as topologically mixing and dense periodic orbits, ergodicity and intrinsic stochasticity, can be used in various applications such as global optimization. In feature selection, chaos search is more capable of escaping from local optima than random search. One way of application with chaos is a chaotic optimization algorithm (COA) [6, 7, 13, 16, 17], which utilizes the nature of chaos sequence including the quasi-stochastic property and ergodicity. The experimental studies assert that the benefits by chaotic variables instead of random variables are more obvious although the mathematical theory can not be formulated.

2.1 Generation of chaotic sequences

In this section, we present the chaotic maps used, which generate chaotic sequences in the process of evolutionary algorithms [12]. Chaos theory studies the behavior of systems that follow deterministic laws but appear to be random and unpredictable, i.e., dynamical systems. Chaotic variables can go through all states in certain ranges according to their own regularity without repetition [10–12]. A chaotic map is a map that exhibits some type of chaotic behavior. In this work, we applied 2-D chaotic maps that are common in the literature, namely, the Lozi map [18] given by

$$\begin{cases} y_1(k) = 1 - a|y_1(k-1)| + by(k-1), \\ y(k) = y_1(k-1), \end{cases} \quad (1)$$

$$z(k) = \frac{y(k) - \alpha}{\alpha' - \alpha}, \tag{2}$$

where k is the iteration number. In this work, the values of y are normalized in the range $[0;1]$ to each decision variable in n -dimensional space of the optimisation problem. Therefore, $y_1 \in [-0.6417; 0.6716]$ and $(\alpha; \alpha') = (-0.6418; 0.6716)$.

The parameters used in this study are $a = 1.7$ and $b = 0.5$, see Figure 1, these values are suggested in [13].

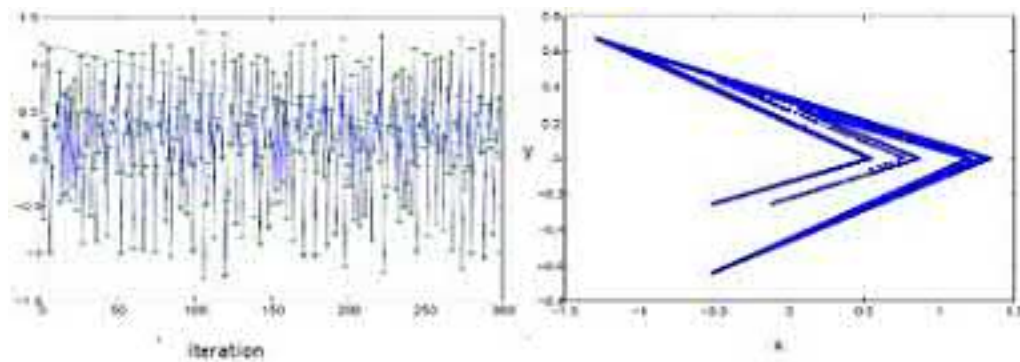


Figure 1: Attractor and temporal series of the Lozi map.

2.2 Two-phase methods and basic BCOA

In this section we briefly recall the BCOA introduced by Ying Song [1]. Many chaotic strategies in global optimization consist of two phases: the global phase and the local phase. During the global phase, chaotic points are drawn from the domain of searches X according to a certain, often uniform, distribution. Then, the objective function is evaluated in these points. During the local phase, the sample points are manipulated by means of local search to yield a candidate global minimum. Consider the following optimization problem for a nonlinear function:

$$\begin{aligned} \min f(X), \quad X &= [x_1, x_2, x_3, \dots, x_n], \\ L_i &\leq x_i \leq U_i. \end{aligned}$$

The chaotic variables are

$$Z^{(k+1)} = g(Z^k),$$

where Z^k are chaotic states generated by the chaotic equation.

The basic process of the BCOA [1] strategy can be described as follows.

Step 1: also called the first carrier wave. Define a chaotic sequences generator based on the Logistic map. Generate a sequence of the chaotic points and map it to a sequence of decision points in the original decision space. Then, calculate the objective functions with respect to the generated decision points, and choose the point with the minimum objective function as the current optimum.

The ergodic area of chaotic variables to the variance range of optimisation variables is

$$X^k = c + d \cdot Z^k,$$

where c and d are constant vectors such as amplification gains and, respectively, consist of n elements $c_i = L_i$ and $d_i = U_i - L_i$.

Step 2: also called the second carrier wave. The current optimum is assumed to be close to the global optimum after certain iterations, and it is viewed as the center with a little chaotic perturbation and the global optimum is obtained through the fine search. Repeat the above two steps until some specified convergence criterion is satisfied, and the global optimum is obtained.

The approach of the second carrier wave is as follows:

$$X = X^* + \beta X^*(0.5 - Z),$$

so the search is on both two sides of the sub-optimal solution. Here X^* is the so far best solution. β is the parameter of the second carrier.

We have

$$-0.5\beta \leq \beta(0.5 - Z) \leq 0.5\beta \quad \text{as} \quad \beta \geq 0, \quad (3)$$

$$0.5\beta \leq \beta(0.5 - Z) \leq -0.5\beta \quad \text{as} \quad \beta \leq 0, \quad (4)$$

so the search is on both two sides of the sub-optimal solution.

3 Proposed EBCOA

3.1 Block flow diagram of EBCOA

Applying the local search technique has been hot and can bring two benefits to the whole search procedure. First, the search can be driven into a better area further from local optima. Second, but not less important, the exploitation of some promising areas of the search space can be enhanced so as to speed up the convergence of the search.

The BCOA method [1] is then improved by the local search around every point obtained by the chaotic series. The logistic map [1, 6, 7] is usually adopted in the COA. But the distribution of chaotic sequences produced by the logistic map is uniformly leading to the slow constrigent. The Lozi map marked by (1) is a Gaussian map with which we replace the logistic map to accelerate the rate of convergence.

The EBCOA can be illustrated as follows, where M_g , M_l and M_{gl} are the maximum number of iterations of the chaotic global search, maximum number of iterations of the chaotic local search and maximum number of iterations of the chaotic local search in the global search, respectively. β is the step size in the chaotic local search, \bar{x}_i is the best solution.

3.2 Step-size control

It is well-established that the convergence of a chaotic optimization algorithm directly depends on how it controls the step size. Moreover, the step-size control influences to a large extent the rate at which a chaotic optimization algorithm approaches the optimum. The step-size adaptation mechanisms are all based on the idea that the smaller the step size, the higher the probability of sampling good solutions.

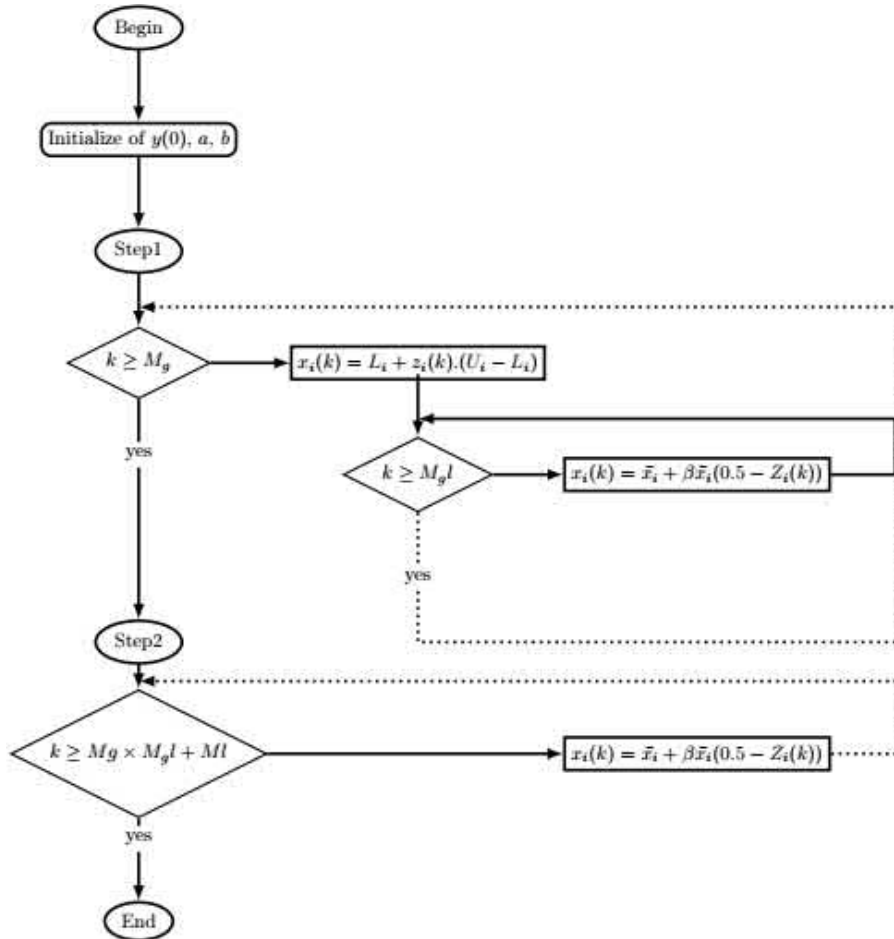


Figure 2: Block flow diagram of the EBCOA.

4 Simulation Results

In applied mathematics, test functions, known as artificial landscapes, are useful to evaluate characteristics of optimization algorithms. For testing our approach, and from the standard set of benchmark problems available in the literature, we use two well known nonlinear benchmark functions [21, 22]. In our study, we overcome this limitation using a number of dimensions 2 and comparing with other heuristic optimization algorithms. The Griewank function has many irregularities but there is only one unique global minimum. The Rastrigin function has many local optimal points and one unique global minimum. Table 1 resumes the global optimum, the function value at global optimum and the search range used for each test function. Figure 2 presents the plot for each test function. All the programs were run on a 2 GHz Pentium IV processor with 2 GB of random access memory in the MATLAB. In each case study, 50 independent runs were made for each of the EBCOA methods. In the tested cases to benchmark problems, the

maximum numbers of iterations $maxK$ and $maxK'$ were 10000 and 10000 iterations.

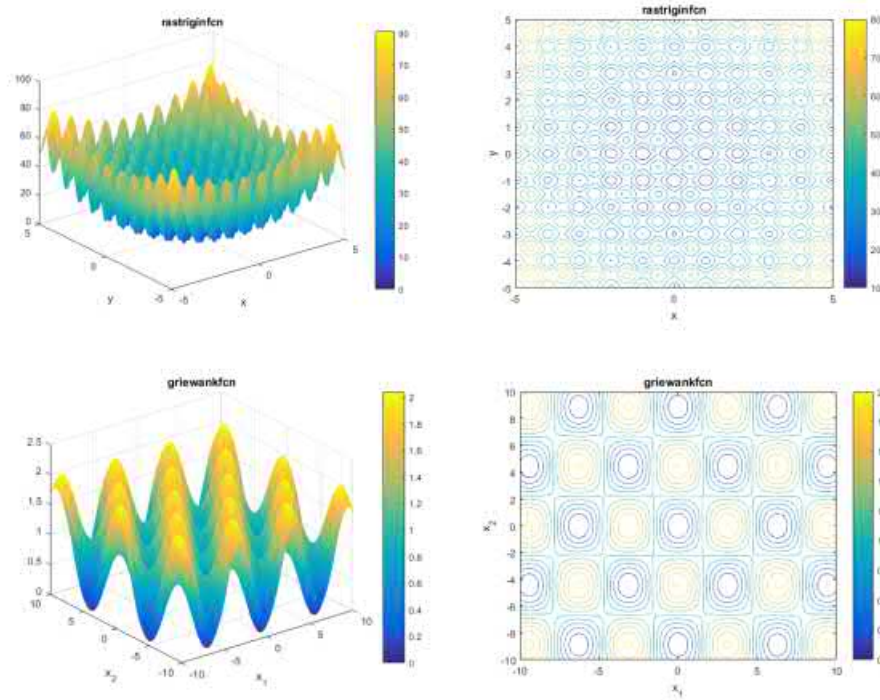


Figure 3: A perspective view and the related contour lines of some of functions when $n = 2$.

4.1 Results for the Rastrigin function

| | | BCOA | EBCOA |
|---------|-----------|------------|----------------------|
| K' | β | optimum | optimum |
| 1001 | 700 | 4.2752e-6 | 0 |
| 1001 | 500 | 4.7997e-9 | 0 |
| 1001 | 400 | 1.1219e-11 | 0 |
| 2405 | 200 | 3.5527e-15 | 0 |
| 1023 | 0.1 | 3.9080e-14 | 3.90798505 e -14 |
| 6965 | 0.01 | 4.3343e-13 | 4.192202141 e -13 |
| $maxK'$ | 1e -3 | 2.6392e-5 | 5.419204974544 e - 6 |
| $maxK'$ | 1e -4 | 4.7111e-4 | 8.3677132572291 e-5 |
| $maxK'$ | -(1 e -3) | 2.8008e-5 | 2.1552183152806 e-5 |
| $maxK'$ | -(1 e -4) | 4.7392e-4 | 5.0020093164866 e -5 |

Table 1: Rastrigin optimum for $n = 2$ with different β .

| | | BCOA | EBCOA |
|---------|---------|------|-------|
| optimum | β | K' | K' |
| 0 | 100 | 1206 | 10 |
| | 10 | 399 | 10 |
| | 1 | 368 | 10 |
| | -100 | 1918 | 10 |
| | -10 | 421 | 10 |

Table 2: Number of iterations with different β .

From Table 2, for $\beta \geq 200$, the EBCOA can find the actual optimum 0. Here $|\beta| \in [1e - 4, 200] \cup [-120, -(1e - 4)]$. The optimum is improved. From Table 3 for $\beta \in]0.1, 100]$, the EBCOA can also find the actual optimum 0 but with the number of iterations less than that in the BCOA.

The optimum value and the convergence speed are better than those in the COA [7] and its improvements, such as the MSCOA [19], COA-BFGS [14] and other evolutionary algorithms (such as the GA, PSO and its improvements) [20–22].

4.2 Results for the Griewank function.

| | | BCOA | EBCOA |
|------|---------|---------|---------|
| K' | β | optimum | optimum |
| 802 | 11.12 | 0 | 0 |
| 346 | 11.10 | 0.2533 | 0 |
| 904 | -9.93 | 0 | 0 |
| 372 | -9.91 | 0.2516 | 0 |

Table 3: Griewank optimum for $n = 2$ with different β .

| | | BCOA | EBCOA |
|---------|---------|------|-------|
| optimum | β | K' | K' |
| 0 | 11.09 | 802 | 10 |
| | 10 | 550 | 10 |
| | 1.60 | 347 | 10 |
| | -9.90 | 904 | 10 |
| | -10 | 489 | 10 |
| | -1.33 | 369 | 10 |

Table 4: Number of iterations with different β .

From Table 4 we find that, for $\beta \geq 11.09$ and $\beta \leq -9.90$, the EBCOA can always find the actual optimum 0, and for $\beta \in [1.60, 11.09] \cup [9.90, -1.33]$, the EBCOA can also find the actual optimum 0 but with the number of iterations less than that in the BCOA. The optimum value and the convergence speed are better than those in the COA [7] and its improvements such as the MSCOA [19], COA-BFGS [14] and other evolutionary algorithms (such as the GA, PSO and its improvements) [20–22].

5 Conclusion

Based on the ergodic property, chaos is adopted to enrich the search behavior and prevent solutions from being trapped in the local optimum in optimization problems. This paper focuses on exploring the effects of chaotic maps and giving guidance for improving the Bi-directional chaotic optimization algorithm in solving optimization problems. Through proposing a new algorithm, the EBCOA, we have improved the BCOA doing some modification in the global step of research, we refined the final solution using a second bi-directional method of local search. The presented study allows us to conclude that the proposed method is fast and converges to a good optimum.

References

- [1] Ying Song. A Bi-directional Chaos Optimization Algorithm. In: *2010 Sixth International Conference on Natural Computation (ICNC 2010)*.
- [2] T. Y. Li and J. A. Yorke. Period three implies chaos. *Amer. Math. Monthly* **82** (1975) 985–992.
- [3] E. Ott, T. Sauer and J. A. Yorke. Coping with Chaos Analysis of Chaotic Data and Exploitation of Chaotic Systems. In: *Wiley Series in Nonlinear Science*, 1st ed. John Wiley: New York, USA, 1994.
- [4] S. H. Strogatz. *Nonlinear Dynamics and Chaos*. Massachusetts: Perseus Publishing, 2000.
- [5] J. C. Sprott. *Chaos and Times-Series Analysis*. Oxford University Press, Oxford, UK, 2003.
- [6] B. Li and W. S. Jiang. Chaos optimization method and its application. *Journal of Control Theory and Application* **14** (4) (1997) 613–615.
- [7] B. Li and W. S. Jiang. Optimizing complex function by chaos search. *Cybernetics and Systems* **29** (4) (1998) 409–419. Oxford, UK, 2003.
- [8] A. Khernane. Numerical Approximation of the Exact Control for the Vibrating Rod with Improvement of the Final Error by Particle Swarm Optimization. *Nonlinear Dynamics and Systems Theory* **20** (2) (2020) 179–190.
- [9] D. P. Niu, F. L. Wang, D. K. He and M. X. Jia. Chaotic differential evolution for multiobjective optimization. *Control Decision* **24** (2009) 361–364.
- [10] L.X. Li, Y.X. Yang, H. Peng and X.D. Wang. An optimization method inspired by chaotic behavior. *Int. J. Bifurcat Chaos* **16** (2006) 2351–2364.
- [11]] D. Yang, Z. Liu and J. Zhou. Chaos optimization algorithms based on chaotic maps with different probability distribution and search speed for global optimization. *Commun. Nonlinear Sci. Numer. Simul* **19** (2014) 1229–1246.
- [12] R. Caponetto, L. Fortuna, S. Fazzino and M. G. Xibilia. Chaotic Sequences to Improve the Performance of Evolutionary Algorithms. *IEEE Transactions on Evolutionary Computation* **7** (3) (2003) 289–304.

- [13] L. S. Coelho. Tuning of PID controller for an automatic regulator voltage system using chaotic optimization approach. *Chaos, Solitons and Fractals* **39** (2009) 1504–1514.
- [14] D. X. Yang, G. Li and G. D. Cheng, On the efficiency of chaos optimization algorithms for global optimization. *Chaos, Soli. Fract* **34** (4) (2007) 1366–1375.
- [15] R. Bououden, M. S. Abdelouahab and F. Jarad. Chaos in New 2-d Discrete Mapping and Its Application in Optimization. *Nonlinear Dynamics and Systems Theory* **20** (2) (2020) 144-152.
- [16] H. Shayeghi, S. Jalilzadeh, H.A. Shayanfar and A. Safari. Robust PSS Design using Chaotic Optimization Algorithm for a Multimachine Power System. In: *ECTI-CON 2009*, Pattaya, Thailand, May 2009, pp. 40–43. 2007.
- [17] T. Hamaizia and R. Lozi. An improved chaotic optimization algorithm using a new global locally averaged strategy. *Journal of Nonlinear Systems and Applications* **3** (2) (2012) 58–63.
- [18] R. Lozi. Un attracteur du type attracteur de Hénon. *J. Phys.* **39** (C5) (1978) 9–10.
- [19] T. Zhang, H. W. Wang and Z. C. Wang. Mutative scale chaos optimization algorithm and its application. *Control & Decision* **14** (3) (1999) 285–288.
- [20] B. Liu, L. Wang, Y. H. Jin, F. Tang and D. X. Huang. Improved particle swarm optimization combined with chaos. *Chaos, Soli. Fract.* **25** (5) (2005) 1261–1271.
- [21] Y. Song, Z. Q. Chen, and Z. Z. Yuan. New chaotic PSO-based neural network predictive control for nonlinear process. *IEEE Trans. Neural Networks* **18** (2) (2007) 595–600.
- [22] S. Janson and M. Middendorf. A hierarchical particle swarm optimizer and its adaptive variant. *IEEE Trans. Syst., Man, Cybern. Part B: Cybernetics* **35** (6) (2005) 1272–1282.



Speed Sensorless Direct Torque Control Strategy of a Doubly Fed Induction Motor Using an ANN and an EKF

T. Djellouli^{1,3}, S. Moulahoum², A. Moualdia^{2*}, M.S. Bouchrit¹
and P. Wira³

¹ *Process Control Laboratory, National Polytechnic School, Algiers, Algeria*

² *Laboratory of Electrical Engineering and Automatics (LREA), University of Medea, Algeria*

³ *IRIMAS, Laboratory of Modeling Intelligence Process Systems (MIPS), University of Haute Alsace, Mulhouse, France.*

Received: March 13 2020; Revised: September 18, 2020

Abstract: This study is devoted to the Direct Torque Control (DTC) strategy of a Doubly Fed Induction Motor (DFIM), with the use of an Artificial Neural Network (ANN) in the switching table, that gives the control sequence of the voltage inverter. This strategy is performed in two methods, the first one is with a mechanical sensor for the motor speed and, consequently, the position of its rotor, and the second one is without a mechanical sensor, using the Extended Kalman Filter (EKF) as a fast observer for the nonlinear closed loop with the obtained variable matrix. The EKF gives the new values of the state variables of the DFIM by minimizing the noise impact. This helps to avoid problems caused by the motor speed sensor and to make better the control robustness and its performances in the situation of any sensor fault. The selected configuration uses two voltage inverters linked to the stator and the rotor windings, which permits adopting the energy distribution between the stator and the rotor, and which is a suitable drive for the changeable speed application.

Keywords: *doubly fed induction motor (DFIM); direct torque control (DTC); artificial neural network (ANN); extended Kalman filter (EKF).*

Mathematics Subject Classification (2010): 03B52, 93C42, 94D05.

* Corresponding author: <mailto:amoualdia@gmail.com>

1 Introduction

In a generator system, the Double Feed Induction Machine (DFIM) is more used in different speed wind systems for electricity production [1], where in motor mode, it is found in high power applications such as traction, marine propulsion and pump storage systems [2, 3]. In this application, the DFIM works in motor operation, it is supplied by two Voltage Inverters (VI), one is for the stator and the second is for the rotor. This case is explained in Figure 1. The switching state of the VI is checked according to the counted values of the flux and the angle of this flux from the measured electrical amounts (voltages and currents). The switching table that gives the control sequence of the inverter is elaborated based on the ANN technique as the developed control ameliorates the torque reply by minimizing the oscillations compared to the conventional table control. The way exposed in this paper is the Direct Torque Control (DTC) which is applied to ensure a good dynamic performance and stability. The control is supported by the initial information on the flux, the rotor position and its fastness. In most cases, the latter is gained by a mechanical sensor. However, this demands a location installation that gives difficulty access or requires more space, decreases reliability in difficult environments and rises the expense of the machine. In this content, the Extended Kalman Filter (EKF) is used to estimate the speed of the DFIM as a work of the measured stator and rotor electrical variables [4].

This paper is organized as follows. Section 2 and Section 3 give, with no details, the modeling and control by DTC-ANN strategy of the DFIM with a speed sensor. Section 4 is dedicated to estimating the rotor speed by the EKF used in the evolved strategy. Section 5 introduces the simulation effects obtained by the application of the DTC-ANN strategy with and without a speed sensor. Concluding remarks are given in Section 6.

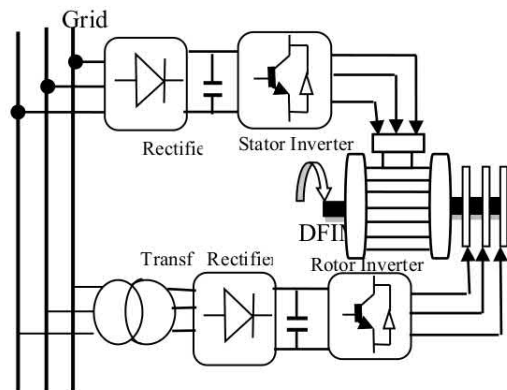


Figure 1: General schema of a DFIM powered by two Inverters.

2 Modeling of the DFIM

In order to achieve a good dynamic performance in DFIM control, it is necessary to have the model which represents the machine's behavior, not only in the permanent regimes, but also in the transient regimes. The modelling of the DFIM is based on the general equations in Concordia transformation applied on the stator and rotor windings, these

equations are given as follows [5]:

$$\begin{cases} V_{\alpha s} = R_s I_{\alpha s} + \frac{d\phi_{\alpha s}}{dt}, \\ V_{\beta s} = R_s I_{\beta s} + \frac{d\phi_{\beta s}}{dt}, \end{cases} \quad (1)$$

$$\begin{cases} V_{\alpha r} = R_r I_{\alpha r} + \frac{d\phi_{\alpha r}}{dt} + \omega \phi_{\beta r}, \\ V_{\beta r} = R_r I_{\beta r} + \frac{d\phi_{\beta r}}{dt} - \omega \phi_{\alpha r}, \end{cases} \quad (2)$$

$$\begin{cases} \phi_{\alpha s} = L_s I_{\alpha s} + M I_{\alpha r}, \\ \phi_{\beta s} = L_s I_{\beta s} + M I_{\beta r}, \end{cases} \quad (3)$$

$$\begin{cases} \phi_{\alpha r} = M I_{\alpha s} + L_r I_{\alpha r}, \\ \phi_{\beta r} = M I_{\beta s} + L_r I_{\beta r}, \end{cases} \quad (4)$$

where ω_s , ω are the stator and rotor pulsations, $\omega = p\Omega$. Ω is the mechanical rotating speed. The angular relationship is defined by Figure 2 [6]:

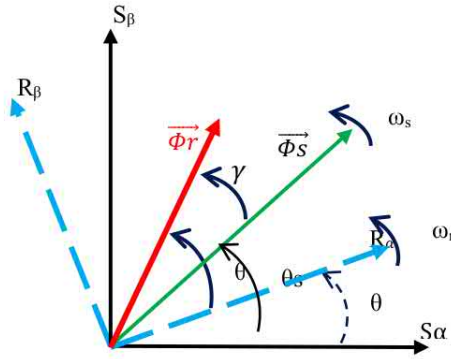


Figure 2: Stator and rotor flux position in the DFIM.

$$\theta_s = \theta_r + \theta - \gamma, \quad (5)$$

θ_s : Angular position of the rotating reference $\alpha - \beta$,

θ_r : Angular position relative to α axis,

θ : The electrical angular position of the rotor relative to the stator reference frame.

So, in the steady state ($d\gamma/dt = 0$) and with

$$\begin{cases} \frac{d\theta_s}{dt} = \omega_s, \\ \frac{d\theta}{dt} = \omega, \\ \omega_s = \omega + \omega_r, \end{cases} \quad (6)$$

the dynamical equation is given by

$$J \frac{d\Omega}{dt} = T_{em} - T_r - K_f \Omega \quad (7)$$

and the electromagnetic torque equation is

$$T_{em} = \frac{P \cdot M}{L_r} (\Phi_{\alpha r} I_{\beta s} - \Phi_{\beta r} I_{\alpha s}). \quad (8)$$

The motor is powered directly by two three-phase voltage inverters, as it is represented in Figure 1.

3 Strategy Applied on DFIM

The system, studied in this work, is the DFIM powered by two voltage inverters (VI) for the stator and the rotor, Fig.1. The switching states of the inverters are generated using a direct torque control (DTC) strategy, where the current and voltage sensors are needed [7]. The DTC makes it possible to control the optimum electromagnetic torque from the flow metrics and their positions. The main advantages of the DTC applied to the induction machine are:

- The DTC has a simple structure and a robust control, if one ensures a good quality of the estimation of the flows during operation, and consequently, a good estimate of the couple.
- The DTC with two ST (switching tables) provides excellent torque dynamics, but the positions of the stator and rotor flows and the angle between these fluxes must be carefully controlled. In this paper, a separate control of the stator and rotor flows is proposed. In order to apply the DTC strategy to two voltage inverters on the DFIM, we define a first ST to control the stator flux vector and a second ST to control the rotor flux vector. The next part of the control strategy controls the interaction between the two streams. As a result, it is possible to regulate the speed as long as the electromagnetic torque is controllable [7].

By using the stator flux $\vec{\Phi}_s$ and the rotor flux $\vec{\Phi}_r$ vectors as state variables, the DFIM electromagnetic torque can be expressed as follows [7, 8]:

$$\begin{cases} \vec{T}_{em} = \frac{3}{2} \cdot \frac{PM}{\sigma_s L_r} (\vec{\Phi}_s \wedge \vec{\Phi}_r), \\ \|T_{em}\| = K \cdot (\|\vec{\Phi}_s\| \cdot \|\vec{\Phi}_r\|) \cdot \sin(\gamma), \end{cases} \quad (9)$$

where P is the number of pole pairs, L_s , L_r are the stator and rotor self-inductances, M is the mutual inductance, and $\sigma = 1 - \frac{M}{L_s L_r}$ is the dispersion coefficient. $\vec{\Phi}_s$ and $\vec{\Phi}_r$ are the stator and rotor flux space vectors and γ is the angle between the fluxes as shown in Figure 2. The constant ' K ' is defined as below:

$$K = \frac{3}{2} \cdot \frac{PM}{\sigma L_s L_r}. \quad (10)$$

By analyzing relation (9), two strategies can be proposed for the torque control:

- by fixing the flux module and adjusting the γ angle,
- by fixing the γ angle and adjusting the flux module.

In this study, the authors [6, 7] chose the first strategy. The DTC strategy applied to this system will provide fast and robust torque and flux responses.

3.1 Stator and rotor inverter control

The first inverter is connected to the stator winding (Stator Inverter (SI)), and the second one is connected to the rotor winding (Rotor Inverter (RI)), S_1 , S_2 , and S_3 are the switching sequence sent to the IGBT gates. The instantaneous value of the stator flux and its position are estimated from the measured electrical quantities. Using hysteresis comparators, the flux and the position are controlled directly and independently with an appropriate selection of the voltage vector imposed by the inverter. The inverter provides eight voltage vectors. These vectors are chosen by a switching table based on the errors of flux and its position. Table 1 is deduced according to the switching sequence from the model of the induction machine in a stationary reference and the expression of the stator voltage.

Table 1. Voltage Inverter Table.

| voltage vector | S_1 | S_2 | S_3 | V_{ab} | V_{bc} | V_{ca} |
|----------------|-------|-------|-------|----------|----------|----------|
| V_0 | 0 | 0 | 0 | 0 | 0 | 0 |
| V_1 | 1 | 0 | 0 | +U | 0 | -U |
| V_2 | 1 | 1 | 0 | 0 | +U | -U |
| V_3 | 0 | 1 | 0 | -U | +U | 0 |
| V_4 | 0 | 1 | 1 | -U | 0 | +U |
| V_5 | 0 | 0 | 1 | 0 | -U | +U |
| V_6 | 0 | 1 | 0 | +U | -U | 0 |
| V_7 | 1 | 1 | 1 | 0 | 0 | 0 |

The stator flux is estimated from the following relation:

$$\Phi_s(t) = \int (V_s - R_s I_s) dt. \quad (11)$$

Over the time interval $[0, T_s]$, corresponding to a sampling period T_e , it is considered that the term $R_s I_s$ is negligible compared to the voltage V_s , thus

$$\Phi_s = \Phi_{s0} + V_s T_e. \quad (12)$$

The stator and rotor flux vectors can be estimated directly into the stator and rotor voltage vectors

$$\begin{cases} \frac{d}{dt} \vec{\phi}_s = \vec{V}_s, \\ \frac{d}{dt} \vec{\phi}_r = \vec{V}_r. \end{cases} \quad (13)$$

We integrate (11) during a sampling period T_e . Thus, the following equation is obtained:

$$\begin{cases} \overline{\Phi_s(t_{n+1})} = \overline{\Phi_s(t_n)} + T_e \cdot \overline{V_s(t_n)}, \\ \overline{\Phi_r(t_{n+1})} = \overline{\Phi_r(t_n)} + T_e \cdot \overline{V_r(t_n)}. \end{cases} \quad (14)$$

The voltage vector application time is T_e . Consequently, V_s and V_r remain constant during the time interval $[t_n, t_{n+1}]$, where $t_{n+1} = t_n + T_e$. Equation (8) can be rewritten as

$$\begin{cases} \overline{\Phi_s^{n+1}} = \overline{\Phi_s^n} + T_e \cdot \overline{V_s^n}, \\ \overline{\Phi_r^{n+1}} = \overline{\Phi_r^n} + T_e \cdot \overline{V_r^n}. \end{cases} \quad (15)$$

For each sampling time, the appropriate output voltage vector of the inverter can be deduced from the estimated values of the flux. In Figure 3, six sectors are defined in the stationary reference frame (α, β) . Therefore, if θ_s (or θ_r) is in the same sector, the use of an identical voltage vector leads to a similar phase and amplitude evolution of the flux vector. The rotor flux vector is defined in the same way [6]. Thus, the applied voltage

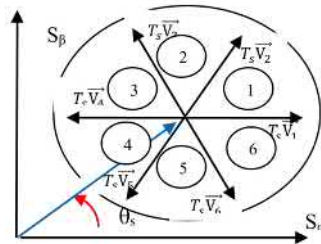


Figure 3: Applicable voltage vectors for the stator flux vector control.

vectors depend on the following:

1. The sector number (according to θ_s and θ_r).
2. The required flux angular position.
3. The required flux magnitude evolution.

This is illustrated in ST shown in Table 2. Two independent STs are implemented in the control system. They allow controlling the rotor and stator fluxes. The DTC strategy is aimed to separate the stator and rotor flux adjustment. In this way, the flux interaction is controlled, and consequently, the electromagnetic torque T_{em} (13).

Table 2. Switch positions and their voltage vectors

| | | Sector number N | | | | | |
|------------------------|----------|-----------------|-------|-------|-------|-------|-------|
| $\vec{\Phi}$ evolution | θ | 1 | 2 | 3 | 4 | 5 | 6 |
| $\ \vec{\Phi}\ $ | | Voltage vector | | | | | |
| | | V_2 | V_3 | V_4 | V_5 | V_6 | V_1 |
| | | V_6 | V_1 | V_2 | V_3 | V_4 | V_5 |
| | | V_3 | V_4 | V_5 | V_6 | V_1 | V_2 |
| | | V_5 | V_6 | V_1 | V_2 | V_3 | V_4 |

3.2 DTC-ANN applied on DFIM

The proposed DTC-ANN consists to replace the switching table which provides the voltage vector, the Artificial Neural Network (ANN) switching table inputs are:

- $\Delta\Phi_s$ The flux error.
- $\Delta\Phi_r$: The angle error.

N_s is the number of sector from 1 to 6. This ANN is based on forward-forward propagation with three hidden layers having, respectively [4, 14], 16 neurons in each layer and one connection as activation functions. The output layer has three neurons providing a voltage vector [9], the proposed ANN switching table is shown in Figure 4. It is well

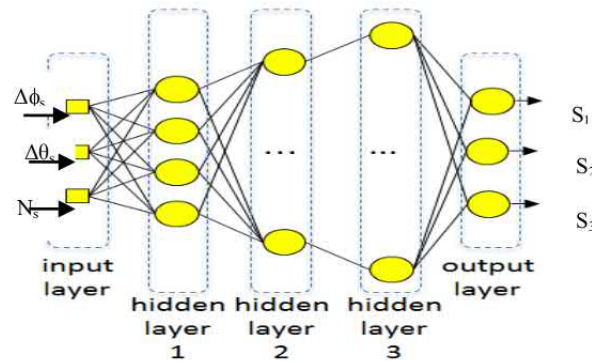


Figure 4: The ANN structure for switching table.

known that the stator windings and the rotor windings are fed by two three-phase systems where the rotor current frequency has a slip. The angular relation of rotor can be deduced as (Figure 2):

$$\theta_r = \gamma + \theta_s - \theta. \quad (16)$$

The global scheme of the proposed control strategy is illustrated in Figure 5. In this diagram, Ω is the mechanical rotation speed measured by a sensor installed on the rotor.

4 Speed Sensorless Control by EKF

The rotor position and DFIM speed data are indispensable in the check. They are always obtained via a mechanical speed sensor. But, this sensor needs a place for its installation, moreover, this leads to some problems in its installation; and it is affected by noises and vibrations. Various techniques have been proposed in the literature to remove this mechanical sensor. Among these techniques, there is the speed estimation using the EKF. This Kalman filter is an observer for the nonlinear closed loop with the obtained variable matrix. In every calculation stage, the Kalman filter gives the new values of the state variables of the DFIM. The prediction values are made by minimizing the noise impact and modeling the parameter faults or the unstable state. Noises are supposed to be white, Gaussian and not correlated with the estimated states [10].

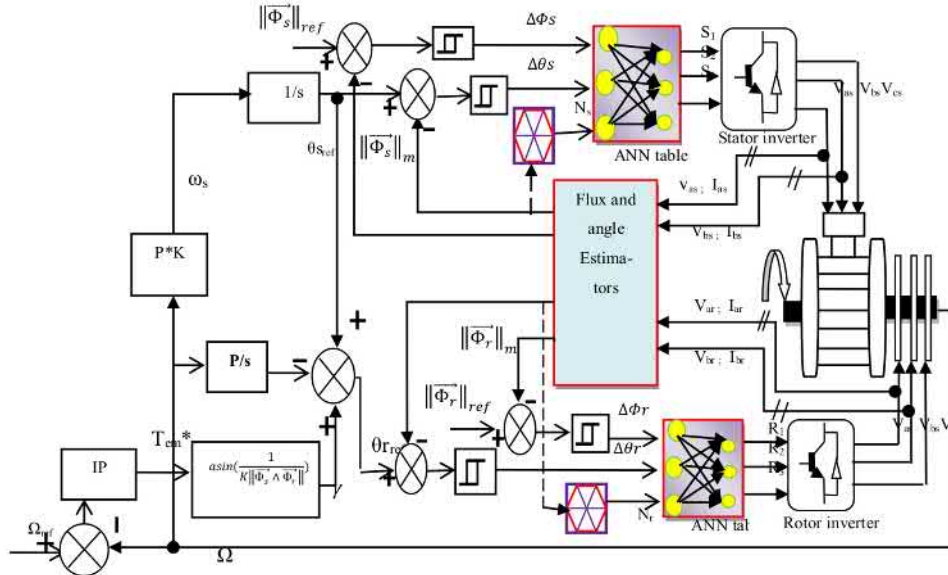


Figure 5: Global block diagram of the DTC with a mechanical speed sensor.

4.1 Selection of DFIM model

We consider the angular rotor speed ω as a state variable which increases the size of the state vector, in this case, this state vector becomes

$$x = [i_{\alpha s} \quad i_{\beta s} \quad i_{\alpha r} \quad i_{\beta r} \quad \omega]^T, \tag{17}$$

$$u = [v_{\alpha s} \quad v_{\beta s} \quad v_{\alpha r} \quad v_{\beta r}]^T. \tag{18}$$

The time-domain of the motor model is given as[11]:

$$\dot{x} = f(x, u) = Ax + Bu, \tag{19}$$

$$y = h(x) = [i_{\alpha s} i_{\beta s}]^T, \tag{20}$$

$$A = \begin{bmatrix} -\frac{R_s}{\sigma L_s} & \frac{(1-\sigma)\omega}{\sigma} & \frac{R_r M}{\sigma L_s L_r} & \frac{M}{\sigma L_s} \omega \\ -\frac{(1-\sigma)\omega}{\sigma} & -\frac{R_s}{\sigma L_s} & -\frac{M}{\sigma L_s L_r} \omega & \frac{R_r M}{\sigma L_s L_r} \\ \frac{R_s M}{\sigma L_s L_r} & -\frac{M}{\sigma L_r} \omega & -\frac{R_r}{\sigma L_r} & -\frac{1}{\sigma} \omega \\ \frac{M}{\sigma L_r} \omega & \frac{R_s M}{\sigma L_s L_r} & \frac{1}{\sigma} \omega & -\frac{R_r}{\sigma L_r} \end{bmatrix}, \tag{21}$$

$$B = \begin{bmatrix} \frac{1}{\sigma L_s} & 0 & -\frac{M}{\sigma L_s L_r} & 0 \\ 0 & \frac{1}{\sigma L_s} & 0 & -\frac{M}{\sigma L_s L_r} \\ -\frac{M}{\sigma L_s L_r} & 0 & \frac{1}{\sigma L_r} & 0 \\ 0 & -\frac{M}{\sigma L_s L_r} & 0 & \frac{1}{\sigma L_r} \end{bmatrix}, \tag{22}$$

$$C = \begin{bmatrix} 1 & 0 & 0 & 0 & 0 \\ 0 & 1 & 0 & 0 & 0 \end{bmatrix}. \tag{23}$$

The above equations can be written also as

$$\frac{d}{dt} \begin{bmatrix} I_{\alpha s} \\ I_{\beta s} \\ I_{\alpha r} \\ I_{\beta r} \\ \omega \end{bmatrix} = \begin{bmatrix} a_1 & a_2 p \Omega & a_3 & a_4 p \Omega & 0 \\ -a_2 p \Omega & a_1 & -a_4 p \Omega & a_3 & 0 \\ a_5 & -a_6 p \Omega & a_7 & -a_8 p \Omega & 0 \\ a_6 p \Omega & a_5 & a_8 p \Omega & a_7 & 0 \\ 0 & 0 & 0 & 0 & 1 \end{bmatrix} \begin{bmatrix} I_{\alpha s} \\ I_{\beta s} \\ I_{\alpha r} \\ I_{\beta r} \\ \omega \end{bmatrix} + Bu \quad (24)$$

with

$$Bu = \begin{bmatrix} b_1 & 0 & b_2 & 0 \\ 0 & b_1 & 0 & b_2 \\ b_2 & 0 & b_3 & 0 \\ 0 & b_2 & 0 & b_3 \\ 0 & 0 & 0 & 0 \end{bmatrix} \begin{bmatrix} V_{\alpha s} \\ V_{\beta s} \\ V_{\alpha r} \\ V_{\beta r} \end{bmatrix}, \quad (25)$$

$$\begin{bmatrix} I_{\alpha s} \\ I_{\beta s} \end{bmatrix} = \begin{bmatrix} 1 & 0 & 0 & 0 & 0 \\ 0 & 1 & 0 & 0 & 0 \end{bmatrix} [I_{\alpha s} \ I_{\beta s} \ I_{\alpha r} \ I_{\beta r} \ \omega]^T, \quad (26)$$

where the parameters a_i and b_i are given by

$$a_1 = -\frac{R_s}{\sigma L_s}, a_2 = \frac{(1-\sigma)}{\sigma}, a_3 = \frac{R_r M}{\sigma L_s L_r}, a_4 = \frac{M}{\sigma L_s}, \quad (27)$$

$$a_5 = \frac{R_s M}{\sigma L_s L_r}, a_6 = \frac{-M}{\sigma L_r}, a_7 = -\frac{R_r}{\sigma L_r}, a_8 = \frac{1}{\sigma}, \quad (28)$$

$$b_1 = \frac{1}{\sigma L_s}, b_2 = -\frac{M}{\sigma L_s L_r}, b_3 = \frac{1}{\sigma L_r}. \quad (29)$$

4.2 DFIM discretization model

The DFIM discrete state space model is obtained from equations (23) and (24) as follows [10, 12]:

$$X_{k+1} = f(X_k, U_k) = A_k X_k + B_k U_k, \quad (30)$$

$$Y_k = h(X_k) = C_k X_k, \quad (31)$$

where A_k, B_k and C_k are the discretized system matrix, input matrix and output matrix, respectively, thus

$$\begin{cases} A_k = 1 + TA, \\ B_k = BT, \\ C_k = C, \end{cases} \quad (32)$$

where T is the sampling time and I is an identity matrix.

$$\begin{cases} A_k = \begin{bmatrix} 1 + a_1 T & a_2 p \Omega T & a_3 T & a_4 p \Omega T & 0 \\ -a_2 p \Omega T & 1 + a_1 T & -a_4 p \Omega T & a_3 T & 0 \\ a_5 T & -a_6 p \Omega T & 1 + a_7 T & -a_8 p \Omega T & 0 \\ a_6 p \Omega T & a_5 T & a_8 p \Omega T & 1 + a_7 T & 0 \\ 0 & 0 & 0 & 0 & 1 \end{bmatrix}, \\ B_k = T \begin{bmatrix} b_1 & 0 & b_2 & 0 \\ 0 & b_1 & 0 & b_2 \\ b_2 & 0 & b_3 & 0 \\ 0 & b_2 & 0 & b_3 \\ 0 & 0 & 0 & 0 \end{bmatrix}, \\ C_k = \begin{bmatrix} 1 & 0 & 0 & 0 & 0 \\ 0 & 1 & 0 & 0 & 0 \end{bmatrix}, \end{cases} \quad (33)$$

$$X_k = \begin{bmatrix} I_{\alpha s}(k) \\ I_{\beta s}(k) \\ I_{\alpha r}(k) \\ I_{\beta r}(k) \\ \omega(k) \end{bmatrix}, X_{k+1} = \begin{bmatrix} I_{\alpha s}(k+1) \\ I_{\beta s}(k+1) \\ I_{\alpha r}(k+1) \\ I_{\beta r}(k+1) \\ \omega(k+1) \end{bmatrix}, U_k = \begin{bmatrix} V_{\alpha s}(k) \\ V_{\beta s}(k) \\ V_{\alpha r}(k) \\ V_{\beta r}(k) \end{bmatrix}. \tag{34}$$

Let v be the noise vector of the system which perturbs the state vector, and w be the measurement noise vector which perturbs the measurement vector [11]

$$\begin{cases} X_{k+1} = f(X_k, U_k) + w_k, \\ Y_k = h(X_k) + v_k. \end{cases} \tag{35}$$

The Kalman filter considers the system noise vector and the measurement noise vector as the Gaussian white noise of zero mean, which is free of the basic state vector and their covariance matrices, these are, respectively, Q and R , defined by

$$\begin{cases} Q = \text{cov}(w) = E \{ww^T\}, \\ R = \text{cov}(v) = E \{vv^T\}. \end{cases} \tag{36}$$

4.3 Determination of the noise and state covariance matrices

To obtain the best considerable speed value, it is necessary to use exact initial values for the covariance system matrices of the noise measurement and the state noise Q , R and P , respectively [12]. They have important results on the stability filter and convergence time. These matrices are supposed to be matrices of diagonal covariance.

4.4 Implementation of the discretized EKF algorithm

The filtering algorithm is formed of two major steps, a prediction step and a filtering step [10, 11].

- ∇ In the prediction process, the following predicted states values $\hat{X}(k+1)$ are got by using a mathematical model (state-variable equations), also the former values of the estimated states. Therefore, the predicted state covariance matrix (P) is gained before the new measurement values. At the end, the mathematical model and also the covariance matrix of the system (Q) are used.
- ∇ During the second step, which is the filtering step, the following estimated states, $\hat{X}(k+1)$, are got from the predicted ones, they estimate $X(k+1)$ by adding a correction term $K(y - \hat{y})$ to the predicted value.

This correction term is a weighted variety between the current output vector (y) and the predicted output vector (\hat{y}). Here K is the Kalman gain. The estimated states are gained from the following stages [13, 14].

- Initialization of the state vector and covariance matrices.
- Prediction of the state vector

$$\hat{X}_{k+1/k} = f(X_{k/k}, U_k). \tag{37}$$

- Covariance estimation of prediction.

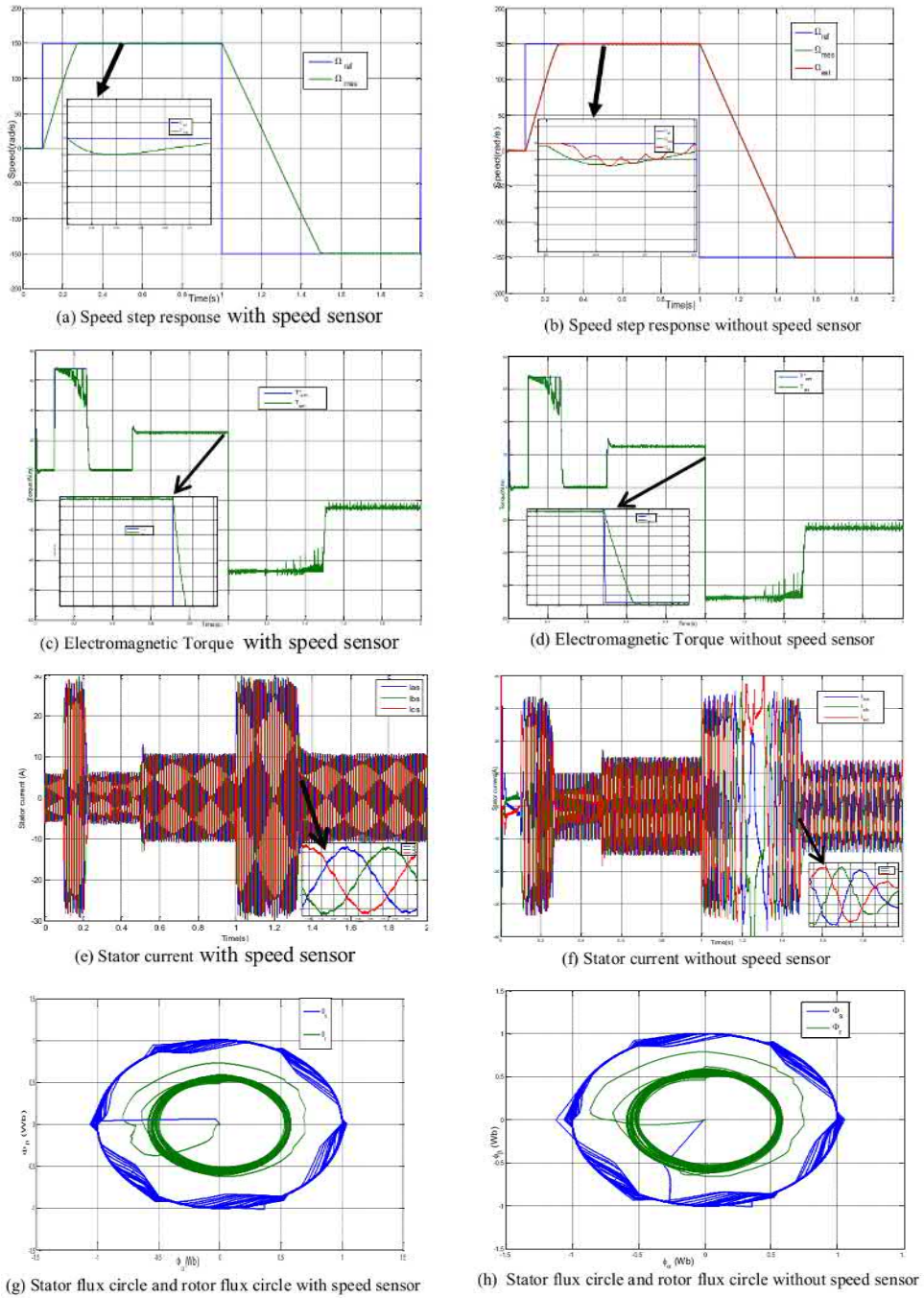


Figure 7: Simulation results.

6 Conclusion

In this paper, the direct torque control strategy by two switching tables developed by ANN technique applied on DFIM, with and without a mechanical sensor, is presented. In order to guarantee a good dynamic performance of the overall system and to solve the problem of control, accompanied generally with the mechanical sensor fault, the EKF approach is used as a speed observer in the DTC, which makes it possible to obtain a good control for the voltages generated by the inverters, and consequently, a good metric of flux and torque, in order to ensure a good dynamic performance of the controlled system without a mechanical speed sensor. The results obtained show a good regulation of the electrical and magnetic quantities, which ensures the efficiency of this strategy without a speed sensor and the stability of the system in the event of load or sensor fault.

Acknowledgment

The research is part of a project PRFU'2020, realized, respectively, in the Laboratory of Process Control (LCP), National Polytechnic School, Algiers, Algeria, and Laboratory of Electrical Engineering and Automatic LREA Research, University of Medea.

References

- [1] T. Douadi, Y. Harbouche, R. Abdessemed and I. Bakhti. Improvement Performances of Active and Reactive Power Control Applied to DFIG for Variable Speed Wind Turbine Using Sliding Mode Control and FOC. *International Journal of Engineering TRANSACTIONS A* **31**(10) (2018) 1689–1697.
- [2] D. Ben Attous and Y. Bekakra. Speed Control of a Doubly Fed Induction Motor using Fuzzy Logic Techniques. *International Journal on Electrical Engineering and Informatics* **2** (3) (2010) 179–191.
- [3] S. Khojet El Khil, I. Slama-Belkhodja, M. Pietrzak-David and B. de Fornel. A Fault Tolerant Operating System in a Doubly Fed Induction Machine Under Inverter Short-circuit Faults. *32nd Annual Conference on IEEE Industrial Electronics, Paris, France*, Nov. (2006).
- [4] M. Abdelrahem, C. Hackl and R. Kennel. Application of Extended Kalman Filter to Parameter Estimation of Doubly-Fed Induction Generators in Variable-Speed Wind Turbine Systems. *International Conference on Clean Electrical Power(ICCEP)* (2015) 226–233.
- [5] S. Lekhchine, T. Bahi, I. Aadlia, Z. Layateb and H. Bouzeria. Speed control of doubly fed induction motor. *Energy Procedia* **74** (2015) 575–586.
- [6] F. Bonnet, P.E. Vidal and M. Pietrzak-David. Dual Direct Torque Control of Doubly Fed Induction Machine. *IEEE Transactions on Industrial Electronics* **54** (5) (2007) 2482–2490.
- [7] M. Abdellatif, M. Debbou, I. Slama-Belkhodja and M. Pietrzak-David. Simple Low-Speed Sensorless Dual DTC for Double Fed Induction Machine Drive. *IEEE Transactions on Industrial Electronics* (**61**) (8) (2014) 3915–3922.
- [8] F. Bonnet and M. Pietrzak-David. Control optimization of a doubly fed induction machine. *IEEE Power Electronics Specialists Conference, Rhodes* (Jun 2008) 2579–2585.
- [9] C. Kamal Basha and M. Suryakalavathi. Estimation of Rotor Flux using Neural Network Observer in Speed Sensorless Induction Motor Drive. *International Journal of Computer Applications* **79** (6) (2014).

- [10] M. Vafaie, B. Dehkordi, P. Moallem and A. Kiyoumars. Minimizing Torque and Flux Ripples and Improving Dynamic Response of PMSM using a Voltage Vector with Optimal Parameters. *Industrial Electronics IEEE Transactions* **63** (2015) 3876–3888.
- [11] H. Hamidi and A. Valizadeh. Improvement of Navigation Accuracy using Tightly Coupled Kalman Filter. *International Journal of Engineering TRANSACTIONS B: Applications* **30**(2) (2017) 215–223.
- [12] Y-R. Kim, S-K. Sul and M-H. Park. Speed sensorless vector control of induction motor using extended Kalman filter. *IEEE Transactions on Industry Applications* **30** (05) (1994) 1225–1233.
- [13] K.C. Wong, S.L. Ho and K.W.E. Cheng. Direct torque control of a doublyfed induction generator with space vector modulation. *Elec. Pow. Comp. and Syst.* **36**(12) (2008) 1337–1350.
- [14] Y. Chedni, D.J. Boudana, A. Moualdia, L. Nezli and P. Wira. Sensorless Two Series Connected Quasi Six-Phase IM Based Direct Torque Control for Torque Ripples Minimization. *Nonlinear Dynamics and System Theory* **20**(2) (2020) 153–167.
- [15] A. Moualdia, M. O. Mahmoudi and L. Nezli. Direct Torque Control of the DFIG and Direct Power Control for Grid Side Converter in wind power generation system. *The Mediterranean Journal of Measurement and Control, MEDJMC* **9**(3) (2013) 101–108.
- [16] S. Boulkhrachef, A. Moualdia, Dj. Boudana and P. Wira. Higher-order sliding mode control of a wind energy conversion system. *Nonlinear Dynamics and System Theory* **19**(4) (2019) 486–496.
- [17] A. Chalanga, S. Kamal and B. Moreno. Implementation of super-twisting control: super-twisting and higher Order sliding-mode observer-based approaches. *IEEE Trans. on Industrial Electronics* **63**(6) (2016) 3677–3685.
- [18] A.G. Mazko. Robust output feedback stabilization and optimization of discrete-time control systems. *Nonlinear Dynamics and System Theory* **18**(1) (2018) 92–106.
- [19] E. Benyoussef, A. Meroufel and S. Barkat. Neural network and fuzzy logic direct torque control of sensorless double star synchronous machine. *Rev. Roum. Sci. Techn. Ectrotechn. et Nerg.* **61**(3) (2016) 239–243.

APPENDIX Table 3. DFIM parameters used in simulation.

| | |
|---------------------------------|-------------------|
| Stator resistance | $R_s = 1.2\Omega$ |
| Rotor resistance | $R_r = 1.8\Omega$ |
| Stator inductance | $L_s = 0.1554H$ |
| Rotor inductance | $L_r = 0.1554H$ |
| mutual inductance | $M = 0.15H$ |
| Inertia moment | $J = 0.07Kg.m^2$ |
| Coefficient of viscous friction | $f = 0.001$ |
| Number of pairs of poles | $P = 2$ |



Solving Laplace Equation within Local Fractional Operators by Using Local Fractional Differential Transform and Laplace Variational Iteration Methods

H. K. Jassim¹, J. Vahidi^{2,3,*} and V. M. Ariyan^{3,4}

¹ *Department of Mathematics, Faculty of Education for Pure Sciences, University of Thi-Qar, Nasiriyah, Iraq*

² *Department of Mathematics, Iran University of Science and Technology, Tehran, Iran*

³ *Department of Mathematical Sciences, University of South Africa, UNISA0003, South Africa*

⁴ *Department of Mathematical Sciences, Mangosuthu University of Technology, Umlazi, South Africa*

Received: May 10, 2018; Revised: October 15, 2020

Abstract: In this paper, we utilize the local fractional differential transform (LFDTM) and Laplace variational iteration methods (LFLVIM) to obtain approximate solutions for the Laplace equation (LE) within local fractional derivative operators (LFDOs). The efficiency of the considered methods is illustrated by some examples. The results obtained by the LFDTM are compared with the results obtained by the LFLVIM. We demonstrate that the two approaches are very effective and convenient for finding the approximate analytical solutions of PDEs with LFDOs.

Keywords: *Laplace equation; local fractional differential transform method; local fractional Laplace variational iteration method; approximate solutions.*

Mathematics Subject Classification (2010): 34A08, 37M99.

* Corresponding author: <mailto:jvahidi@iust.ac.ir>

1 Introduction

The LFDTM and LFM are powerful approximate methods for various kinds of linear and nonlinear PDEs with LFDOs. For example, the Laplace variational iteration method (LFLVIM) has been applied to PDEs in physics and mathematics. Jassim et al. applied this method to diffusion and wave equations [1] and the Laplace equation [2]. Furthermore, Liu et al. [3] used the LFLVIM for a fractal vehicular traffic flow, and Li et al. to a fractal heat conduction problem [4]. Furthermore, the LFDTM has been applied to solve ordinary and partial differential equations on the Cantor sets. Jafari et al. utilized this method to find the approximate solution of ODEs [5–7]. Yang et al. applied the LFDTM to solve a two dimensional diffusion equation [8].

Our aim is to extend the applications of the proposed methods to obtain the analytical approximate solutions to the Laplace equation within local fractional derivative operators of the form

$$\frac{\partial^{2\vartheta}\psi(\eta, \kappa)}{\partial\kappa^{2\vartheta}} + \frac{\partial^{2\vartheta}\psi(\eta, \kappa)}{\partial\eta^{2\vartheta}} = 0 \tag{1}$$

with

$$\psi(\eta, 0) = \phi_1(\eta), \quad \frac{\partial^\vartheta}{\partial\kappa^\vartheta}\psi(\eta, 0) = \phi_2(\eta), \tag{2}$$

where $\phi_1(\eta)$ and $\phi_2(\eta)$ are given functions.

There are many approximate and numerical methods utilized to solve PDEs within LFDOs, namely, the LFFDM [9], LFD [10], LFSEM [11,12], LFM [13–15], LFLDM [16], RDTM [17] and SVM [18].

2 Local Fractional DTM

In the following the basic definitions and fundamental operations of the LFDTM are shown [8].

The two dimensional differential transform of the LF analytic function $\psi(\eta, \kappa)$ via LFDOs is

$$\Psi(\beta, \varepsilon) = \frac{1}{\Gamma(1 + \beta\vartheta)} \frac{1}{\Gamma(1 + \varepsilon\vartheta)} \left[\frac{\partial^{(\beta+\varepsilon)\vartheta}\psi(\eta, \kappa)}{\partial\eta^{\beta\vartheta}\partial\kappa^{\varepsilon\vartheta}} \right]_{\eta=\eta_0, \kappa=\kappa_0}, \tag{3}$$

where $\beta, \varepsilon = 0, 1, \dots, n$ and $0 < \vartheta \leq 1$.

The 2D differential inverse transform of $\Psi(\beta, \varepsilon)$ via LFDOs is

$$\psi(\eta, \kappa) = \sum_{\beta=0}^{\infty} \sum_{\varepsilon=0}^{\infty} \Psi(\beta, \varepsilon) (\eta - \eta_0)^{\beta\vartheta} (\kappa - \kappa_0)^{\varepsilon\vartheta}. \tag{4}$$

By combining (3) and (4), it can be obtained that

$$\psi(\eta, \kappa) = \sum_{\beta=0}^{\infty} \sum_{\varepsilon=0}^{\infty} \frac{1}{\Gamma(1 + \beta\vartheta)} \frac{1}{\Gamma(1 + \varepsilon\vartheta)} \left[\frac{\partial^{(\beta+\varepsilon)\vartheta}\psi(\eta, \kappa)}{\partial\eta^{\beta\vartheta}\partial\kappa^{\varepsilon\vartheta}} \right]_{\eta=\eta_0, \kappa=\kappa_0} (\eta - \eta_0)^{\beta\vartheta} (\kappa - \kappa_0)^{\varepsilon\vartheta}. \tag{5}$$

If $\eta_0 = 0$ and $\kappa_0 = 0$, then (3) is shown as follows:

$$\Psi(\beta, \varepsilon) = \frac{1}{\Gamma(1 + \beta\vartheta)} \frac{1}{\Gamma(1 + \varepsilon\vartheta)} \left[\frac{\partial^{(\beta+\varepsilon)\vartheta}\psi(\eta, \kappa)}{\partial\eta^{\beta\vartheta}\partial\kappa^{\varepsilon\vartheta}} \right]_{\eta=0, \kappa=0}, \tag{6}$$

and (4) is expressed as follows:

$$\psi(\eta, \kappa) = \sum_{\beta=0}^{\infty} \sum_{\varepsilon=0}^{\infty} \Psi(\beta, \varepsilon) \eta^{\beta\vartheta} \kappa^{\varepsilon\vartheta}. \quad (7)$$

Theorem 2.1 Suppose that $\psi(\eta, \kappa)$, $\varphi(\eta, \kappa)$ and $\theta(\eta, \kappa)$ are local fractional analytic functions and $\Psi(\beta, \varepsilon)$, $\Phi(\beta, \varepsilon)$ and $\Theta(\beta, \varepsilon)$ are their corresponding local fractional differential transforms with order of fraction ϑ , then we have

1. If $\psi(\eta, \kappa) = \varphi(\eta, \kappa) + \theta(\eta, \kappa)$, then $\Psi(\beta, \varepsilon) = \Phi(\beta, \varepsilon) + \Theta(\beta, \varepsilon)$.
2. If $\psi(\eta, \kappa) = \varphi(\eta, \kappa) + \theta(\eta, \kappa)$, then $\Psi(\beta, \varepsilon) = \sum_{r=0}^{\beta} \sum_{s=0}^{\varepsilon} \Phi(\beta, \varepsilon - s) \Theta(\beta - r, \varepsilon)$.
3. If $\psi(\eta, \kappa) = a\varphi(\eta, \kappa)$, where a is a constant, then $\Psi(\beta, \varepsilon) = \Phi(\beta, \varepsilon)$.
4. If $\psi(\eta, \kappa) = \frac{\partial^\vartheta}{\partial \eta^\vartheta} \varphi(\eta, \kappa)$, then $\Psi(\beta, \varepsilon) = \frac{\Gamma(1 + (\beta + 1)\vartheta)}{\Gamma(1 + \beta\vartheta)} \Phi(\beta + 1, \varepsilon)$.
5. If $\psi(\eta, \kappa) = \frac{\partial^\vartheta}{\partial \kappa^\vartheta} \varphi(\eta, \kappa)$, then $\Psi(\beta, \varepsilon) = \frac{\Gamma(1 + (\varepsilon + s)\vartheta)}{\Gamma(1 + \varepsilon\vartheta)} \Phi(\beta, \varepsilon + 1)$.
6. If $\psi(\eta, \kappa) = \frac{\partial^{(r+s)\vartheta}}{\partial \eta^{r\vartheta} \partial \kappa^{s\vartheta}} \varphi(\eta, \kappa)$, then

$$\Psi(\beta, \varepsilon) = \frac{\Gamma(1 + (\beta + r)\vartheta)}{\Gamma(1 + \beta\vartheta)} \frac{\Gamma(1 + (\varepsilon + s)\vartheta)}{\Gamma(1 + \varepsilon\vartheta)} \Phi(\beta + r, \varepsilon + s).$$
7. If $\psi(\eta, \kappa) = \frac{(\eta - \eta_0)^{r\vartheta}}{\Gamma(1 + r\vartheta)} \frac{(\kappa - \kappa_0)^{s\vartheta}}{\Gamma(1 + s\vartheta)}$, $\Psi(\beta, \varepsilon) = \frac{\delta_\vartheta(\beta - r)}{\Gamma(1 + r\vartheta)} \frac{\delta_\vartheta(\varepsilon - s)}{\Gamma(1 + s\vartheta)}$, where the local fractional Dirac delta function is given by

$$\delta_\vartheta(\beta - r) = \begin{cases} 1, & \beta = r, \\ 0, & \beta \neq r, \end{cases} \quad \text{and} \quad \delta_\vartheta(\varepsilon - s) = \begin{cases} 1, & \varepsilon = s, \\ 0, & \varepsilon \neq s. \end{cases}$$

3 Local Fractional LVIM

Let us consider the following local fractional PDEs on the Cantor sets with LFDOs:

$$L_\vartheta \varphi(\eta, \kappa) + R_\vartheta \varphi(\eta, \kappa) + N_\vartheta \varphi(\eta, \kappa) = \omega(\eta, \kappa), \quad (8)$$

where $L_\vartheta = \frac{\partial^{m\vartheta}}{\partial \kappa^{m\vartheta}}$ denotes the linear LFDO, R_ϑ is the remaining linear operator, N_ϑ represents the general nonlinear LFDO, and ω is the source term.

According to the rule of LFM, the correction local fractional functional for (8) is [13–15]

$$\varphi_{n+1}(\kappa) = \varphi_n(\kappa) + \frac{1}{\Gamma(1 + \vartheta)} \int_0^\kappa \frac{\sigma(\kappa - \xi)^\vartheta}{\Gamma(1 + \vartheta)} (L_\vartheta [\varphi_n(\xi)] + R_\vartheta [\tilde{\varphi}_n(\xi)] + N_\vartheta [\tilde{\varphi}_n(\xi)] - \omega(\xi)) (d\xi)^\vartheta, \quad (9)$$

where $\frac{\sigma(\kappa - \xi)^\vartheta}{\Gamma(1 + \vartheta)}$ is a fractal Lagrange multiplier.

For initial value problems of (8), we can start with

$$\varphi_0(\eta, \kappa) = \varphi(\eta, 0) + \frac{\kappa^\vartheta}{\Gamma(1 + \vartheta)} \varphi^{(\vartheta)}(\eta, 0) + \dots + \frac{\kappa^{(m-1)\vartheta}}{\Gamma(1 + (m-1)\vartheta)} \varphi^{((m-1)\vartheta)}(\eta, 0). \quad (10)$$

We now take the local fractional Laplace transform for (9), we get

$$\begin{aligned} \tilde{L}_\vartheta \{ \varphi_{n+1}(\kappa) \} &= \tilde{L}_\vartheta \{ \varphi_n(\kappa) \} + \\ \tilde{L}_\vartheta \left\{ \frac{1}{\Gamma(1 + \vartheta)} \int_0^\kappa \frac{\sigma(\kappa - \xi)^\vartheta}{\Gamma(1 + \vartheta)} (L_\vartheta [\varphi_n(\xi)] + R_\vartheta [\tilde{\varphi}_n(\xi)] + N_\vartheta [\tilde{\varphi}_n(\xi)] - \omega(\xi)) (d\xi)^\vartheta \right\}, \end{aligned} \quad (11)$$

or, equivalently,

$$\begin{aligned} \tilde{L}_\vartheta \{ \varphi_{n+1}(\kappa) \} &= \tilde{L}_\vartheta \{ \varphi_n(\kappa) \} + \tilde{L}_\vartheta \left\{ \frac{\sigma(\kappa)^\vartheta}{\Gamma(1 + \vartheta)} \right\} \times \\ &\tilde{L}_\vartheta \{ L_\vartheta [\varphi_n(\xi)] + R_\vartheta [\tilde{\varphi}_n(\xi)] + N_\vartheta [\tilde{\varphi}_n(\xi)] - \omega(\xi) \}. \end{aligned} \quad (12)$$

Take the local fractional variation of (12), which is given by

$$\begin{aligned} \delta^\vartheta \left(\tilde{L}_\vartheta \{ \varphi_{n+1}(\kappa) \} \right) &= \delta^\vartheta \left(\tilde{L}_\vartheta \{ \varphi_n(\kappa) \} \right) + \\ \delta^\vartheta \left(\tilde{L}_\vartheta \left\{ \frac{\sigma(\kappa)^\vartheta}{\Gamma(1 + \vartheta)} \right\} \tilde{L}_\vartheta \{ (L_\vartheta [\varphi_n(\kappa)] + R_\vartheta [\tilde{\varphi}_n(\kappa)] + N_\vartheta [\tilde{\varphi}_n(\kappa)] - \omega(\kappa)) \} \right). \end{aligned} \quad (13)$$

By using the computation of (13), we get

$$\begin{aligned} \delta^\vartheta \left(\tilde{L}_\vartheta \{ \varphi_{n+1}(\kappa) \} \right) &= \delta^\vartheta \left(\tilde{L}_\vartheta \{ \varphi_n(\kappa) \} \right) + \tilde{L}_\alpha \left\{ \frac{\sigma(\kappa)^\vartheta}{\Gamma(1 + \vartheta)} \right\} \delta^\vartheta \left(\tilde{L}_\vartheta \{ L_\vartheta [\varphi_n(\kappa)] \} \right) \\ &= 0. \end{aligned} \quad (14)$$

Hence, from (14) we get

$$1 + \tilde{L}_\vartheta \left\{ \frac{\sigma(\kappa)^\vartheta}{\Gamma(1 + \vartheta)} \right\} s^{m\vartheta} = 0, \quad (15)$$

where

$$\begin{aligned} \delta^\vartheta \left(\tilde{L}_\vartheta \{ L_\vartheta [\varphi_n(\kappa)] \} \right) &= \delta^\vartheta \left(s^{m\vartheta} \tilde{L}_\vartheta \{ \varphi_n(\kappa) \} - s^{(m-1)\vartheta} \varphi_n(0) - \dots - \varphi_n^{((m-1)\vartheta)}(0) \right) \\ &= s^{m\vartheta} \delta^\vartheta \left(\tilde{L}_\vartheta \{ \varphi_n(\kappa) \} \right). \end{aligned} \quad (16)$$

Therefore, we have

$$\tilde{L}_\vartheta \left\{ \frac{\sigma(\kappa)^\vartheta}{\Gamma(1 + \vartheta)} \right\} = -\frac{1}{s^{m\vartheta}}. \quad (17)$$

Taking the inverse version of the Yang-Laplace transform into (17), we have

$$\frac{\sigma(\kappa)^\vartheta}{\Gamma(1 + \vartheta)} = \tilde{L}_\vartheta \left(-\frac{1}{s^{m\vartheta}} \right) = -\frac{\kappa^{(m-1)\vartheta}}{\Gamma(1 + (m-1)\vartheta)}. \quad (18)$$

Hence, we have the following iteration algorithm:

$$\begin{aligned}
\tilde{L}_\vartheta \{\varphi_{n+1}(\kappa)\} &= \tilde{L}_\vartheta \{\varphi_n(\kappa)\} - \frac{1}{s^{m\vartheta}} \tilde{L}_\vartheta \{L_\vartheta [\varphi_n(\kappa)] + R_\vartheta [\varphi_n(\kappa)] + N_\vartheta [\varphi_n(\kappa)] - \omega(\kappa)\} \\
&= \tilde{L}_\vartheta \{\varphi_n(\kappa)\} - \frac{1}{s^{m\vartheta}} \tilde{L}_\vartheta \left\{ s^{m\vartheta} \varphi_n(\kappa) - \dots - \varphi_n^{((m-1)\vartheta)}(0) \right\} \\
&\quad - \frac{1}{s^{m\vartheta}} \tilde{L}_\vartheta \{R_\vartheta [\varphi_n(\kappa)] + N_\vartheta [\varphi_n(\kappa)] - \omega(\kappa)\} \\
&= \frac{1}{s^\vartheta} \varphi_n(0) - \frac{1}{s^{2\vartheta}} \varphi_n^{(\vartheta)}(0) - \dots - \frac{1}{s^{m\vartheta}} \varphi_n^{((m-1)\vartheta)}(0) \\
&\quad - \frac{1}{s^{m\vartheta}} \tilde{L}_\vartheta \{R_\vartheta [\varphi_n(\kappa)] + N_\vartheta [\varphi_n(\kappa)] - \omega(\kappa)\},
\end{aligned} \tag{19}$$

where the initial value reads as

$$\tilde{L}_\vartheta \{\varphi_0(\eta, \kappa)\} = \frac{1}{s^\vartheta} \varphi(\eta, 0) + \frac{1}{s^{2\vartheta}} \varphi^{(\vartheta)}(\eta, 0) + \dots + \frac{1}{s^{m\vartheta}} \varphi^{((m-1)\vartheta)}(\eta, 0). \tag{20}$$

Therefore, the local fractional series solution of (8) is

$$\varphi(\eta, \kappa) = \lim_{n \rightarrow \infty} \tilde{L}_\vartheta^{-1} \left(\tilde{L}_\vartheta \{\varphi_n(\eta, \kappa)\} \right). \tag{21}$$

4 Applications

In this section, an example for the Laplace equation involving LFDOs is presented in order to demonstrate the simplicity and the efficiency of the above methods.

Example 4.1 Let us consider the Laplace equation within LFDOs:

$$\frac{\partial^{2\vartheta} \varphi(\eta, \kappa)}{\partial \kappa^{2\vartheta}} + \frac{\partial^{2\vartheta} \varphi(\eta, \kappa)}{\partial \eta^{2\vartheta}} = 0, \tag{22}$$

$$\varphi(\eta, 0) = -E_\vartheta(\eta^\vartheta), \quad \frac{\partial^\vartheta \varphi(\eta, \kappa)}{\partial \kappa^\vartheta} = 0. \tag{23}$$

I. Below we present the LFDTM.

Using the LFDTM on both sides of (22), we can write

$$\frac{\Gamma(1 + (\varepsilon + 2)\vartheta)}{\Gamma(1 + \varepsilon\vartheta)} \Phi(\beta, \varepsilon + 2) + \frac{\Gamma(1 + (\beta + 2)\vartheta)}{\Gamma(1 + \beta\vartheta)} \Psi(\beta + 2, \varepsilon) = 0. \tag{24}$$

The transformed initial conditions are

$$\Phi(\beta, 0) = -\frac{1}{\Gamma(1 + \beta\vartheta)}, \quad \Phi(\beta, 1) = 0. \tag{25}$$

In view of (24) and (25), the results are listed as follows:

$$\begin{aligned}
 \Psi(0, 0) &= -1, & \Psi(0, 1) &= 0, & \Psi(0, 2) &= \frac{1}{\Gamma(1 + 2\vartheta)}, & \Psi(0, 3) &= 0, \\
 \Psi(0, 4) &= \frac{1}{\Gamma(1 + 4\vartheta)}, & \Psi(0, 5) &= 0, & \Psi(0, 6) &= \frac{1}{\Gamma(1 + 6\vartheta)}, & \Psi(1, 0) &= -\frac{1}{\Gamma(1 + \vartheta)}, \\
 \Psi(1, 1) &= 0, & \Psi(1, 2) &= \frac{1}{\Gamma(1 + \vartheta)} \frac{1}{\Gamma(1 + 2\vartheta)}, & \Psi(1, 3) &= 0, \\
 \Psi(1, 4) &= -\frac{1}{\Gamma(1 + \vartheta)} \frac{1}{\Gamma(1 + 4\vartheta)}, & \Psi(1, 5) &= 0, & \Psi(1, 6) &= \frac{1}{\Gamma(1 + \vartheta)} \frac{1}{\Gamma(1 + 6\vartheta)}, \\
 \Psi(2, 0) &= -\frac{1}{\Gamma(1 + 2\vartheta)}, & \Psi(2, 1) &= 0, \\
 \\
 \Psi(2, 2) &= \frac{1}{\Gamma(1 + 2\vartheta)} \frac{1}{\Gamma(1 + 2\vartheta)}, & \Psi(2, 3) &= 0, & \Psi(2, 4) &= -\frac{1}{\Gamma(1 + 2\vartheta)} \frac{1}{\Gamma(1 + 4\vartheta)}, \\
 \Psi(2, 5) &= 0, & \Psi(2, 6) &= \frac{1}{\Gamma(1 + 2\vartheta)} \frac{1}{\Gamma(1 + 6\vartheta)}, & \Psi(3, 0) &= -\frac{1}{\Gamma(1 + 3\vartheta)}, & \Psi(3, 1) &= 0, \\
 \Psi(3, 2) &= \frac{1}{\Gamma(1 + 3\vartheta)} \frac{1}{\Gamma(1 + 2\vartheta)}, & \Psi(3, 3) &= 0, & \Psi(3, 4) &= -\frac{1}{\Gamma(1 + 3\vartheta)} \frac{1}{\Gamma(1 + 4\vartheta)}, \\
 \Psi(3, 5) &= 0, & \Psi(3, 6) &= \frac{1}{\Gamma(1 + 3\vartheta)} \frac{1}{\Gamma(1 + 6\vartheta)}, & \Psi(4, 0) &= -\frac{1}{\Gamma(1 + 4\vartheta)}, & \Psi(3, 1) &= 0, \\
 \Psi(4, 2) &= \frac{1}{\Gamma(1 + 4\vartheta)} \frac{1}{\Gamma(1 + 2\vartheta)}, & \Psi(4, 3) &= 0, & \Psi(4, 4) &= -\frac{1}{\Gamma(1 + 4\vartheta)} \frac{1}{\Gamma(1 + 4\vartheta)}, \\
 \Psi(4, 5) &= 0, & \Psi(4, 6) &= \frac{1}{\Gamma(1 + 4\vartheta)} \frac{1}{\Gamma(1 + 6\vartheta)}, \dots
 \end{aligned}$$

and so on. Hence, $\psi(\eta, \kappa)$ is evaluated as follows:

$$\begin{aligned}
 \psi(\eta, \kappa) &= \sum_{\beta=0}^{\infty} \sum_{\varepsilon=0}^{\infty} \Psi(\beta, \varepsilon) \eta^{\beta\vartheta} \kappa^{\varepsilon\vartheta} \tag{26} \\
 &= - \left[1 + \frac{\eta^\vartheta}{\Gamma(1 + \vartheta)} + \frac{\eta^{2\vartheta}}{\Gamma(1 + 2\vartheta)} + \dots \right] \left[1 - \frac{\kappa^{2\vartheta}}{\Gamma(1 + 2\vartheta)} + \frac{\kappa^{4\vartheta}}{\Gamma(1 + 4\vartheta)} - \dots \right],
 \end{aligned}$$

which is exactly the same as the solution obtained by the LFFDM [11] and it converges to the closed form solution:

$$\psi(\eta, \kappa) = -E_\vartheta(\eta^\vartheta) \cos_\vartheta(\kappa^\vartheta). \tag{27}$$

II. As the next step we apply the LFLVIM.

In view of (19) and (22), we get the following iterative formula:

$$\begin{aligned}
 \tilde{L}_\vartheta \{\varphi_{n+1}(\eta, \kappa)\} &= \tilde{L}_\vartheta \{\varphi_n(\eta, \kappa)\} - \frac{1}{s^{2\vartheta}} \tilde{L}_\vartheta \left\{ \frac{\partial^{2\vartheta} \varphi_n}{\partial \kappa^{2\vartheta}} + \frac{\partial^{2\vartheta} \varphi_n}{\partial \eta^{2\vartheta}} \right\} \\
 &= \tilde{L}_\vartheta \{\varphi_n(\eta, \kappa)\} - \frac{1}{s^{2\vartheta}} \left[s^{2\vartheta} \tilde{L}_\vartheta \{\varphi_n(\eta, \kappa)\} - s^\vartheta \varphi_n(\eta, 0) - \varphi_n^{(\vartheta)}(\eta, 0) \right] \\
 &\quad - \frac{1}{s^{2\vartheta}} \tilde{L}_\vartheta \left\{ \frac{\partial^{2\vartheta} \varphi_n(\eta, \kappa)}{\partial \eta^{2\vartheta}} \right\} \\
 &= \frac{1}{s^\vartheta} \varphi_n(\eta, 0) + \frac{1}{s^{2\vartheta}} \varphi_n^{(\vartheta)}(\eta, 0) - \frac{1}{s^{2\vartheta}} \tilde{L}_\vartheta \left\{ \frac{\partial^{2\vartheta} \varphi_n(\eta, \kappa)}{\partial \eta^{2\vartheta}} \right\}. \tag{28}
 \end{aligned}$$

From (23), the initial value reads

$$\varphi_0(\eta, \kappa) = -E_\vartheta(\eta^\vartheta). \tag{29}$$

Hence, we get the first approximation, namely,

$$\begin{aligned}
 \tilde{L}_\vartheta \{\varphi_1(\eta, \kappa)\} &= \frac{1}{s^\vartheta} \varphi_0(\eta, 0) + \frac{1}{s^{2\vartheta}} \varphi_0^{(\vartheta)}(\eta, 0) - \frac{1}{s^{2\vartheta}} \tilde{L}_\vartheta \left\{ \frac{\partial^{2\vartheta} \varphi_0(\eta, \kappa)}{\partial \eta^{2\vartheta}} \right\} \\
 &= -\frac{1}{s^\vartheta} E_\vartheta(\eta^\vartheta) + \frac{1}{s^{3\vartheta}} E_\vartheta(\eta^\vartheta). \tag{30}
 \end{aligned}$$

The second approximation reads

$$\begin{aligned}
 \tilde{L}_\vartheta \{\varphi_2(\eta, \kappa)\} &= \frac{1}{s^\vartheta} \varphi_1(\eta, 0) + \frac{1}{s^{2\vartheta}} \varphi_1^{(\vartheta)}(\eta, 0) - \frac{1}{s^{2\vartheta}} \tilde{L}_\vartheta \left\{ \frac{\partial^{2\vartheta} \varphi_1(\eta, \kappa)}{\partial \eta^{2\vartheta}} \right\} \\
 &= -\frac{1}{s^\vartheta} E_\vartheta(\eta^\vartheta) + \frac{1}{s^{3\vartheta}} E_\vartheta(\eta^\vartheta) - \frac{1}{s^{5\vartheta}} E_\vartheta(\eta^\vartheta). \tag{31}
 \end{aligned}$$

The other approximations are written as

$$\begin{aligned}
 \tilde{L}_\vartheta \{\varphi_3(\eta, \kappa)\} &= \frac{1}{s^\vartheta} \varphi_2(\eta, 0) + \frac{1}{s^{2\vartheta}} \varphi_2^{(\vartheta)}(\eta, 0) - \frac{1}{s^{2\vartheta}} \tilde{L}_\vartheta \left\{ \frac{\partial^{2\vartheta} \varphi_2(\eta, \kappa)}{\partial \eta^{2\vartheta}} \right\} \\
 &= -\frac{1}{s^\vartheta} E_\vartheta(\eta^\vartheta) + \frac{1}{s^{3\vartheta}} E_\vartheta(\eta^\vartheta) - \frac{1}{s^{5\vartheta}} E_\vartheta(\eta^\vartheta) + \frac{1}{s^{7\vartheta}} E_\vartheta(\eta^\vartheta). \tag{32}
 \end{aligned}$$

Proceeding in this manner, we can derive the following formula:

$$\begin{aligned}
 \tilde{L}_\vartheta \{\varphi_n(\eta, \kappa)\} &= \frac{1}{s^\vartheta} \varphi_{n-1}(\eta, 0) + \frac{1}{s^{2\vartheta}} \varphi_{n-1}^{(\vartheta)}(\eta, 0) - \frac{1}{s^{2\vartheta}} \tilde{L}_\vartheta \left\{ \frac{\partial^{2\vartheta} \varphi_{n-1}(\eta, \kappa)}{\partial \eta^{2\vartheta}} \right\} \\
 &= \sum_{r=0}^n (-1)^{r+1} \frac{1}{s^{(2r+1)\vartheta}} E_\vartheta(\eta^\vartheta). \tag{33}
 \end{aligned}$$

Consequently, the LF series solution is

$$\begin{aligned}
 \varphi(\eta, \kappa) &= \lim_{n \rightarrow \infty} \tilde{L}_\vartheta^{-1} \left(\tilde{L}_\vartheta \{\varphi_n(\eta, \kappa)\} \right) = \tilde{L}_\vartheta^{-1} \left[\sum_{r=0}^{\infty} (-1)^{r+1} \frac{1}{s^{(2r+1)\vartheta}} E_\vartheta(\eta^\vartheta) \right] \\
 &= -E_\vartheta(\eta^\vartheta) \left[\sum_{r=0}^{\infty} (-1)^r \frac{\kappa^{2r\vartheta}}{\Gamma(1+2r\vartheta)} \right] = -E_\vartheta(\eta^\vartheta) \cos_\vartheta(\kappa^\vartheta), \tag{34}
 \end{aligned}$$

from Eqs. (27) and (34), the approximate solution of the Laplace equation (22) by using the LFLVIM is the same result as that obtained by the LFDTM and it clearly appears that the approximate solution remains closed form to the exact solution.

5 Conclusions

In this work, the LFDTM and LFLVIM have been successfully applied to finding the approximate analytical solutions for the Laplace equation with LFDOs. The solutions obtained by the proposed methods are an infinite power series for the appropriate initial condition, which can, in turn, be expressed in a closed form to the exact solution. The example shows that the results of the LFDTM are in excellent agreement with the results given by the LFLVIM and local fractional function decomposition method.

References

- [1] H. K. Jassim, C. Unlu, S. P. Moshokoa and C. M. Khalique. Local Fractional Laplace Variational Iteration Method for Solving Diffusion and Wave Equations on Cantor Sets within Local Fractional Operators. *Mathematical Problems in Engineering*. **2015** Article ID 309870 (2015) 1–9.
- [2] H. Jafari and H. K. Jassim, A Coupling Method of Local Fractional Variational Iteration Method and Yang-Laplace Transform for Solving Laplace Equation on Cantor Sets. *International Journal of pure and Applied Sciences and Technology*. **26** (2015) 24–33.
- [3] C. F. Liu, S. S. Kong and J. Zhao. Local Fractional LVIM for Fractal Vehicular Traffic Flow. *Advance in Mathematical Physics*. **2014** Article ID 649318 (2014) 1–7.
- [4] Y. Li, L. F. Wang and S. J. Yuan. Reconstructive schemes for VIM within Yang-Laplace transform with application to fractal heat conduction problem. *Thermal Science*. **17** (2013) 715–721.
- [5] H. Jafari and A. Azad, A computational Method for Solving a System of Volterra Integro-differential Equations. *Nonlinear Dynamics and Systems Theory* **12** (4) (2012) 389–396.
- [6] H. Jafari and M. Azadi. Lie Symmetry Reductions of a Coupled KdV System of Fractional Order. *Nonlinear Dynamics and Systems Theory* **18** (1) (2018) 22–28.
- [7] H. Jafari, H. K. Jassim, F. Tchier and D. Baleanu. On the Approximate Solutions of Local Fractional Differential Equations with Local Fractional Operator. *Entropy*. **18** (2016) 1–12.
- [8] X. J. Yang, J. A. Tenreiro Machado and H. M. Srivastava. A new numerical technique for solving the local fractional diffusion equation: Two dimensional extended differential transform approach. *Applied Mathematics and Computation*. **274** (2016) 143–151.
- [9] S. P. Yan, H. Jafari, and H. K. Jassim. Local Fractional Adomian Decomposition and Function Decomposition Methods for Solving Laplace Equation within Local Fractional Operators. *Advances in Mathematical Physics*. **2014** Article ID 161580 (2014) 1–7.
- [10] Z. P. Fan, H. K. Jassim, R. K. Rainna and X. J. Yang. Adomian Decomposition Method for Three-Dimensional Diffusion Model in Fractal Heat Transfer Involving Local Fractional Derivatives. *Thermal Science*. **19** (2015) S137–S141.
- [11] H. Jafari and H. K. Jassim. Application of the Local fractional Adomian Decomposition and Series Expansion Methods for Solving Telegraph Equation on Cantor Sets Involving Local Fractional Derivative Operators. *Journal of Zankoy Sulaimani-Part A*. **17** (2015) 15–22.
- [12] H. K. Jassim and D. Baleanu. A novel approach for Korteweg-de Vries equation of fractional order. *International Journal of Mathematics and Computer Research*. **5** (2019) 192–198.
- [13] Y. J. Yang, D. Baleanu and X. J. Yang. A Local Fractional Variational Iteration Method for Laplace Equation with LFDOs. *Abstract and Applied Analysis*. **2014** Article ID 202650 (2014) 1–6.

- [14] Y. Wang, Z. Y. Feng and L. Z. Jiang. An Explanation of Local Fractional Variational Iteration Method and Its Application to local fractional modified Korteweg-de Vries equation. *Thermal science*. **22** (2018) 23–27.
- [15] S. Xu, X. Ling, Y. Zhao, H. K. Jassim. A Novel Schedule for Solving the Two-Dimensional Diffusion in Fractal Heat Transfer. *Thermal Science*. **19** (2015) 99–103.
- [16] H. K. Jassim. On Approximate Methods for Fractal Vehicular Traffic Flow. *TWMS Journal of Applied and Engineering Mathematics*. **7** (2017) 58–65.
- [17] H. Jafari and H. K. Jassim and J. Vahidi. Reduced Differential Transform and Variational Iteration Methods for 3D Diffusion Model in Fractal Heat Transfer within Local Fractional Operators. *Thermal Science*. **22** (2018) S301–S307.
- [18] D. Ziane. Local Fractional Sumudu Variational Iteration Method for solving PDEs with local fractional derivative. *Int. J. Open Problems Compt. Math.* **10** (2017) 29–42.



Solution to the Critical Burgers Equation for Small Data in a Bounded Domain

M. B. Kania*

Institute of Mathematics, University of Silesia in Katowice, Bankowa 14, 40-007 Katowice, Poland

Received: March 23, 2020; Revised: September 24, 2020

Abstract: Solvability of Dirichlet’s problem for the subcritical fractional Burgers equation is discussed here in the base spaces $D((-\Delta)^{\frac{s}{2}})$, $s \geq 0$ fixed. A unique solution in the *critical case* ($\alpha = \frac{1}{2}$) for small data is obtained next as a limit of the $X^{\frac{1}{2\alpha}}$ solutions to the subcritical equations, when the exponent α of $(-\Delta)^\alpha$ tends to $\frac{1}{2}^+$.

Keywords: *fractional Burgers equation; global solvability; critical equation.*

Mathematics Subject Classification (2010): 35S11.

1 Introduction

We consider the Dirichlet boundary value problem for the fractional Burgers equation in a bounded interval $I \subset \mathbb{R}$

$$\begin{aligned} u_t + \frac{1}{2}\nabla u^2 + (-\Delta)^\alpha u &= 0, \quad x \in I \subset \mathbb{R}, t > 0, \\ u &= 0 \text{ on } \partial I, \\ u(0, x) &= u_0(x), \end{aligned} \tag{1}$$

where $\alpha \in [\frac{1}{2}, 1]$ is a fractional exponent.

In our work we use the following Balakrishnan’s definition of the fractional Laplacian (see [14]):

$$(-\Delta)^\beta g = \frac{\sin(\beta\pi)}{\pi} \int_0^\infty s^{\beta-1} (sI - \Delta)^{-1} (-\Delta)g ds, \quad g \in D(-\Delta), \quad \beta \in (0, 1).$$

* Corresponding author: <mailto:maria.kania@us.edu.pl>

Equivalence between the semigroup definition, Balakrishnan's formula and Bochner's formula is a general result, see [14]. The above definition can be used to study problems both in the case of a bounded and unbounded domain.

Over the last three decades a number of papers devoted to the Burgers equation with fractional dissipation in \mathbb{R} have been published (see [2, 3, 11, 12, 15]). In paper [12], Kiselev, Nazarov and Shterenberg have conducted an extensive study for the 1-dimensional Burgers equation in the periodic setting, which concerned the subcritical cases $\frac{1}{2} < \alpha < 1$, the critical case $\alpha = \frac{1}{2}$, as well as the supercritical cases $0 < \alpha < \frac{1}{2}$. Karch, Miao and Xu investigated the asymptotics for the subcritical case in [11] whereas Alibaud, Imbert and Karch studied the asymptotics for the critical as well as supercritical case in [2]. In paper [15], the authors made use of the modulus of the continuity method and Fourier localization technique to prove the global well-posedness of the critical Burgers equation in critical Besov spaces $\dot{B}_{p,1}^{\frac{1}{p}}(\mathbb{R})$ with $p \in [1, \infty)$.

The global in time solvability of one-dimensional subcritical Burgers equation in bounded domain was studied recently in [10] in two base spaces $L^2(I)$ and $D((-\Delta)^{\frac{s}{2}})$ with $s > \frac{1}{2}$. Moreover, it was shown there that the solutions to subcritical problems (1) converge to the solution (not necessarily unique) of the critical problem when $\alpha \rightarrow \frac{1}{2}^+$.

1.1 Description of the results

This paper is devoted to the global in time solvability and properties of solutions to problem (1) for $\alpha \in [\frac{1}{2}, 1]$ in a bounded domain I . Our aim is to include, in the subcritical case of exponent $\alpha \in (\frac{1}{2}, 1]$, the problem of interest in the framework of semilinear parabolic equations with a sectorial positive operator (see [5, 9]). This offers a simple but formalized proof of local solvability as well as the regularity of solutions. There are different possible choices of the phase spaces for this problem. We choose $D((-\Delta)^{\frac{s}{2}})$ with $s > 0$ as the *base spaces* (in which the equation is fulfilled). The second section of the paper is devoted to the local and then the global in time solvability of the subcritical Burgers equation. Moreover, for small data we obtain a *uniform in $\alpha \in (\frac{1}{2}, 1]$* estimate of the solutions u_α in $L^\infty(0, T; D((-\Delta)^{\frac{1}{2}}))$ and $L^2(0, T; D((-\Delta)^{\frac{3}{4}}))$, where $T > 0$ is fixed but arbitrarily large. In Section 3, we show that for the small data the solutions to subcritical problems (1) converge to the unique solution of the critical problem when $\alpha \rightarrow \frac{1}{2}^+$. It is a consequence of the well known compactness theorems. In this study, we use a technique proposed in our recent publications [6–8, 10].

Notation. Standard notation for Sobolev spaces is used. We indicate the dependence of solution u of (1) on $\alpha \in (\frac{1}{2}, 1]$, calling it u_α . Let r^- denote a number strictly less than r but arbitrarily close to it.

2 Solvability of Subcritical Problem (1), $\alpha \in (\frac{1}{2}, 1]$

Formulation of the problem and its local solvability. Our first task is the local in time solvability of the subcritical problem (1) for $\alpha \in (\frac{1}{2}, 1]$. We will use the standard approach proposed by Dan Henry [9] for semilinear 'parabolic' equations. We start from recalling some useful facts concerning Henry's approach. So, when we have the abstract Cauchy problem

$$\begin{cases} u_t + Au = F(u), & t > 0, \\ u(0) = u_0, \end{cases} \quad (2)$$

where

1. X is a Banach space. The space X is called the *base space*, that is, the space in which the equation is fulfilled,
2. $A: D(A) \rightarrow X$ is a sectorial positive operator in X ,
3. $F: X^\gamma \rightarrow X$ is Lipschitz continuous on the bounded subset of X^γ for some non-negative $\gamma \in [0, 1)$,
4. $u(0) = u_0 \in X^\gamma$,

then by local X^γ solution of this problem we understood the function u , which satisfies the following conditions.

Definition 2.1 The function u is called a local X^γ solution of (2) if, for some real $\tau > 0$, it satisfies

- $u(0) = u_0$,
- $u \in C([0, \tau); X^\gamma)$,
- $u \in C^1((0, \tau); X)$,
- $u(t)$ belongs to $D(A)$ for each $t \in (0, \tau)$,
- the equation $u_t + Au = F(u)$ holds in X for all $t \in (0, \tau)$.

The following theorem concerns the local X^γ solution of the abstract problem (2).

Theorem 2.1 Let X be a Banach space, $A: D(A) \rightarrow X$ be a sectorial positive operator in X and $F: X^\alpha \rightarrow X$ be Lipschitz continuous on the bounded subset of X^α for some non-negative $\alpha \in [0, 1)$. Then for each $u(0) = u_0 \in X^\alpha$, there exists a unique local X^α solution $u = u(t, u_0)$ of (2) defined on its maximal interval of existence $[0, \tau_{u_0})$.

Now we use Henry’s approach to our problem. There are different possible choices of the base space. We choose $X = D((-\Delta)^{\frac{s}{2}}) \subset H^s(I)$, where $s \geq 0$ is fixed, as the base space. The operator $A_\alpha := (-\Delta)^\alpha$ acting in the Banach space X is equipped with the domain $D(A_\alpha) \subset H^{s+2\alpha}(I)$. The resulting phase space is $X^{\frac{1}{2\alpha}} = [X, D(A_\alpha)]_{\frac{1}{2\alpha}} = D((-\Delta)^{\frac{s+1}{2}}) \subset H^{s+1}(I)$ (since $(A_\alpha)^{\frac{1}{2\alpha}} = (-\Delta)^{\frac{1}{2}}$). Moreover, when Ω is a domain in \mathbb{R}^N , then $W^{m,r}(\Omega)$ is the Banach algebra provided $mr > N$ (see [1, p. 115]). Note that in our case, $H^{s+1}(I)$ is a *Banach algebra*.

Working with the *sectorial positive operator* $A_\alpha : D(A_\alpha) \rightarrow X$, $\alpha \in (\frac{1}{2}, 1]$, in I with the zero boundary condition (e.g. [5, 9]), we rewrite equation (1) in an abstract form:

$$\begin{aligned} (u_\alpha)_t + A_\alpha u_\alpha &= F(u_\alpha), \quad t > 0, \\ u_\alpha(0, x) &= u_0(x), \end{aligned} \tag{3}$$

where

$$F(u_\alpha) = -\frac{1}{2} \nabla u_\alpha^2 \tag{4}$$

is the Nemytskii operator corresponding to a nonlinear term $-\frac{1}{2} \nabla u_\alpha^2$. The following local existence result holds.

Theorem 2.2 *Let $s \geq 0$ be fixed and $\alpha \in (\frac{1}{2}, 1]$. Then for arbitrary $u_0 \in X^{\frac{1}{2\alpha}} = D((-\Delta)^{\frac{s+1}{2}})$, there exists a unique local in time $X^{\frac{1}{2\alpha}}$ solution $u_\alpha(t)$ to the subcritical problem (3) defined on its maximal interval of existence $[0, \tau_{u_0})$. Moreover,*

$$u_\alpha \in C((0, \tau_{u_0}); X^1) \cap C([0, \tau_{u_0}); X^{\frac{1}{2\alpha}}), \quad (u_\alpha)_t \in C((0, \tau_{u_0}); X^\gamma),$$

with arbitrary $\gamma < 1$, $(X^1 = D(A_\alpha) \subset H^{s+2\alpha}(I))$.

Proof. To guarantee the local solvability we need to check if the nonlinearity (4) is Lipschitz continuous on bounded sets as a map from $X^{\frac{1}{2\alpha}}$ into X (see Theorem 2.1; [5], p. 55 for more details), that is, for any $r > 0$ there exists $L(r) > 0$ such that

$$\|F(v) - F(w)\|_X \leq L(r)\|v - w\|_{X^{\frac{1}{2\alpha}}}$$

for all $v, w \in B(r)$, where $B(r)$ denotes an open ball in $X^{\frac{1}{2\alpha}}$ centered at zero of radius r . Since $H^{s+1}(I)$ is the Banach algebra, for $v, w \in B(r)$, we get

$$\begin{aligned} \|F(v) - F(w)\|_{H^s(I)} &= \frac{1}{2} \|\nabla(v^2 - w^2)\|_{H^s(I)} \leq c\|v^2 - w^2\|_{H^{s+1}(I)} \\ &\leq \|v + w\|_{H^{s+1}(I)}\|v - w\|_{H^{s+1}(I)}. \end{aligned}$$

Consequently, we obtain

$$\|F(v) - F(w)\|_{H^s(I)} \leq c'(\|v\|_{H^{s+1}(I)}, \|w\|_{H^{s+1}(I)})\|v - w\|_{H^{s+1}(I)},$$

which proves the local solvability of (1) in the phase space $X^{\frac{1}{2\alpha}}$.

Remark 2.1 The local solution constructed above fulfills Cauchy’s integral formula (see [5, Lemma 2.2.1]):

$$u_\alpha(t) = e^{-A_\alpha t}u_0 + \int_0^t e^{-A_\alpha(t-s)}F(u_\alpha(s))ds, \quad t \in [0, \tau_{u_0}),$$

where $e^{-A_\alpha t}$ denotes the linear semigroup corresponding to the operator $A_\alpha := (-\Delta)^\alpha$ in $D((-\Delta)^{\frac{s}{2}})$ and $F(u_\alpha) = -\frac{1}{2}\nabla u_\alpha^2$.

Remark 2.2 Note that since the function F is Lipschitz continuous on bounded subsets of $X^{\frac{1}{2\alpha}}$, as a consequence of the embeddings between the fractional power space, it possesses this property as a map from X^β to X for each $\beta \in [\frac{1}{2\alpha}, 1)$. Consequently, for each $\beta \in [\frac{1}{2\alpha}, 1)$ and $u_0 \in X^\beta$, there exists a unique local in time X^β solution to the subcritical problem (3) defined on its maximal interval of existence.

Remark 2.3 Let $\epsilon = 2\alpha - 1 > 0$ and $t_0 > 0$ be chosen arbitrarily close to 0. From Theorem 2.2, we know that $u_\alpha(t_0, \cdot) \in D((-\Delta)^{\frac{s}{2}+\alpha}) \subset H^{s+2\alpha}(I)$. Since ∂I is regular, considering the equation (3) in the base space $D((-\Delta)^{\frac{s+\epsilon}{2}})$ with a new initial condition $u_\alpha(t_0, x) = (u_\alpha)_{t_0}(x)$, we obtain that $u_\alpha(t, \cdot)$ varies continuously in $D((-\Delta)^{\frac{s+\epsilon}{2}+\alpha})$ for $t > t_0$. Next, repeating this procedure n times with $t_n = \sum_{i=0}^n \frac{t_0}{2^i}$ and the base space $D((-\Delta)^{\frac{s+(n+1)\epsilon}{2}})$, we get additional regularity of the solution of (3), that is, $u_\alpha(t, \cdot) \in D((-\Delta)^{\frac{s+(n+1)\epsilon}{2}+\alpha}) \subset H^{s+(n+1)\epsilon+2\alpha}(I)$ for $t > t_n = t_0(2 - \frac{1}{2^n})$. This phenomenon is known in the literature as bootstrapping.

Global solvability. Having obtained the local in time solution of (1), to guarantee its global extensibility we need suitable *a priori estimates*. We start from the Maximum Principle.

Lemma 2.1 *Let $k \in \mathbb{N}$. Then, for a sufficiently regular solution u_α of (1), the following estimates hold:*

$$\|u_\alpha(t, \cdot)\|_{L^{2^k}(I)} \leq \|u_0\|_{L^{2^k}(I)}, \tag{5}$$

$$\|u_\alpha(t, \cdot)\|_{L^{2^k}(I)} \leq \|u_0\|_{L^{2^k}(I)} e^{-2^{1-k}\lambda_1^\alpha t}, \tag{6}$$

where λ_1 is the Poincaré constant (see [7])

$$\lambda_1^\alpha \|\phi\|_{L^2(I)}^2 \leq \|(-\Delta)^{\frac{\alpha}{2}} \phi\|_{L^2(I)}^2. \tag{7}$$

Proof. Multiplying (1) by $u_\alpha^{2^k-1}$, $k = 1, 2, \dots$, we get

$$\frac{1}{2^k} \frac{d}{dt} \int_I u_\alpha^{2^k} dx + \int_I (-\Delta)^\alpha u_\alpha |u_\alpha|^{2^k-1} \operatorname{sgn} u_\alpha dx + \int_I (u_\alpha)_x u_\alpha^{2^k} dx = 0.$$

Using the Kato-Beurling-Deny inequality in the bounded domain [7, Corollary 3.2] with $q = 2^k$, we have

$$\frac{2^k - 1}{2^{2k-2}} \int_I [(-\Delta)^{\frac{\alpha}{2}} (|u_\alpha|^{2^k-1})]^2 dx \leq \int_I [(-\Delta)^\alpha u_\alpha |u_\alpha|^{2^k-1} \operatorname{sgn} u_\alpha dx. \tag{8}$$

Since

$$\int_I (u_\alpha)_x u_\alpha^{2^k} dx = \frac{1}{2^k + 1} \int_I (u_\alpha^{2^k+1})_x dx = 0,$$

and $2 \leq \frac{2^k-1}{2^{k-2}}$, thanks to (8) and (7), we obtain

$$\frac{d}{dt} \int_I u_\alpha^{2^k} dx \leq \frac{d}{dt} \int_I u_\alpha^{2^k} dx + 2\lambda_1^\alpha \int_I |u_\alpha|^{2^k} dx \leq 0,$$

which leads to estimates (5) and (6).

Remark 2.4 Let $q \in \mathbb{N}$. Since $u_\alpha(t) \in L^\infty(I)$, the following convergence holds:

$$\lim_{q \rightarrow \infty} \|u_\alpha(t, \cdot)\|_{L^q(I)} = \|u_\alpha(t, \cdot)\|_{L^\infty(I)}$$

(see [1, Theorem 2.8]). Consequently, letting $k \rightarrow +\infty$ in estimate (5), we obtain

$$\|u_\alpha(t, \cdot)\|_{L^\infty(I)} \leq \|u_0\|_{L^\infty(I)}. \tag{9}$$

Remark 2.5 The constant $\lambda_1^{\alpha-\frac{1}{2}}$ can be estimated independently of $\alpha \in (\frac{1}{2}, 1]$. We have

$$\mu_b := \min\{1, \lambda_1^{\frac{1}{2}}\} \leq \lambda_1^{\alpha-\frac{1}{2}} \leq \max\{1, \lambda_1^{\frac{1}{2}}\} =: \mu_a. \tag{10}$$

Remark 2.6 Multiplying (1) by u_α , due to (7) and Remark 2.5, we obtain a differential inequality of the form

$$0 = \frac{d}{dt} \|u_\alpha\|_{L^2(I)}^2 + 2\|(-\Delta)^{\frac{\alpha-\frac{1}{2}}{2}} (-\Delta)^{\frac{1}{4}} u_\alpha\|_{L^2(I)}^2 \geq \frac{d}{dt} \|u_\alpha\|_{L^2(I)}^2 + 2\mu_b \|(-\Delta)^{\frac{1}{4}} u_\alpha\|_{L^2(I)}^2. \tag{11}$$

Integrating (11) over $(0, T)$, we get

$$\int_0^T \|(-\Delta)^{\frac{1}{4}} u_\alpha\|_{L^2(I)}^2 ds = \frac{1}{2\mu_b} \left(\|u_0\|_{L^2(I)}^2 - \|u_\alpha(T)\|_{L^2(I)}^2 \right) \leq \frac{1}{2\mu_b} \|u_0\|_{L^2(I)}^2.$$

This implies a uniform in $\alpha \in (\frac{1}{2}, 1]$ estimate of u_α in $L^2(0, T; D((-\Delta)^{\frac{1}{4}}))$, where $T > 0$ is fixed but arbitrarily large.

The $L^p(I)$ a priori estimates obtained in Lemma 2.1 and Remark 2.4 are, unfortunately, too weak to guarantee the global in time solvability of (3) in $X^{\frac{1}{2\alpha}}$. For this purpose, we need to estimate higher Sobolev norms of the solutions to (3). We will show that $\|u_\alpha\|_{H^{s+1}(I)}$ is bounded on the solutions. Consequently, we will obtain Lipschitz continuity and boundedness of the nonlinear term F as a map from $X^{\frac{1}{2\alpha}}$ to X .

We will start from the $H^1(I)$ a priori estimate.

Lemma 2.2 *For a sufficiently regular solution u_α of (1), the following estimate holds:*

$$\|u_\alpha\|_{H^1(I)} \leq c(\|u_0\|_{H^1(I)}, \alpha). \quad (12)$$

Proof. Multiplying (1) by $-(u_\alpha)_{xx}$, we get

$$\frac{1}{2} \frac{d}{dt} \int_I ((u_\alpha)_x)^2 dx + \int_I [(-\Delta)^{\frac{1+\alpha}{2}} u_\alpha]^2 dx - \int_I u_\alpha (u_\alpha)_x (u_\alpha)_{xx} dx = 0.$$

Since

$$- \int_I u_\alpha (u_\alpha)_x (u_\alpha)_{xx} dx = \frac{1}{2} \int_I ((u_\alpha)_x)^3 dx,$$

we have

$$\frac{d}{dt} \int_I ((u_\alpha)_x)^2 dx + 2 \int_I [(-\Delta)^{\frac{1+\alpha}{2}} u_\alpha]^2 dx + \int_I ((u_\alpha)_x)^3 dx = 0. \quad (13)$$

Note that (see [10, p. 63])

$$\|u_\alpha\|_{W^{1,3}(I)}^3 \leq c(\alpha) \|u_\alpha\|_{H^{1+\alpha}(I)}^{3\theta} \|u_\alpha\|_{L^\infty(I)}^{3(1-\theta)} \quad (14)$$

with $\frac{4}{3(2\alpha+1)} \leq \theta < \frac{2}{3}$. Consequently, using the Young inequality, we get

$$\begin{aligned} \frac{d}{dt} \int_I ((u_\alpha)_x)^2 dx + c \int_I ((u_\alpha)_x)^2 dx &\leq \frac{d}{dt} \int_I ((u_\alpha)_x)^2 dx + \int_I [(-\Delta)^{\frac{1+\alpha}{2}} u_\alpha]^2 dx \\ &\leq c(\|u_\alpha\|_{L^\infty(I)}, \alpha), \end{aligned}$$

where an equivalent norm in $H^{1+\alpha}(I)$ is used.

Lemma 2.3 *For a sufficiently regular solution u_α of (1), which satisfies the smallest data condition (17), the following uniform in $\alpha \in (\frac{1}{2}, 1]$ estimate*

$$\|(u_\alpha)_x(t)\|_{L^2(I)} \leq \|u_0\|_{H^1(I)} e^{-(2\mu_b - C^3 \|u_0\|_{L^\infty(I)})t} \quad (15)$$

holds.

Proof. Note that, when the Nirenberg–Gagliardo inequality (and an equivalent norm in $H^{\frac{3}{2}}(I)$)

$$\|u_\alpha\|_{W^{1,3}(I)} \leq c \|u_\alpha\|_{L^\infty(I)}^{\frac{1}{3}} \|u_\alpha\|_{H^{\frac{3}{2}}(I)}^{\frac{2}{3}} \leq C \|u_\alpha\|_{L^\infty(I)} \|(-\Delta)^{\frac{3}{4}} u_\alpha\|_{L^2(I)}^{\frac{2}{3}}$$

is used instead of (14), thanks to the Poincaré inequality (7) and (9), due to Remark 2.5, the estimate (13) extends to

$$\frac{d}{dt} \int_I ((u_\alpha)_x)^2 dx + (2\mu_b - C^3 \|u_0\|_{L^\infty(I)}) \int_I [(-\Delta)^{\frac{3}{4}} u_\alpha]^2 dx \leq 0. \tag{16}$$

Consequently, when the data are small

$$\|u_0\|_{L^\infty(I)} < \frac{2\mu_b}{C^3} \tag{17}$$

we obtain the thesis.

Remark 2.7 Under the assumption (17) the estimate (16) implies a uniform in $\alpha \in (\frac{1}{2}, 1]$ estimate of u_α in $L^\infty(0, T; H_0^1(I))$ and $L^2(0, T; D((-\Delta)^{\frac{3}{4}}))$. So, we have

$$\|u_\alpha\|_{L^\infty(0,T;H_0^1(I))} + \|u_\alpha\|_{L^2(0,T;D((-\Delta)^{\frac{3}{4}}))} \leq \text{const}, \tag{18}$$

where $T > 0$ is fixed but arbitrarily large and the constant on the right-hand side is independent of α .

Lemma 2.4 For a sufficiently regular solution u_α of (1), the following estimate holds:

$$\|\Delta u_\alpha\|_{L^2(I)} \leq c(\|u_0\|_{H^2(I)}, \alpha). \tag{19}$$

Proof. Multiplying (1) by $(-\Delta)^2 u_\alpha$, we get

$$\frac{d}{dt} \|\Delta u_\alpha\|_{L^2(I)}^2 + 2 \|(-\Delta)^{\frac{2+\alpha}{2}} u_\alpha\|_{L^2(I)}^2 + 3 \int_I (\Delta u_\alpha)^2 \nabla u_\alpha dx = 0.$$

Using the Nirenberg–Gagliardo inequality

$$\|u\|_{W^{2,4}(I)}^2 \leq c \|u\|_{H^{\frac{5}{2}}(I)}^{\frac{5}{3}} \|u\|_{H^1(I)}^{\frac{1}{3}} \tag{20}$$

and the Young inequality, we can estimate the nonlinear term as follows:

$$\int_I |(\Delta u_\alpha)^2 \nabla u_\alpha| dx \leq \|\Delta u_\alpha\|_{L^4(I)}^2 \|\nabla u_\alpha\|_{L^2(I)} \leq \frac{\mu_b}{3} \|u_\alpha\|_{H^{\frac{5}{2}}(I)}^2 + c \|u_\alpha\|_{H^1(I)}^8.$$

Consequently, thanks to the Poincaré inequality (7), we get

$$\frac{d}{dt} \|\Delta u_\alpha\|_{L^2(I)}^2 + \mu_b \|(-\Delta)^{\frac{5}{4}} u_\alpha\|_{L^2(I)}^2 \leq c \|u_0\|_{H^1(I)}^8. \tag{21}$$

Remark 2.8 Since for the small data we have uniform in α estimate of solution u_α in $H^1(I)$, we get a uniform in $\alpha \in (\frac{1}{2}, 1]$ estimate

$$\|u_\alpha\|_{L^\infty(0,T;H^2(I))} + \|u_\alpha\|_{L^2(0,T;H^{\frac{5}{2}}(I))} \leq \text{const},$$

where $T > 0$ is fixed but arbitrarily large.

Further we get the $H^l(I)$ estimate of solutions by recurrence.

Lemma 2.5 *Let $l = \frac{k}{2}$, $k \geq 5$. Then, for a sufficiently regular solution of (1), the following estimate holds:*

$$\|u_\alpha\|_{H^l(I)} \leq c(\|u_0\|_{H^{l-\alpha}(I)}, \alpha). \tag{22}$$

Proof. Note first that by (12) we have $\|u_\alpha\|_{H^1(I)} \leq c(\|u_0\|_{H^1(I)}, \alpha)$. Multiplying (1) by $(-\Delta)^l u_\alpha$ we obtain

$$\frac{1}{2} \frac{d}{dt} \int_I [(-\Delta)^{\frac{l}{2}} u_\alpha]^2 dx + \int_I [(-\Delta)^{\frac{l+\alpha}{2}} u_\alpha]^2 dx = \int_I (-\Delta)^{\frac{l-\alpha}{2}} (u_\alpha(u_\alpha)_x) (-\Delta)^{\frac{l+\alpha}{2}} u_\alpha dx. \tag{23}$$

Since $H^{l-\alpha}(I)$ is a Banach algebra for $l - \alpha > \frac{1}{2}$, the nonlinear term can be estimated as follows:

$$\begin{aligned} \left| \int_I (-\Delta)^{\frac{l-\alpha}{2}} (u_\alpha(u_\alpha)_x) (-\Delta)^{\frac{l+\alpha}{2}} u_\alpha dx \right| &\leq c \|u_\alpha(u_\alpha)_x\|_{H^{l-\alpha}(I)} \|u_\alpha\|_{H^{l+\alpha}(I)} \\ &\leq c \|u_\alpha\|_{H^{l-\alpha}(I)} \|u_\alpha\|_{H^{l+1-\alpha}(I)} \|u_\alpha\|_{H^{l+\alpha}(I)}. \end{aligned}$$

By the Nirenberg-Gagliardo inequality, we get

$$\|u_\alpha\|_{H^{l+1-\alpha}(I)} \leq c \|u_\alpha\|_{H^{l+\alpha}(I)}^{\frac{1}{2\alpha}} \|u_\alpha\|_{H^{l-\alpha}(I)}^{1-\frac{1}{2\alpha}},$$

hence

$$\left| \int_I (-\Delta)^{\frac{l-\alpha}{2}} (u_\alpha(u_\alpha)_x) (-\Delta)^{\frac{l+\alpha}{2}} u_\alpha dx \right| \leq c \|u_\alpha\|_{H^{l+\alpha}(I)}^{1+\frac{1}{2\alpha}} \|u_\alpha\|_{H^{l-\alpha}(I)}^{2-\frac{1}{2\alpha}}.$$

Consequently, using the Young inequality, we obtain from (23) a differential inequality

$$\frac{d}{dt} \int_I [(-\Delta)^{\frac{l}{2}} u_\alpha]^2 dx + \int_I [(-\Delta)^{\frac{l+\alpha}{2}} u_\alpha]^2 dx \leq c(\|u_\alpha\|_{H^{l-\alpha}(I)}, \alpha).$$

The following global existence result holds.

Theorem 2.3 *The local solution u_α of (3) constructed in Theorem 2.2 exists globally in time.*

Lemma 2.6 *Let $\alpha \in (\frac{1}{2}, \frac{3}{4}]$. For solution u_α of (3) satisfying the smallest data restriction (17) we have a uniform with respect to α estimate*

$$\|(u_\alpha)_t\|_{L^2(0,T;L^2(I))} \leq C(T), \tag{24}$$

where $T > 0$ is fixed but arbitrarily large.

Proof. Since $H^1(I)$ is a Banach algebra from equation (1), thanks to the Poincaré inequality (7), we obtain for $\alpha \in (\frac{1}{2}, \frac{3}{4}]$

$$\|(u_\alpha)_t\|_{L^2(I)}^2 \leq 2\lambda_1^{\frac{4\alpha-3}{2}} \|(-\Delta)^{\frac{3}{4}} u_\alpha\|_{L^2(I)}^2 + c\|u_\alpha\|_{H^1(I)}^2 \leq 2\mu_b^{-1} \|(-\Delta)^{\frac{3}{4}} u_\alpha\|_{L^2(I)}^2 + c\|u_\alpha\|_{H^1(I)}^4.$$

Integrating the result over $(0, T)$, due to (18), we get

$$\int_0^T \|(u_\alpha)_t\|_{L^2(I)}^2 dt \leq c(T; \|u_0\|_{H^1(I)}), \tag{25}$$

with a positive constant c independent of α .

3 Critical Problem (1) with $\alpha = \frac{1}{2}$ for Small Data

Passing to the limit in equation (1). Using the Lions-Aubin compactness lemma we will show now that for the small data (the condition (17)) the solutions of subcritical problems (1) converge, as $\alpha \rightarrow \frac{1}{2}^+$, to the unique solution of the critical problem. The below lemma will be useful in the limiting procedure.

Lemma 3.1 *For any sequence $\alpha_n \rightarrow \frac{1}{2}$ such that $\{\alpha_n : n \in \mathbb{N}\} \subset (\frac{1}{2}, \frac{3}{4}]$ there are a subsequence (denoted in the same way) $\alpha_n \rightarrow \frac{1}{2}$ and a function u such that for any $T > 0$*

1. $u_{\alpha_n} \rightarrow u$ weakly in $L^2(0, T; D((-\Delta)^{\frac{3}{4}}))$ and weakly- $*$ in $L^\infty(0, T; D((-\Delta)^{\frac{1}{2}}))$,
2. $u_{\alpha_n} \rightarrow u$ in $L^2(0, T; D((-\Delta)^{\frac{3}{4}-}))$,
3. $(u_{\alpha_n})_t \rightarrow u_t$ weakly in $L^2(0, T; L^2(I))$.

Proof. Part (1). Note that uniform in α estimate (18) means that any sequence $\{u_{\alpha_n}\}$ is bounded in $L^2(0, T; D((-\Delta)^{\frac{3}{4}}))$. Consequently (see [4, Theorem 3.18]), there exist a subsequence (denoted in the same way) and $u \in L^2(0, T; D((-\Delta)^{\frac{3}{4}}))$ such that $\{u_{\alpha_n}\}$ converges to u weakly when $\alpha_n \rightarrow \frac{1}{2}$.

Part (2). Let

$$\mathbf{U} = \left\{ u_\alpha; \quad \alpha \in \left(\frac{1}{2}, \frac{3}{4} \right] \right\} \quad \text{and} \quad \frac{\partial \mathbf{U}}{\partial t} = \{(u_\alpha)_t : u_\alpha \in U\}. \tag{26}$$

Since the set \mathbf{U} is bounded in $L^2(0, T; D((-\Delta)^{\frac{3}{4}}))$ and $\frac{\partial \mathbf{U}}{\partial t}$ is bounded in $L^2(0, T; L^2(I))$ (see (18) and (24)), using the Lions-Aubin compactness lemma (see [13], [16, Corollary 4]) we claim that the set \mathbf{U} is relatively compact in the space $L^2(0, T; D((-\Delta)^{\frac{3}{4}-}))$. Consequently, for any sequence $\{u_{\alpha_n}\}$ there exist a subsequence (denoted in the same way) and $u \in L^2(0, T; D((-\Delta)^{\frac{3}{4}-}))$ such that $\{u_{\alpha_n}\}$ converges to u strongly.

Part(3) is a consequence of estimate (24) (see [4, Theorem 3.18]).

Remark 3.1 Since the set \mathbf{U} is bounded in $L^\infty(0, T; D((-\Delta)^{\frac{1}{2}}))$ and $\frac{\partial \mathbf{U}}{\partial t}$ is bounded in $L^2(0, T; L^2(I))$ (see (18) and (24)), using the Corollary 4 from [16] we claim that the set \mathbf{U} is also relatively compact in the space $C(0, T; D((-\Delta)^{\frac{1}{2}-}))$.

Theorem 3.1 *Let $\{\alpha_n : n \in \mathbb{N}\} \subset (\frac{1}{2}, \frac{3}{4}]$ and let u_α be the solution of the subcritical problem (1) (constructed in Theorem 2.3 in $D((-\Delta)^{\frac{3}{2}})$) corresponding to the initial*

condition $u_0 \in D((-\Delta)^{\frac{s+1}{2}})$ satisfying the smallest data restriction (17). Then, passing over a subsequence (denoted in the same way), with α_n to $\frac{1}{2}$ in equation (1), we get a weak solution u (not necessarily unique) to the critical problem ($\alpha = \frac{1}{2}$) satisfying a.e. in each time interval $[0, T]$ the equality

$$\frac{d}{dt} \langle u, \phi \rangle + \frac{1}{2} \langle \nabla u^2, \phi \rangle + \langle (-\Delta)^{\frac{1}{2}} u, \phi \rangle = 0,$$

for every function $\phi \in H_0^1(I)$, where $\langle \cdot, \cdot \rangle$ is a scalar product in $L^2(I)$ and $\frac{d}{dt}$ stands for the distributional derivative.

Proof. Multiplying equation (1) by a 'test function' $\phi \in H_0^1(I)$ (note, $H_0^1(I) \subset L^\infty(I)$, $N = 1$), we obtain

$$\int_I (u_\alpha)_t \phi \, dx + \int_I (-\Delta)^\alpha u_\alpha \phi \, dx = -\frac{1}{2} \int_I \nabla u_\alpha^2 \phi \, dx.$$

Next for each smooth scalar test function $\eta \in D((0, T))$, we get

$$\int_0^T \int_I (u_\alpha)_t \phi \, dx \, \eta \, dt + \int_0^T \int_I (-\Delta)^\alpha u_\alpha \phi \, dx \, \eta \, dt = -\frac{1}{2} \int_0^T \int_I \nabla u_\alpha^2 \phi \, dx \, \eta \, dt.$$

We will discuss now the convergence of components in the above equality one by one. In the term containing the time derivative $(u_\alpha)_t$, thanks to [18, Lemma 1.1, Chapt.III], we have

$$\int_0^T \langle (u_\alpha)_t, \phi \rangle \eta \, dt = \int_0^T \frac{d}{dt} \langle u_\alpha, \phi \rangle \eta \, dt = - \int_0^T \langle u_\alpha, \phi \rangle \eta' \, dt$$

for all $\phi \in H_0^1(I)$. Since

$$\begin{aligned} \int_0^T \int_I |u_\alpha - u| |\phi| |\eta'| \, dx \, dt &\leq \int_0^T \|u_\alpha - u\|_{L^2(I)} \|\phi\|_{L^2(I)} |\eta'| \, dt \\ &\leq \|u_\alpha - u\|_{L^2(0,T;L^2(I))} \|\phi\|_{L^2(I)} \|\eta'\|_{L^2(0,T)}, \end{aligned}$$

using part (2) of Lemma 3.1, we obtain

$$\int_0^T \langle u_\alpha, \phi \rangle \eta' \, dt \rightarrow \int_0^T \langle u, \phi \rangle \eta' \, dt.$$

For the linear term

$$\int_0^T \int_I (-\Delta)^\alpha u_\alpha \phi \, dx \, \eta \, dt = \int_0^T \int_I (-\Delta)^{\frac{1}{2}} u_\alpha (-\Delta)^{\alpha-\frac{1}{2}} \phi \, dx \, \eta \, dt \tag{27}$$

we get

$$\begin{aligned} &\left| \int_0^T \int_I (-\Delta)^{\frac{1}{2}} u_\alpha (-\Delta)^{\alpha-\frac{1}{2}} \phi \, dx \, \eta \, dt - \int_0^T \int_I (-\Delta)^{\frac{1}{2}} u \phi \, dx \, \eta \, dt \right| \\ &\leq \int_0^T \int_I \left| (-\Delta)^{\frac{1}{2}} u_\alpha \right| \left| \left((-\Delta)^{\alpha-\frac{1}{2}} - I \right) \phi \right| \, dx \, |\eta| \, dt \\ &+ \int_0^T \int_I |\phi| \left| (-\Delta)^{\frac{1}{2}} (u_\alpha - u) \right| \, dx \, |\eta| \, dt \\ &\leq \|u_\alpha\|_{L^2(0,T;D((-\Delta)^{\frac{1}{2}}))} \left\| \left((-\Delta)^{\alpha-\frac{1}{2}} - I \right) \phi \right\|_{L^2(I)} \|\eta\|_{L^2(0,T)} \\ &+ \|\phi\|_{L^2(I)} \|\eta\|_{L^2(0,T)} \|u_\alpha - u\|_{L^2(0,T;D((-\Delta)^{\frac{1}{2}}))}. \end{aligned} \tag{28}$$

Passing to the limit, by [14, Theorem 3.1.6] and part (2) of Lemma 3.1, we obtain the convergence

$$\int_0^T \int_I (-\Delta)^{\frac{1}{2}} u_\alpha (-\Delta)^{\alpha - \frac{1}{2}} \phi \, dx \, \eta \, dt \rightarrow \int_0^T \int_I (-\Delta)^{\frac{1}{2}} u \phi \, dx \, \eta \, dt. \tag{29}$$

Next, for the nonlinear term, since $H^1(I)$ is Banach algebra, we prove that

$$\begin{aligned} \left| \int_0^T \int_I \nabla u_\alpha^2 \phi \eta - \nabla u^2 \phi \eta \, dx \, dt \right| &\leq \int_0^T \|u_\alpha^2 - u^2\|_{H^1(I)} \|\phi\|_{L^2(I)} |\eta| \, dt \\ &\leq c \|u_\alpha - u\|_{L^2(0,T;D((-\Delta)^{\frac{1}{2}}))} \|u_\alpha + u\|_{L^\infty(0,T;D((-\Delta)^{\frac{1}{2}}))} \|\phi\|_{L^2(I)} \|\eta\|_{L^2(0,T)}. \end{aligned}$$

By collecting all the limits together, we find the form of the limit *critical equation*

$$\int_0^T \frac{d}{dt} \langle u, \phi \rangle \eta \, dt + \frac{1}{2} \int_0^T \langle \nabla u^2, \phi \rangle \eta \, dt + \int_0^T \langle (-\Delta)^{\frac{1}{2}} u, \phi \rangle \eta \, dt = 0.$$

Properties of the weak solutions to the critical fractional Burgers equation.

We will start from collecting the properties inherited by the solution u of the critical problem(1) in the process of passing to the limit. We have the following results

Corollary 3.1 *For arbitrary $T > 0$ we have*

- $u \in L^2(0, T; D((-\Delta)^{\frac{3}{4}})) \cap L^\infty(0, T; D((-\Delta)^{\frac{1}{2}})),$
- $u_t \in L^2(0, T; L^2(I)),$
- $u \in C_w(0, T; D((-\Delta)^{\frac{1}{2}})).$

Proof. Using the properties of the weak limit, due to Lemma 3.1 (1) and (3), we obtain the first two regularities. Next, the Corollary 2.1 from [17] implies that there exists a weakly continuous function on $[0, T]$ with the values in $D((-\Delta)^{\frac{1}{2}})$ which is equal to u almost everywhere.

We will show now that the local solutions of the critical fractional Burgers equation obtained in Theorem 3.1, are locally unique.

Lemma 3.2 *The solution of the critical fractional Burgers equation satisfying*

$$u \in L^\infty([0, \tau); H^1(I))$$

is locally unique.

Proof. Let $U = u_1 - u_2$, where u_1 and u_2 are the local in time solutions of the critical problem (1) (in the above class) corresponding to the same initial condition u_0 . Then U satisfies

$$\begin{aligned} U_t + u_1 \nabla U + \nabla u_2 U + (-\Delta)^{\frac{1}{2}} U &= 0, \quad x \in I \subset \mathbb{R}, t > 0, \\ U &= 0 \text{ on } \partial I, \\ U(0, x) &= 0. \end{aligned}$$

Multiplying the above equation in $L^2(I)$ by U , thanks to the integration by parts, we obtain

$$\frac{d}{dt} \int_I U^2 \, dx + \int_I \nabla u_2 U^2 \, dx + 2 \int_I \left[(-\Delta)^{\frac{1}{4}} U \right]^2 \, dx = 0.$$

From the Hölder and the Nirenberg-Gagliardo inequality the nonlinear term can be transformed as follows:

$$\int_I \nabla u_2 U^2 dx \leq \|\nabla u_2\|_{L^2(I)} \|U\|_{L^4(I)}^2 \leq \|\nabla u_2\|_{L^2(I)} \|U\|_{L^2(I)} \|U\|_{H^{\frac{1}{2}}(I)}.$$

Since $\|u_2\|_{H^1(I)}$ is bounded, using the Cauchy inequality, we get a differential inequality of the form

$$\begin{aligned} \frac{d}{dt} \|U(t, \cdot)\|_{L^2(I)}^2 &\leq c(\|u_2\|_{H^1(I)}) \|U(t, \cdot)\|_{L^2(I)}^2, \\ U(0, x) &= 0, \end{aligned}$$

having only a zero solution on $[0, \tau)$.

Theorem 3.2 *The solution of the critical fractional Burgers equation obtained in Theorem 3.1, is unique.*

4 Conclusion

This paper is devoted to the global in time solvability and properties of solutions to the critical problem (1) ($\alpha = \frac{1}{2}$) in a bounded domain I . For this purpose we constructed first the local and then the global in time $X^{\frac{1}{2\alpha}}$ solution u_α of the subcritical fractional Burgers equation ($\alpha \in (\frac{1}{2}, 1]$) in the base spaces $D((-\Delta)^{\frac{s}{2}})$, $s \geq 0$ fixed. Moreover, for small data we obtained a *uniform in $\alpha \in (\frac{1}{2}, 1]$* estimate of the solutions u_α in $L^\infty(0, T; D((-\Delta)^{\frac{1}{2}}))$ and $L^2(0, T; D((-\Delta)^{\frac{3}{4}}))$, where $T > 0$ is fixed but arbitrarily large. Using the Lions-Aubin compactness lemma, thanks to the above uniform in α estimates, we showed that, for the small data (the condition (17)), the solutions of subcritical problems (1) converge, as $\alpha \rightarrow \frac{1}{2}^+$, to the unique solution of the critical problem. For any data, the uniqueness of the solution to the critical problem (1) is an open problem.

References

- [1] R.A. Adams. *Sobolev Spaces*. Academic Press, New York, 1975.
- [2] N. Alibaud, C. Imbert and G. Karch. Asymptotic Properties of Entropy Solutions to Fractal Burgers Equation. *SIAM Journal on Mathematical Analysis* **42** (1) (2010) 354–376.
- [3] P. Biler, T. Funaki and W. Woyczynski. Fractal Burgers Equations. *J. Differential Equ.* **148** (1998) 9–46.
- [4] H. Brezis. *Functional Analysis, Sobolev Spaces and Partial Differential Equations*. Springer, New York, 2011.
- [5] J.W. Cholewa and T. Dlotko. *Global Attractors in Abstract Parabolic Problems*. Cambridge University Press, Cambridge, 2000.
- [6] T. Dlotko M.B. Kania and C. Sun. Pseudodifferential parabolic equations in uniform spaces. *Applicable Anal.* **93** (2014) 14–34.
- [7] T. Dlotko M.B. Kania and C. Sun. Pseudodifferential parabolic equations; two examples. *Topol. Methods Nonlinear Anal.* **43** (2014) 463–492.
- [8] T. Dlotko M.B. Kania and C. Sun. Quasi-geostrophic equation in \mathbb{R}^2 . *J. Differential Equ.* **259** (2015) 531–561.

- [9] D. Henry. *Geometric Theory of Semilinear Parabolic Equations*. Springer-Verlag, Berlin, 1981.
- [10] M.B. Kania. Fractional Burgers equation in a bounded domain. *Colloquium Mathematicum* **151** (2018) 57–70,
- [11] G. Karch, C. Miao and X. Xu. On convergence of solutions of fractal Burgers equation toward rarefaction waves. *SIAM Journal on Mathematical Analysis* **39** (5) (2008) 1536–1549.
- [12] A. Kiselev, F. Nazarov and R. Shterenberg. Blow up and regularity for fractal Burgers equation. *Dynamics of PDE* **5** (2008) 211–240.
- [13] J.L. Lions. *Quelques méthodes de résolution des problèmes aux limites non linéaires*. Dunod Gauthier-Villars, Paris, 1969.
- [14] C. Martínez Carracedo and M. Sanz Alix. *The Theory of Fractional Powers of Operators*. Elsevier, Amsterdam, 2001.
- [15] C. Miao and G. Wu. Global well-posedness of the critical Burgers equation in critical Besov spaces. *J. Differential Equations* **247** (2009) 1673–1693.
- [16] J. Simon. Compact Sets in the $L^p(0, T; B)$. *Ann. Mat. Pura Appl.* **146** (1987) 65–96.
- [17] W. A. Strauss. On continuity of functions with values in various Banach spaces. *Pacific J. Math.* **19** (1966) 543–551.
- [18] R. Temam. *Navier-Stokes Equations, Theory and Numerical Analysis*. North-Holland, Amsterdam, 1979.



Application of the Direct Power Control Strategy in a Shunt Active Filter by Exploiting the Solar Photovoltaic Energy as a Continuous Source

A. Morsli¹, A. Tlemçani^{1*}, A. Krama², A. Abbadi¹, L. Zellouma²
and H. Nouri³

¹ *Electrical Engineering and Automation Research Laboratory (LREA), University of Medea, 26000, Medea, Algeria.*

² *Saharan Energy Resources Exploitation and Valorization Laboratory (LEVRES) of El-Oued, B.P. 789 El-Oued 39000, Algeria.*

³ *Power Systems, Electronics and Control Research Group, Department of Engineering Design and Mathematics, University of West of England, Bristol, BS16 1QY, U.K.*

Received: January 11, 2020; Revised: October 1, 2020

Abstract: In order to follow the standard recommendations of the electrical energy quality (IEEE519) on the distribution network, the active filters have responded to these recommendations, which require that the Total Harmonic Distortion (THD) must be less than 5%. The purpose of this paper is to improve the waveform of the electric current that is distorted due to the non-linear load by the shunt active filtering system by exploiting photovoltaic solar energy as a source of the continuous bus of the inverter and obtain a waveform of the sinusoidal source current with a THD in accordance with the recommendations cited above. To show what we have said, we used a SAPF powered by a PV system (module type MSX120 and a DC-DC boost converter controlled by the (P and O) method) controlled by the Direct Power Control (DPC) technique. The simulation results under *MATLAB/Simulink* showed us the effectiveness of the proposed system.

Keywords: *direct power control (DPC); perturbation and observation (P and O); photovoltaic solar system; shunt active power filter (SAPF).*

Mathematics Subject Classification (2010): 93C42, 03B52, 93E11, 93Cxx.

* Corresponding author: mailto:h_tlemcani@yahoo.fr

1 Introduction

The shunt active power filter is powered by a DC voltage source or a capacitor which is expensive. Our paper proposes another free continuous source by the sun, it is the photovoltaic solar energy which transforms the light energy into electrical energy via the PV sensor.

Fig. 1 shows the principle schematics of the SAPF.

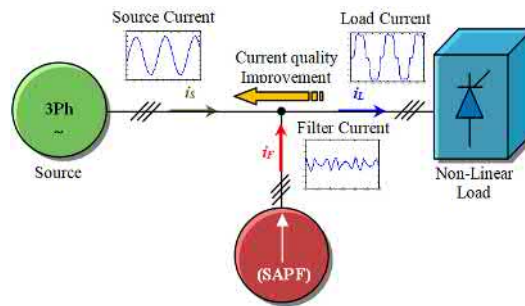


Figure 1: Principle Schematics of the Shunt Active Power Filter.

In this paper, the supply of the SAPF is provided by a photovoltaic solar module as a clean and free source. In order to output active power in the electrical network lines, it guarantees the harmonics compensation of the source current and a reduced cost of the SAPF. The regulation of the voltage of the PV system allowed us to obtain the reference of the active power by means of a PI regulator. Thus, the MPPT command by the (P and O) controller of the Boost converter is made to maintain the output voltage of the PV module constant and to follow the reference value. The three-phase two-level inverter is controlled by the DPC technique which is based on hysteresis comparators using a switchboard. This control approach shows a significant difference in terms of dynamics, robustness and stability compared to the traditional P-Q method.

2 The Photovoltaic Solar System

Fig. 2 shows the photovoltaic system which supplies the shunt active filter by a delivered voltage V_{dc} which is equal to 96 V.

2.1 Modeling of photovoltaic module

The basic element of each photovoltaic system is the photovoltaic module. It has PV cells connected together [1–3]. The PV modules are of type BP-MSX120, their characteristics are given in Tab. 1.

For PV solar module modeling, we applied the frequently used model to describe the electrical characteristics of this module which takes into account the different internal resistances (Fig. 3) [4, 5].

The equivalent circuit mathematical expression of the PV module is presented by

$$I_{PV} = I_{ph} - I_D - I_R, \quad (1)$$

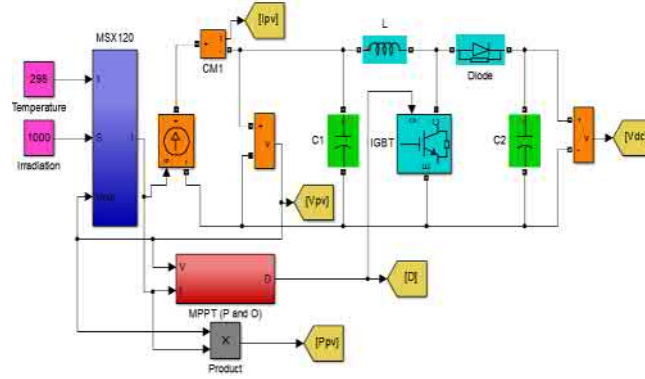


Figure 2: PV solar system (Panel, Boost converter and MPPT).

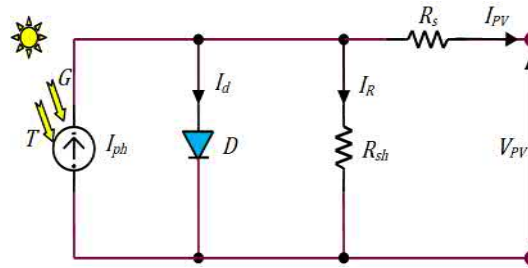


Figure 3: Equivalent circuit of a PV solar module.

$$I_{PV} = I_{ph} - I_0 \left[\exp \left(\frac{q(V_{PV} + z \cdot R_s \cdot I_{PV})}{z \cdot n \cdot k \cdot T_{ck}} \right) - 1 \right] - \frac{V_{PV} + z \cdot R_s \cdot I_{PV}}{z \cdot R_{sh}}. \quad (2)$$

Or,

I_{PV} : PV current [A],

I_{ph} : Photo-current [A],

I_0 : Reverse saturation current [A],

q : Electron charge

$$q = 1.6 \cdot 10^{-19} \text{ coulomb}$$

V_{PV} : PV Voltage [V],

z : Number of cells in series,

R_s : Series resistance [Ω],

R_{sh} : Shunt resistance [Ω],

n : Ideality factor varies between 1 and 2,

k : constant of Boltzmann

$$k = 1.38 \cdot 10^{-23} \text{ J} \cdot \text{K}^{-1}$$

| BP SOLAR MSX 120 | |
|--|------------------------|
| Maximum Power Point P_{max} | 120 W |
| Voltage at P_{max} V_{mp} | 33.7 V |
| Current at P_{max} I_{mp} | 3.56 A |
| Open-circuit voltage V_{oc} | 42.1 V |
| Short-circuit current I_{sc} | 3.87 A |
| Series resistance R_s | 0.473 Ω |
| Shunt resistance R_{sh} | 1367 Ω |
| Ideality factor n | 1.3977 |
| Temperature coefficient of I_{sc} k_i | (0.065 \pm 0.015)%/C |
| Temperature coefficient of V_{oc} k_v | – (80 \pm 10) mV/C |
| Temperature coefficient of P_{max} k_p | – (0.5 \pm 0.05)%/C |
| NOCT | (47 \pm 2)C |
| Number of cells connected in series n_s | 72 |

Table 1: Datasheet parameters of the PV module.

2.2 Modeling of DC-DC converter and MPPT controller

In order to guarantee the level of voltage required to supply the shunt active power filter, the voltage delivered by the PV module is insufficient ($V_{PV} = 42.1$ V), while the inverter must supply a voltage greater than V_{PV} . For this, we used a DC-DC boost converter (Fig. 4) [8].

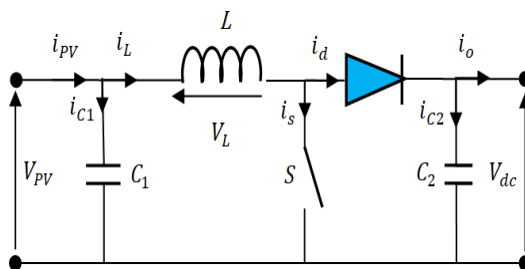


Figure 4: Ideal circuit of boost converter.

The following equations are obtained from Fig. 3 when the switch S is open.

$$i_{c1}(t) = C_1 \frac{dv_{PV}(t)}{dt} = i_{PV}(t) - i_L(t), \tag{3}$$

$$i_{c2}(t) = C_2 \frac{dv_{dc}(t)}{dt} = i_L(t) - i_o(t), \tag{4}$$

$$v_1(t) = L \frac{di_L(t)}{dt} = v_{PV}(t) - v_{dc}(t). \tag{5}$$

This transistor controlled by the (P and O) algorithm aims to tracking the maximum power point MPPT. The latter is then controlled using a MPPT controller with the Perturbation and Observation (P and O) algorithm, as shown in Fig. 5.

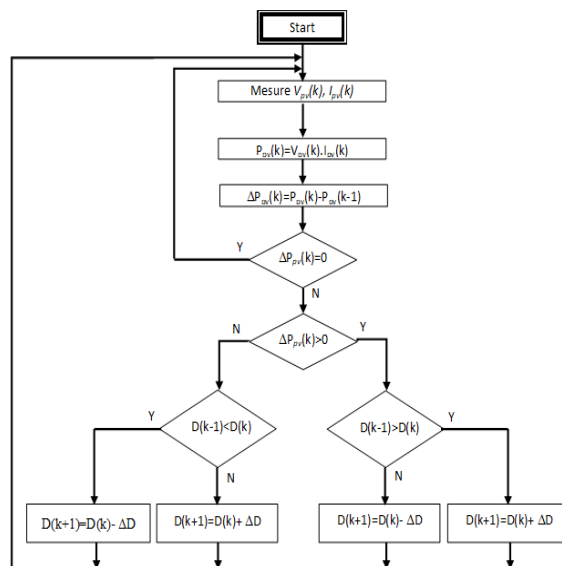


Figure 5: Perturbation and Observation algorithm [9].

The switch S is a MOSFET transistor and internal diode in parallel with a series RC snubber circuit. When a gate signal is applied, the MOSFET conducts and acts as a resistance (R_{on}) in both directions. If the gate signal falls to zero when current is negative, current is transferred to the antiparallel diode. Their parameters are shown in Tab. 2.

| MOSFET Transistor | |
|--------------------------------------|---------------|
| FET resistance R_{on} | 0.1 Ω |
| Internal diode inductance L_{on} | 0 H |
| Internal diode resistance R_d | 0.01 Ω |
| Internal diode forward voltage V_f | 0 V |

Table 2: MOSFET Transistor parameters [10].

3 Modeling of Shunt Active Power Filter

Recently, there are fast switching power devices controlled by different strategies. These devices can compensate the harmonics due to the nonlinear charge by producing counter-harmonic currents [11]. The used SAPF is an inverter with two levels of IGBT Transistor and internal diode in parallel. Their parameters are shown in Tab. 3.

| IGBT Transistor | |
|---------------------------|-----------------|
| IGBT resistance R_{on} | 0.001 Ω |
| Snubber resistance R_s | 100000 Ω |
| Snubber capacitance C_s | Inf F |

Table 3: IGBT Transistor parameters [10].

The work of the simulation model is as follows:

- Mainly the circuit consists of an inverter which consists of 6 IGBTs.
- The inverter is basically used to convert DC into AC. The input of the inverter is 96V dc and the output is connected between the supply network and non linear load through the RL filter in order to inject the filter current i_f .

The simple voltages of the three phases a, b and c at the output of the inverter are given as follows:

$$v_{fa} = V_{An} = 2U_c \frac{2S_a - S_b - S_c}{3} = V_{dc} \frac{2S_a - S_b - S_c}{3}, \tag{6}$$

$$v_{fb} = V_{Bn} = 2U_c \frac{2S_b - S_a - S_c}{3} = V_{dc} \frac{2S_b - S_a - S_c}{3}, \tag{7}$$

$$v_{fc} = V_{Cn} = 2U_c \frac{2S_c - S_a - S_b}{3} = V_{dc} \frac{2S_c - S_a - S_b}{3}. \tag{8}$$

Thus, we can express eight possible cases of the output voltage of the active filter V_{fk} (referred to the neutral N of the source) as shown in Tab. 4 [12].

| Case | S_a | S_b | S_c | v_{fa}/V_{dc} | v_{fb}/V_{dc} | v_{fc}/V_{dc} |
|----------|-------|-------|-------|-----------------|-----------------|-----------------|
| 0 | 0 | 0 | 0 | 0 | 0 | 0 |
| 1 | 1 | 0 | 0 | 2/3 | -1/3 | -1/3 |
| 2 | 0 | 1 | 0 | -1/3 | 2/3 | -1/3 |
| 3 | 1 | 1 | 0 | 1/3 | 1/3 | -2/3 |
| 4 | 0 | 0 | 1 | -1/3 | -1/3 | 2/3 |
| 5 | 1 | 0 | 1 | 1/3 | -2/3 | 1/3 |
| 6 | 0 | 1 | 1 | -2/3 | 1/3 | 1/3 |
| 7 | 1 | 1 | 1 | 0 | 0 | 0 |

Table 4: Possible voltages in the output of the inverter.

The structure of inverter is shown in Fig. 6.

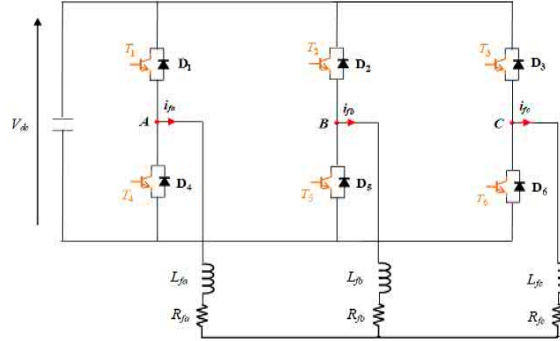


Figure 6: Structure of the three-phase inverter with two levels [13].

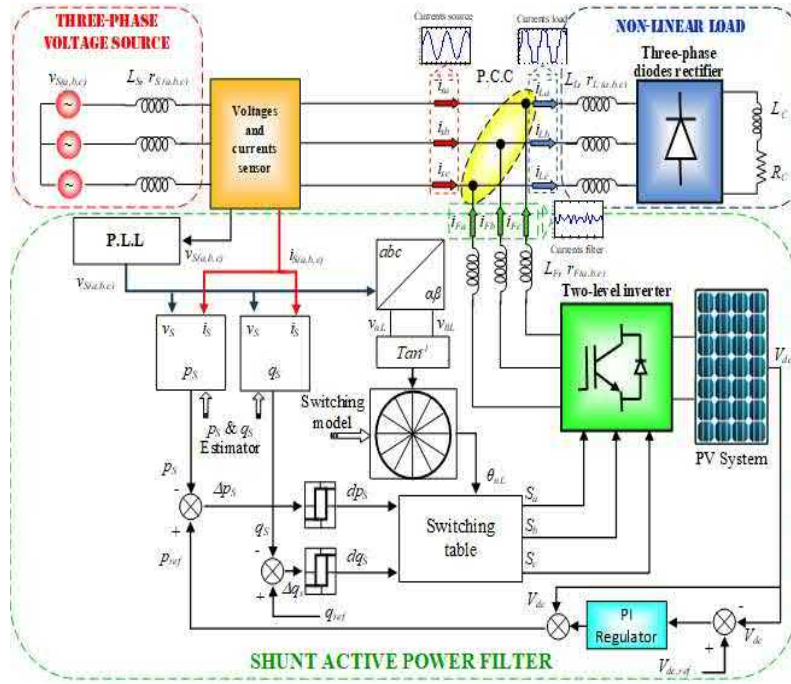


Figure 7: Block diagram of the SAPF controlled by the DPC connected with a PV solar panel.

3.1 Direct power control (DPC) technique

Fig. 7 shows the system of a shunt active power filtering controlled by the DPC technique and connected with a solar photovoltaic panel.

These powers are expressed, respectively, by the following relations [10, 12, 14]:

$$p_s(t) = v_{sa} \cdot i_{sa} + v_{sb} \cdot i_{sb} + v_{sc} \cdot i_{sc}, \tag{9}$$

$$q_s(t) = \frac{1}{\sqrt{3}} [(v_{sb} - v_{sc}) \cdot i_{sa} + (v_{sc} - v_{sa}) \cdot i_{sb} + (v_{sa} - v_{sb}) \cdot i_{sc}]. \tag{10}$$

For this purpose, the stationary coordinates are divided into 12 sectors, as shown in Fig. 8. The digitized signal errors d_{ps} , d_{qs} and voltage phase θ_n are the inputs of switching table shown in Table 1 whose output is the switching state (S_a , S_b , S_c) of the converter. By using this switching table, the optimal state of the converter can be selected uniquely during each time interval according to the combination of the table inputs. The selection of the optimal switching state is performed so that the power errors can be restricted within the hysteresis bands [10, 15].

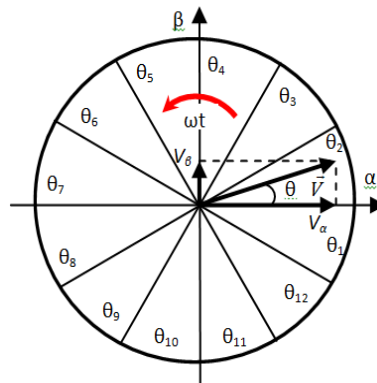


Figure 8: (α, β) twelve (12) sectors representation.

The digitized variables d_{ps} , d_{qs} and grid voltage vector position θ (equation (11)), form a digital word, for access to the address of switching table select the appropriate control voltage vector

$$\theta = \arctan \frac{v_\beta}{v_\alpha}. \tag{11}$$

Determination of the number of sector is given by

$$(n - 2) \frac{\pi}{6} < \theta_n < (n - 1) \frac{\pi}{6}, \tag{12}$$

where n indicates the sector number ($n = 1, 2, \dots, 12$) [10, 16]. The input voltage can be estimated by the following equation:

$$\begin{bmatrix} v_\alpha \\ v_\beta \end{bmatrix} = \frac{1}{i_\alpha^2 + i_\beta^2} \begin{bmatrix} i_\alpha & -i_\beta \\ i_\beta & i_\alpha \end{bmatrix} \begin{bmatrix} \hat{p} \\ \hat{q} \end{bmatrix}. \tag{13}$$

The same observation can be made for d_q and even sectors (θ_i), i =even. So, this shows the limits of this switching table DPC (Tab.5) [10, 17]. The knowledge of the estimated voltage sector is necessary to determine optimal switching states.

The conversion in the $\alpha - \beta$ coordinate system by the system voltages with the Concordia transformation gives

$$\begin{bmatrix} v_{s\alpha}(\theta) \\ v_{s\beta}(\theta) \end{bmatrix} = [T_{32}]^t \cdot \begin{bmatrix} v_{sa}(\theta) \\ v_{sb}(\theta) \\ v_{sc}(\theta) \end{bmatrix}. \tag{14}$$

| d_p | d_q | θ_1 | θ_2 | θ_3 | θ_4 | θ_5 | θ_6 | θ_7 | θ_8 | θ_9 | θ_{10} | θ_{11} | θ_{12} |
|----------|----------|------------|------------|------------|------------|------------|------------|------------|------------|------------|---------------|---------------|---------------|
| 1 | 0 | 101 | 111 | 100 | 000 | 110 | 111 | 010 | 000 | 011 | 111 | 001 | 000 |
| 1 | 1 | 111 | 111 | 000 | 000 | 111 | 111 | 000 | 000 | 111 | 111 | 000 | 000 |
| 0 | 0 | 101 | 100 | 100 | 110 | 110 | 010 | 010 | 011 | 011 | 001 | 001 | 101 |
| 0 | 1 | 100 | 110 | 110 | 010 | 010 | 011 | 011 | 001 | 001 | 101 | 101 | 100 |

Table 5: Switching sectors of the DPC.

The $d - q$ voltage components are derived by the Park transformation, where $\hat{\theta}$ represents the instantaneous reference voltage vector angle,

$$\begin{bmatrix} v_{sd} \\ v_{sq} \end{bmatrix} = p(\hat{\theta}) \cdot \begin{bmatrix} v_{s\alpha}(\theta) \\ v_{s\beta}(\theta) \end{bmatrix} \quad (15)$$

with

$$p(\hat{\theta}) = \frac{1}{i_{\alpha}^2 + i_{\beta}^2} \begin{bmatrix} \cos \hat{\theta} & \sin \hat{\theta} \\ -\sin \hat{\theta} & \cos \hat{\theta} \end{bmatrix} \quad (16)$$

and after substituting (14) in (16), the voltages v_{sd} and v_{sq} are given by:

$$\begin{bmatrix} v_{sd} \\ v_{sq} \end{bmatrix} = \sqrt{3} \cdot V_m \cdot \begin{bmatrix} \sin(\theta - \hat{\theta}) \\ -\cos(\theta - \hat{\theta}) \end{bmatrix}. \quad (17)$$

4 Simulation Results and Discussions

The simulation of the system made with the *MATLAB/Simulink* environment allowed us to obtain the results below. Fig. 9 shows the voltage delivered by the PV module. We note that this voltage is reached at its open-circuit value which is equal to 42.1 V in a very fast time at time $t = 0.005$ s.

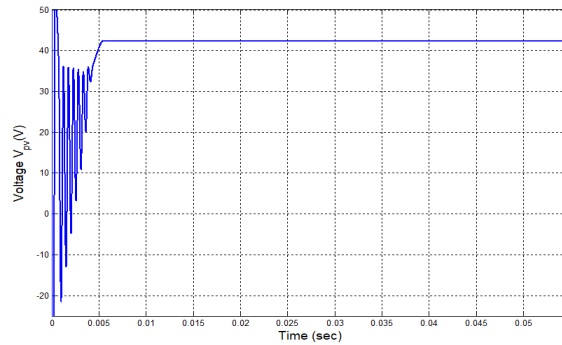


Figure 9: Photovoltaic voltage V_{pv} .

The curves (shown in Fig. 10) express current and power as a function of time. We

observe that the parameters shown in Tab.1 are completed according to the *datasheet* of this module.

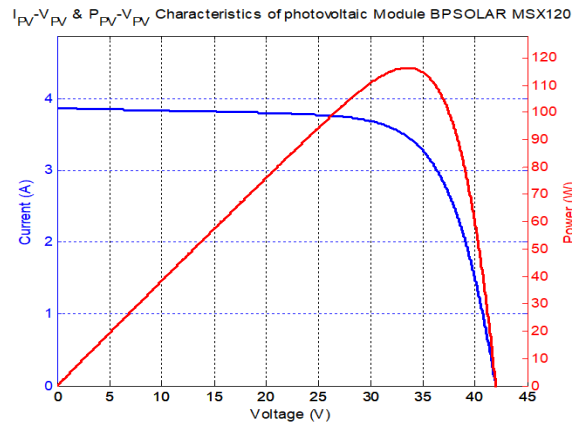


Figure 10: Current I_{pv} and power P_{pv} in the function of voltage V_{pv} for a PV solar module of type BP-MSX120.

Fig. 11 shows the Duty cycle as a function of time. D increases from the value null to the value 0.5 at the instant 0.01 s.

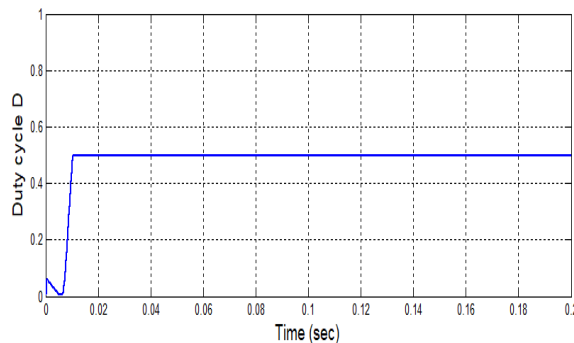


Figure 11: Duty cycle D in the function of time.

Fig. 12 shows the DC link voltage delivered by the boost DC-DC converter. We clearly see that the voltage V_{dc} reaches the reference value which is equal to 96 V at the instant 0.035 s.

Fig. 13 shows the load current delivered by the non-linear load without the SAPF. We see that the signal is distorted because of the harmonics injected by the rectifier with an amplitude value equal to 2.402 A.

Its spectral analysis gives a total harmonic distortion and shows a very high THD to the value accepted by the supply grid which requires a current THD of less than 5%. We see that $THD_{iLa} = 25.32\%$, which is unacceptable. The harmonics that have appeared are of order $(6h \pm 1)$ because of the three-phase source and the non-linear load, i.e., in

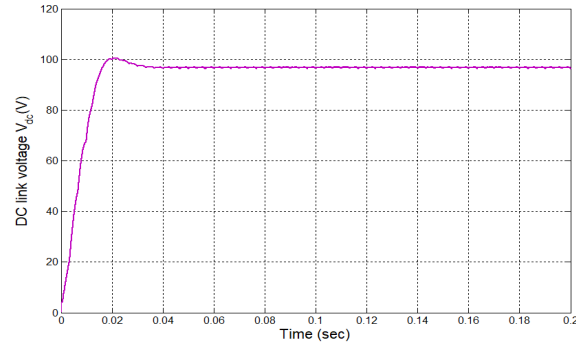


Figure 12: DC link voltage in the output of the boost converter V_{dc} .

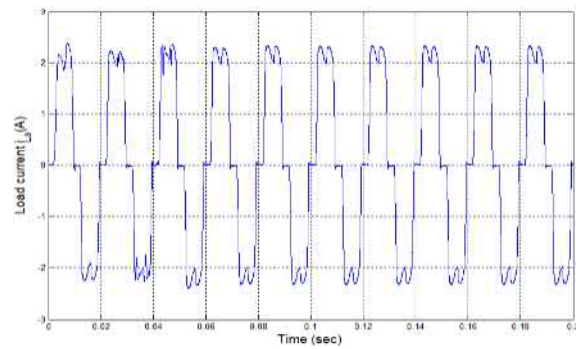


Figure 13: Load current i_{La} without the SAPF.

the range of 30 orders, the order harmonics 5, 7, 11, 13, 17, 19, 23, 25 and 29 appeared (Fig. 14).

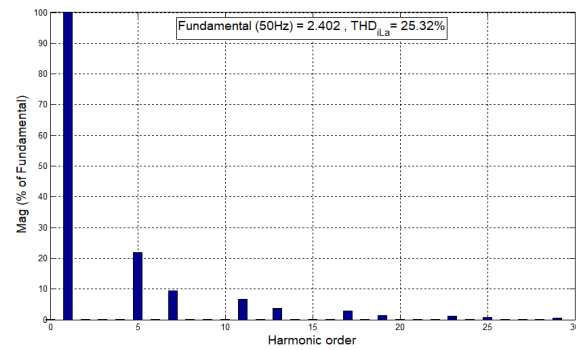


Figure 14: Total Harmonic Distortion of i_{La} .

After connecting the SAPF, we obtained the signal illustrated in Fig. 15. This is the

source current i_{Sa} which becomes almost sinusoidal with an amplitude value equal to 4.412 A.

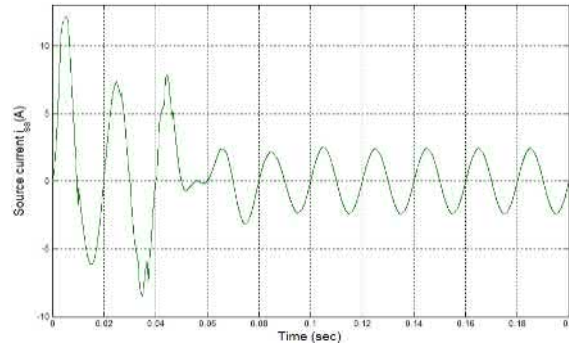


Figure 15: Source current i_{Sa} with the SAPF.

Its spectral analysis gives a THD is less than 5%. We see that $THD_{i_{Sa}} = 2.94\%$, which is acceptable.

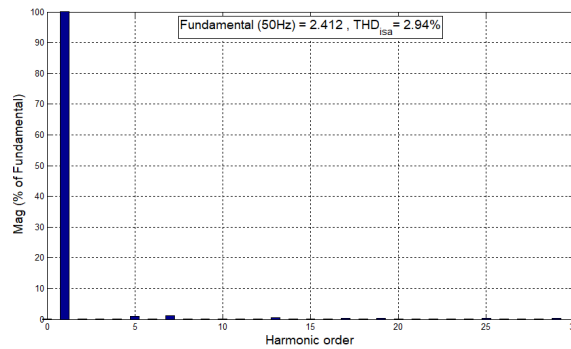


Figure 16: Total Harmonic Distorsion of i_{Sa} .

Fig. 17 shows the filter current i_{Fa} delivered by the SAPF.

Fig. 18 shows the system currents in same figure. The filter current i_{Fa} delivered by the SAPF which compensates for the load current i_{La} by the following formula:

$$i_{Sa} = i_{La} - i_{Fa}. \tag{18}$$

Fig. 19 represents the active P_s and its reference P_s^* powers. This shows us that the active power follows its reference which is equal to 200 W at permanent regime after closing the switch placed between the shunt active filter and the line.

Fig. 20 represents the reactive Q_s and its reference Q_s^* powers. This shows us that the reactive power follows its reference which is equal to 0 VAR at permanent regime after closing the switch placed between the shunt active filter and the line.

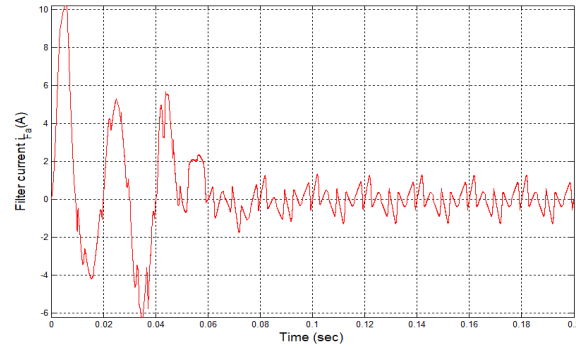


Figure 17: Filter current i_{Fa} .

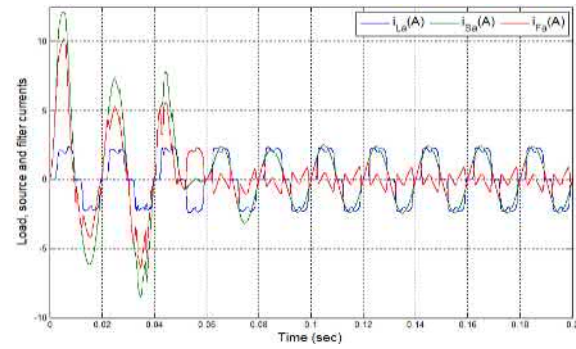


Figure 18: Load, source and filter currents i_{La} , i_{sa} and i_{Fa} .

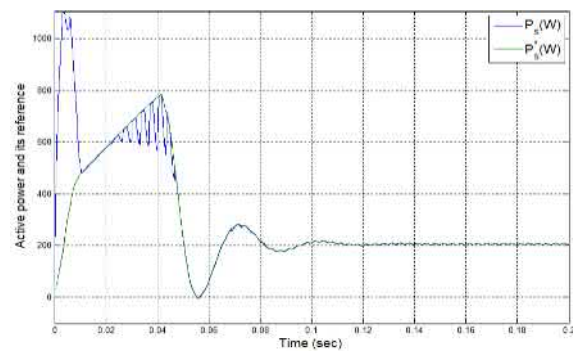


Figure 19: Active power P_s and its reference P_s^* .

5 Conclusion

The harmonics injected into the electricity grid by the nonlinear charges pollute the lines of this network, which causes the deformation of the electric currents on the one

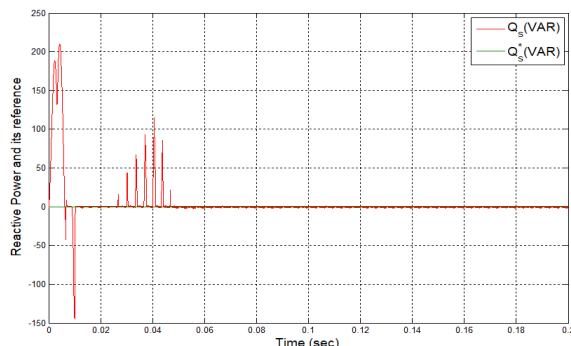


Figure 20: Reactive power Q_s and its reference Q_s^* .

hand and the malfunction of the electrical appliances on the other hand. To clean up the supply network, several methods have been proposed between liabilities and assets. Our proposal is parallel active filtering controlled by the Direct Power Control (DPC) technique. The DC bus is powered by a photovoltaic source. The simulation results under *MATLAB/Simulink* show us that the filter has improved the quality of electrical energy, and especially the wave of electric current i_{Sa} source. We clearly see that:

1. $THD_{iLa}=25.32\%$ before filtering decreased to $THD_{iSa}=2.94\%$ after filtering;
2. The SAPF i_{La} current compensated the reagent in the feed lines;
3. The active and reactive powers have followed their references.

Finally, we can say that the application of the PV system in parallel active filters has a better harmonic compensation performance and reactive power.

References

- [1] K. Ishaque, Z. Salam, H. Taheri and S. Syafaruddin. Modeling and Simulation of Photovoltaic PV System During Partial Shading Based on a Two-Diode Model. *Simulation Modeling Practice and Theory* **19** (07) (2011) 1613–1626.
- [2] K. Ishaque, Z. Salam and S. Syafaruddin. A Comprehensive MATLAB Simulink PV System Simulator with Partial Shading Capability Based on Two-Diode Model. *Solar Energy* **85** (09) (2011) 2217–2227.
- [3] N. Belhaouas, M. S. Ait-Cheikh, A. Malek and C. Larbes. Matlab-Simulink of photovoltaic system based on a two-diode model simulator with shaded solar cells. *Revue des Energies Renouvelables* **16** (01) (2013) 65–73.
- [4] A. Hoque and K. A. Wahid. New Mathematical Model of a Photovoltaic Generator PVG. *Bangladesh Journal of Electrical Engineering* **28** (01) (2000).
- [5] A. Hansen, P. Sorensen, L. Hansen and H. Bindner. Models for Stand-Alone PV System. *Riso National Laboratory, Roskilde, Denmark*, ISBN 87-550-2774-1.
- [6] A. S. Golder. Photovoltaic Generator Modeling for Large Scale Distribution System Studies. *Thesis Master of Science in Electrical Engineering*. October, 2006.

- [7] A. Morsli. Etude d'un système solaire photovoltaïque utilisant des supercondensateurs. *Mémoire de Magistère en électricité solaire. Ecole Nationale Polytechnique ENP, Algeria*, 2010.
- [8] A. Krama, L. Zellouma and B. Rabhi. Improved Control of Shunt Active Power Filter Connected to a Photovoltaic System Using Technique of Direct Power Control. In: *8th International Conference on Modelling, Identification and Control ICMIC2016*, Algiers, Algeria. November 15 – 17, 2016.
- [9] F. Hamidia, A. Abbadi, A. Tlemçani and M. S. Boucherit. Dual star induction motor supplied with double photovoltaic panels based on fuzzy logic type-2. *Nonlinear Dynamics and Systems Theory* **18** (04) (2018) 359–371.
- [10] A. Morsli, A. Tlemçani and M. S. Boucherit. Shunt Active Power Filter Based Harmonics Compensation of a Low-Voltage Network Using Fuzzy Logic System. In: *2018 International Conference on Applied Smart Systems ICASS2018*, Medea, Algeria. November 24–25, 2018.
- [11] A. Morsli, A. Tlemçani, and M. S. Boucherit. Shunt Active Power Filter Based Harmonics Compensation of a Low-Voltage Network Using Fuzzy Logic System. *Nonlinear Dynamics and Systems Theory* **17** (01) (2017) 70–85.
- [12] A. Morsli. Réduction de la pollution des réseaux électriques basses tensions fondée sur les compensateurs actifs : Théorie et réalisation. *Thèse de Doctorat en Génie Electrique. Option: Automatique. Ecole Nationale Polytechnique ENP, Algeria*, 2018.
- [13] R. Chibani, E. Berkouk and M. S. Boucherit. Study of a new DC voltage equalising circuit for Five-Level Neutral Point Clamped-Voltage Source Inverter. *Electrical Systems* **07** (02) (2011) 131–148.
- [14] R. S. Herrera, P. Salmeron and H. Kim. Instantaneous reactive power theory applied to active power filter compensation: different approaches, assessment and experimental results. *IEEE Trans. on Industrial Electronics* **55** (01) (2008) 184–196.
- [15] A. Chaoui, J. P. Gaubert and F. Krim. Power quality improvement using DPC controlled three-phase shunt active filter. *Electr. Power Syst. Res.* **80** (2010) 657–666.
- [16] A. Semmah, A. Massoum, H. Hamdaoui and P. Wira. Comparative Study of PI and Fuzzy DC Voltage Control for a DPC- PWM Rectifier. *Przeegląd Elektrotechniczny* **87** (10) (2011) 355–359.
- [17] A. Chaoui, J. P. Gaubert and A. Bouafia. Direct Power Control Switching Table Concept and Analysis for Three-phase Shunt Active Power Filter. *Journal of Electrical Systems* **09** (01) (2013) 52–65.



Uniqueness of Solution to the von Karman Equations with Free Boundary Conditions

J. Oudaani ^{1*}, A. El Mouatasim ² and B. El-Aqqad ³

^{1,2} *Department of Mathematics, Informatics and Management, Ibn Zohr University,
Poly-Disciplinary Faculty, Code Postal 638, Ouarzazate, Morocco.*

³ *College of Idlssan-Ouarzazate, Morocco.*

Received: April 11, 2020; Revised: September 18, 2020

Abstract: The purpose of this paper is to give some theoretical results, under weaker hypotheses imposed on the external, internal, linear potential loads and three measurable portions with non null area of the boundary of the shallow shell, for the local existence and uniqueness of solution to the stationary von Karman equations, with free-type boundary conditions of the elastic shallow shell. Finally, in some theoretical results, we describe an iterative method for constructing a unique weak solution for the problem.

Keywords: *static von Karman equations; free-type boundary; elastic shallow shell.*

Mathematics Subject Classification (2010): 74F10, 74B20, 74K25, 65N05.

1 Introduction

In nonlinear three-dimensional elasticity theory, the stationary von Karman equations are two dimensional equations for the nonlinearly elastic shallow shell. The mathematical model is a modeling of the physical situation of buckling phenomenon of the elastic shallow shell, which is perturbed by the external and internal forces and potentially non conservative loads $L(\cdot)$ applied to the system, see [3]. In case of free-type and mixed homogenous boundary conditions, we know the static von Karman equations for vertical displacement u of the middle surface of the reference configuration of the shell from a plane, and the Airy stress function ϕ has the form, see, for instance, [3].

* Corresponding author: <mailto:oudaani1970@gmail.com>

Find $(u, \phi) \in (H_0^2(\omega))^2$ such that

$$(\mathbb{P}) \left\{ \begin{array}{ll} \Delta^2 u - [\phi + F_0, u + \theta] + L(u) = p(x) & \text{in } \omega, \\ \Delta^2 \phi + [u, u + 2\theta] = 0 & \text{on } \omega, \\ u = \partial_\nu u = 0 & \text{on } \Gamma_0, \\ u = 0, \quad \Delta u + (1 - \mu)B_1 u = 0 & \text{on } \Gamma_1, \\ \Delta u + (1 - \mu)B_1 u = 0, \quad \partial_\nu(\Delta u) + (1 - \mu)B_2 u - \vartheta u = 0 & \text{on } \Gamma_2, \\ \phi = 0, \partial_\nu \phi = 0 & \text{on } \Gamma. \end{array} \right.$$

Here ω is the middle surface of the initial configuration of the shell, the parameter μ is the Poisson ratio, $\vartheta \geq 0$ is a positive reel and $[u, v]$ is a von Karman bracket defined by [15]

$$[\phi, u] = \partial_{11}\phi\partial_{22}u + \partial_{11}u\partial_{22}\phi - 2\partial_{12}\phi\partial_{12}u. \quad (1)$$

The shell is subjected to the internal force F_0 , which is a given function determined by the in-plane mechanical loads, and the shell is subjected also to the external force p , and $\theta(x, y)$, see [3, 7], is a mapping measuring the deviation of the middle surface of the reference configuration of the shell from a plane. This function determines the initial form of the shell and the case $\theta = 0$ corresponds to the plate theory.

In [3], I.Chueshov and I.Lasiecka studied the stationary and dynamic von Karman equations and established different theoretical results for generalized, strong and weak solutions under weaker hypotheses imposed at different loads, namely, for free-type boundary conditions the authors take the assumption $F_0 \in H^{\frac{5}{2}+\epsilon}(\omega)$, by using the theory of nonlinear semi-group. To justify the uniqueness, the authors used the limit definition of generalized solution along weak continuity of the nonlinear terms involving the Airy stress function and knowing the Lipschitz continuity of von Karman bracket with the Airy stress function. Moreover, in [4], P.G. Ciarlet and L. Gratie justified the generalized von Karman equations by means of a formal asymptotic analysis and established the existence of the system.

The aim of this paper is to find a condition verified by the internal and external loads, the linear bounded operator L and, also, three measurable portions $\Gamma_0, \Gamma_1, \Gamma_2$ with non null area of the boundary $\Gamma = \Gamma_0 \cup \Gamma_1 \cup \Gamma_2$ of the shallow shell. Moreover, in this paper, for justifying some theoretical results, we take only the following weak assumption $F_0 \in H^2(\omega)$.

This paper will be organized as follows. After this introduction, Section 2 contains some basic results and tools that will be needed later. Section 3 is devoted to the description of the mathematical structure of the model under consideration by using an iterative method for establishing the existence and uniqueness of the weak solution associated to the static von Karman equations.

2 Preliminary Results and Needed Tools

In this paper, ω denotes a nonempty connected and bounded open domain in IR^2 , with its boundary $\Gamma = \partial\omega$ of C^∞ -regularity. We assume that in this section $\Gamma =$

$\Gamma_0 \cup \Gamma_1 \cup \Gamma_2$, where Γ_0 , Γ_1 and Γ_2 are three measurable portions of Γ with non null area and $\Gamma_0 \cap \Gamma_1 \cap \Gamma_2 = \emptyset$.

Let us consider the following problem [3]. Find $(u, \phi) \in H^2(\omega) \times H_0^2(\omega)$ such that

$$(\mathbb{P}) \begin{cases} \Delta^2 u - [\phi + F_0, u + \theta] + L(u) = p(x) & \text{in } \omega, \\ \Delta^2 \phi + [u, u + 2\theta] = 0 & \text{on } \omega, \\ u = \partial_\nu u = 0 & \text{on } \Gamma_0, \\ u = 0, \quad \Delta u + (1 - \mu)B_1 u = 0 & \text{on } \Gamma_1, \\ \Delta u + (1 - \mu)B_1 u = 0, \quad \partial_\nu(\Delta u) + (1 - \mu)B_2 u - \vartheta u = 0 & \text{on } \Gamma_2, \\ \phi = 0, \partial_\nu \phi = 0 & \text{on } \Gamma, \end{cases}$$

where $[u, v]$ is defined in (1) and

$$B_1 u = 2n_1 n_2 \partial_{12} u - n_1^2 \partial_{11} u - n_2^2 \partial_{22} u,$$

$$B_2 u = \partial_\tau [(n_1^2 - n_2^2) \partial_{12} u + n_1 n_2 (\partial_{22} u - \partial_{11} u)]$$

with $n = (n_1, n_2)$ being the outer normal to Γ and $\tau = (-n_2, n_1)$ being the unit tangent vector along Γ .

Let $p \geq 1$ and $m \in \mathbb{N}^*$, we denote

$$|u|_p = \left(\int_\omega |u|^p \right)^{1/p}, \quad \|u\| = \sum_{\alpha, \beta=1,2} |\partial_{\alpha\beta} u|_2 \quad \text{and} \quad \|u\|_0^2 = \int_\omega (\Delta u)^2$$

and $\|u\|_{m,\omega}$ is the classical norm in $H^m(\omega)$. For the sake of simplicity, we define

$$\mathbb{V} = \{u \in H^2(\omega) / u = \partial_\nu u = 0 \text{ on } \Gamma_0 \text{ and } u = 0 \text{ on } \Gamma_1\},$$

which is a subspace of $H^2(\omega)$, and

$$a_0(u, v) = \int_\omega (\Delta u \Delta v - (1 - \mu)[u, v]). \tag{2}$$

The following result is of interest.

Proposition 2.1 *Let Γ_0 and Γ_1 be two portions of Γ , if we do not choose the next two portions Γ_0 or Γ_1 of Γ in a linear segment, then the semi norm $\|\cdot\|$ is a norm in \mathbb{V} equivalent to the usual norm of $H^2(\omega)$.*

Proof. To establish that the semi-norm $\|\cdot\|$ is a norm in the subspace \mathbb{V} , we show the following result:

$$\forall u \in \mathbb{V}; \quad \|u\| = \sum_{\alpha, \beta=1,2} |\partial_{\alpha\beta} u|_2 = 0 \Rightarrow u = 0.$$

Then, for $\forall u \in \mathbb{V}$, we have

$$\|u\| = 0 \Rightarrow \forall \alpha, \beta = 1, 2, \quad \partial_{\alpha\beta} u = 0.$$

Now, by using a classical result from distribution theory [5], and since the set ω is connected, with $\forall \alpha, \beta = 1, 2, \partial_{\alpha\beta} u = 0$, we have that

$$\forall (x, y) \in \bar{\omega}, \exists (a, b, c) \in \mathbb{R}^3 \text{ such that } u(x, y) = ax + by + c.$$

If Γ_0 or Γ_1 is not in a linear segment, then

$$u_{\Gamma_0} = (ax + by + c)|_{\Gamma_0} = 0 \text{ and } u_{\Gamma_1} = (ax + by + c)|_{\Gamma_1} = 0,$$

this implies that

$$\Gamma_0 \subset \{(x, y) \in \mathbb{R}^2 / ax + by + c = 0\}$$

or

$$\Gamma_1 \subset \{(x, y) \in \mathbb{R}^2 / ax + by + c = 0\},$$

that contradicts the assumption that one of two portions Γ_0 or Γ_1 is not in a linear segment, and we conclude that $a = b = c = 0$.

Now, if we have that two portions Γ_0 and Γ_1 are in linear segments, then

$$\Gamma_0 \subset \{(x, y) \in \mathbb{R}^2 / ax + by + c = 0\} \text{ and } \Gamma_1 \subset \{(x, y) \in \mathbb{R}^2 / ax + by + c = 0\}.$$

Since Γ_0 and Γ_1 are not in the identical linear segment, we deduce that

$$a = b = c = 0 \Rightarrow u = 0.$$

Finally, the semi-norm $\|\cdot\|$ is a norm in \mathbb{V} .

Now we show that the subspace \mathbb{V} is a Banach space in $H^2(\omega)$. Let $(u_n)_{n \geq 0}$ be the sequence elements in the space \mathbb{V} such that $(u_n)_{n \geq 0}$ converge to u in $H^2(\omega)$.

Since the operator "trace" and ∂_ν are continuous, we have the sequences $(u_n)|_{\Gamma_0}$, $(u_n)|_{\Gamma_1}$ and $\partial_\nu(u_n)|_{\Gamma_0}$ converge to $u|_{\Gamma_0}$, $u|_{\Gamma_1}$ and $\partial_\nu u|_{\Gamma_0}$, then $u|_{\Gamma_0} = u|_{\Gamma_1} = 0$ and $\partial_\nu u|_{\Gamma_0} = 0$. Hence $u \in \mathbb{V}$, then \mathbb{V} is a closed subspace in $H^2(\omega)$.

Moreover, we prove that the norm $\|\cdot\|$ in the space \mathbb{V} is equivalent to the usual norm of $H^2(\omega)$.

The inequality $\|u\| \leq \|u\|_{2,\omega}$ clearly holds. But if we suppose that the other inequality is false, then there exists a sequence (u_n) in \mathbb{V} , such that

$$\forall n \in \mathbb{N}, \|u_n\|_{2,\omega} = 1 \text{ and } \lim_{n \rightarrow +\infty} \|u_n\| = 0. \quad (3)$$

For more detail, see [5].

So, u_n is bounded in the space $H^2(\omega)$. We use the compact injection $H^2(\omega) \hookrightarrow_c L^2(\omega)$, then there exists a subsequence u_m such that, with (3), we have u_m converges in the space $L^2(\omega)$ and also u_m converges to 0, with the norm $\|\cdot\|$ in the space \mathbb{V} .

Finally, we conclude that u_m is a Cauchy sequence with the norm $(\|\cdot\|_2^2 + \|\cdot\|^2)^{1/2}$. In [5], the norm $(\|\cdot\|_2^2 + \|\cdot\|^2)^{1/2}$ is equivalent to the usual norm of $H^2(\omega)$, this implies that u_m converges to u in \mathbb{V} , therefore the limit u satisfies

$$\|u\| = \lim_{m \rightarrow +\infty} \|u_m\| = 0 \Rightarrow u = 0,$$

but this result contradicts the equality $\forall m \in \mathbb{N}, \|u_m\|_{2,\omega} = 1$ and the desired result is obtained.

Remark 2.1 *The norm $\|\cdot\|$ is equivalent to the norm $\|\cdot\|_0$ in the space \mathbb{V} .*

Proof. By the analogous method as in Proposition 2.1, we prove that

$$\forall u \in \mathbb{V}, \exists \alpha > 0, \beta > 0; \alpha \|u\|_0 \leq \|u\|_{2,\omega} \leq \beta \|u\|_0,$$

and, with the result of Proposition 2.1, we have

$$\forall u \in \mathbb{V}, \exists \alpha_1 > 0, \beta_1 > 0; \alpha_1 \|u\| \leq \|u\|_{2,\omega} \leq \beta_1 \|u\|,$$

then

$$\forall u \in \mathbb{V}, \quad \frac{\alpha_1}{\beta} \|u\| \leq \|u\|_0 \leq \frac{\beta_1}{\alpha} \|u\|.$$

Finally, the desired result is verified.

We recall the following results, see [1, 3, 8, 10, 11] for instance.

Theorem 2.1 *Let $u \in H^4(\omega)$, $v \in H^2(\omega)$ and $\mu \in IR$, we have that, with (2),*

$$\int_{\omega} \Delta^2 uv = a_0(u, v) + \int_{\Gamma} [(\partial_{\nu} \Delta u + (1 - \mu) B_2 u) v - (\Delta u + (1 - \mu) B_1 u) \partial_{\nu} v].$$

Lemma 2.1 *The space $\mathbb{V} \cap H^4(\omega)$ is dense in the space \mathbb{V} for the induct norm of $H^4(\omega)$ and for every u and v in \mathbb{V} the equality*

$$\int_{\omega} \Delta^2 uv = a_0(u, v) + \int_{\Gamma} [(\partial_{\nu} \Delta u + (1 - \mu) B_2 u) v - (\Delta u + (1 - \mu) B_1 u) \partial_{\nu} v]$$

holds.

Theorem 2.2 *Let $f \in L^1(\omega)$, then the following problem*

$$\begin{cases} \Delta^2 v = f & \text{in } \omega, \\ v = 0 & \text{on } \Gamma, \\ \partial_{\nu} v = 0 & \text{on } \Gamma \end{cases}$$

has one and only one solution v in $H_0^2(\omega)$ satisfying the relation

$$\|v\|_0 \leq c_0 \|f\|_1,$$

where $c_0 > 0$ is a constant which depends only on $\text{mes}(\omega)$.

We are now in a position to state the following result.

Theorem 2.3 *Let $f \in L^1(\omega)$, the following problem*

$$(Q) \begin{cases} \Delta^2 u = f & \text{in } \omega, \\ u = \partial_{\nu} u = 0 & \text{on } \Gamma_0, \\ u = 0, \Delta u + (1 - \mu) B_1 u = 0 & \text{on } \Gamma_1, \\ \Delta u + (1 - \mu) B_1 u = 0 & \text{on } \Gamma_2, \\ \partial_{\nu}(\Delta u) + (1 - \mu) B_2 u - \vartheta u = 0 & \text{on } \Gamma_2, \end{cases}$$

has one and only one solution in \mathbb{V} such that

$$\|u\| \leq c_{00} \|f\|_1,$$

where $c_{00} > 0$ is a constant which depends only on $\text{mes}(\omega)$.

Proof. By virtue of Lemma 2.1, for all $(u, v) \in \mathbb{V}^2$ we have

$$\int_{\omega} \Delta^2 uv = a_0(u, v) + \int_{\Gamma} [(\partial_{\nu} \Delta u + (1 - \mu) B_2 u)v - (\Delta u + (1 - \mu) B_1 u) \partial_{\nu} v]. \quad (4)$$

Since $v \in \mathbb{V}$, we have

$$v|_{\Gamma_0} = 0, \quad v|_{\Gamma_1} = 0, \quad \partial_{\nu} v|_{\Gamma_0} = 0, \quad (\partial_{\nu} \Delta u + (1 - \mu) B_2 u)|_{\Gamma_2} = 0,$$

and

$$(\Delta u + (1 - \mu) B_1 u)|_{\Gamma_1 \cup \Gamma_2} = 0, \quad \int_{\Gamma_2} (\partial_{\nu} \Delta u + (1 - \mu) B_2 u)v = \vartheta \int_{\Gamma_2} uv,$$

hence, with (4) we deduce that

$$a_0(u, v) + \vartheta \int_{\Gamma_2} uv = \int_{\omega} fv = l(v).$$

The mapping $a_0(\cdot, \cdot)$ is a bilinear, symmetric and continuous in the Hilbert space \mathbb{V} . Moreover, the linear operator $l(\cdot)$ is also continuous.

So

$$\forall u \in \mathbb{V}, \quad a_0(u, u) = \int_{\omega} (\Delta u)^2 - (1 - \mu) \int_{\omega} [u, u] = \|u\|_0^2 - (1 - \mu) \int_{\omega} [u, u]$$

and

$$\int_{\omega} [u, u] = \int_{\omega} (2\partial_{11} u \partial_{22} u - 2(\partial_{12} u)^2) \leq \int_{\omega} 2\partial_{11} u \partial_{22} u.$$

Moreover,

$$\int_{\omega} (\Delta u)^2 = \int_{\omega} (\partial_{11} u + \partial_{22} u)^2 = \int_{\omega} (\partial_{11} u)^2 + (\partial_{22} u)^2 + 2 \int_{\omega} (\partial_{11} u \partial_{22} u).$$

It follows that

$$\int_{\omega} [u, u] \leq \|u\|_0^2,$$

this implies that

$$a_0(u, u) = \int_{\omega} (\Delta u)^2 - (1 - \mu) \int_{\omega} [u, u] \geq \|u\|_0^2 - (1 - \mu) \|u\|_0^2 = \mu \|u\|_0^2.$$

Using Remark 2.1, we have

$$\exists \alpha > 0, \quad a_0(u, u) \geq \alpha \|u\|^2.$$

Then the map $a_0(\cdot, \cdot)$ is coercive.

It turns out that, by the Lax-Milgramme theorem, the following problem

$$\forall v \in \mathbb{V}, \quad a_0(u, v) + \vartheta \int_{\Gamma_2} uv = \int_{\omega} fv = l(v)$$

has one and only one solution in \mathbb{V} .

To prove completely the theorem we show that

$$\|u\| \leq c_0 \|f\|_1.$$

Since u is a solution of the following problem

$$\forall v \in \mathbb{V}, \quad a_0(u, v) + \vartheta \int_{\Gamma_2} uv = \int_{\omega} fv = l(v),$$

and using the injection $H^2(\omega) \hookrightarrow C(\bar{\omega})$, we have

$$\forall u \in \mathbb{V}, \quad \exists \beta > 0 \text{ such that } \|u\|_{\infty} \leq \beta \|u\|,$$

with $a_0(u, u) + \vartheta \int_{\Gamma_1} u^2$ being coercive, then there exists $\alpha > 0$ such that

$$\alpha \|u\|^2 \leq a_0(u, u) + \vartheta \int_{\Gamma_2} u^2 = \int_{\omega} fu \leq \|u\|_{\infty} \|f\|_1 \leq \beta \|u\| \|f\|_1.$$

Finally,

$$\|u\| \leq c_{00} \|f\|_1$$

with $c_{00} = \frac{\beta}{\alpha}$.

Now, let us put

$$F_1(u, \phi) = [\phi + F_0, u + \theta] - L(u). \tag{5}$$

Before giving our main result, we now state the following results.

Proposition 2.2 *Let $(u, v) \in (H_0^2(\omega))^2$, $\theta \in H^2(\omega)$ and $F_0 \in H^2(\omega)$ be with small norms. Let $\phi, \varphi \in H_0^2(\omega)$ be the solutions of the following two problems:*

$$\Delta^2 \phi = -[u, u] \quad \text{and} \quad \Delta^2 \varphi = -[v, v].$$

Then the following estimations

$$\left| [u, \phi] - [v, \varphi] \right|_2 \leq c_1 \|u - v\|$$

and

$$|F_1(u, \phi) - F_1(v, \varphi)|_1 \leq c_1 \|u - v\|$$

hold for some $0 < c_1 < 1$.

Proof. Following [3] and Proposition 2.1 we have

$$\left| [u, \phi] - [v, \varphi] \right|_2 \leq k(\|u\|^2 + \|v\|^2) \|u - v\|$$

for some $k > 0$. Let $c > 0$ be small enough so that $\|u\| \leq c$ and $\|v\| \leq c$. We have

$$\left| [u, \phi] - [v, \varphi] \right|_2 \leq 2kc^2 \|u - v\|,$$

and

$$\left| [u, \phi] - [v, \varphi] \right|_1 \leq k_1 \left| [u, \phi] - [v, \varphi] \right|_2 \leq 2kk_1c^2 \|u - v\|.$$

Moreover, we have

$$\begin{aligned}
|[u - v, F_0]|_1 &\leq (\int_{\omega} |\partial_{11}(u - v)| |\partial_{22}F_0|) + (\int_{\omega} |\partial_{22}(u - v)| |\partial_{11}F_0|) \\
&\quad + 2(\int_{\omega} |\partial_{12}(u - v)| |\partial_{12}F_0|) \\
&\leq \|\partial_{22}F_0\|_2 |\partial_{11}(u - v)|_2 + \|\partial_{11}F_0\|_2 |\partial_{22}(u - v)|_2 \\
&\quad + 2 \|\partial_{12}F_0\|_2 |\partial_{12}(u - v)|_2 \\
&\leq 4c_2 \|F_0\|_{2,\omega} \|u - v\|.
\end{aligned}$$

Using the similar proof for the next inequality, with Proposition 2.1 and Theorem 2.2 we have

$$\begin{aligned}
|[\phi - \varphi, \theta]|_1 &\leq 4c_2 \|\theta\|_{2,\omega} \|\phi - \varphi\| \leq 4c_0c_2 \|\theta\|_{2,\omega} |[u, u] - [v, v]|_1 \\
&\leq 4c_0c_2 \|\theta\|_{2,\omega} \left(|[u, u - v]|_1 + |[v, u - v]|_1 \right) \\
&\leq 16c_0c_2 \|\theta\|_{2,\omega} (\|u\| + \|v\|) \|u - v\| \\
&\leq 32c_0c_2c \|\theta\|_{2,\omega} \|u - v\|,
\end{aligned}$$

and so, with $c_3 = 3 \max(4c_2c_0, 32cc_0c_2, 1)$

$$\begin{aligned}
|F_1(u, \phi) - F_1(v, \varphi)|_1 &\leq \left| [\phi + F_0, u + \theta] - [\varphi + F_0, v + \theta] \right|_1 + |L(u - v)|_1 \\
&\leq \left| [\phi, u] - [\varphi, v] \right|_1 + \left| [F_0, u - v] \right|_1 + \left| [\theta, \phi - \varphi] \right|_1 \\
&\quad + \|L\| \|u - v\| \\
&\leq (2kk_1c^2 + 4c_2c_0 \|F_0\|_{2,\omega} + 32cc_0c_2 \|\theta\|_{2,\omega} + \|L\|) \|u - v\| \\
&\leq (2kk_1c^2 + c_3(\|F_0\|_{2,\omega} + \|\theta\|_{2,\omega} + \|L\|)) \|u - v\|.
\end{aligned}$$

If we choose

$$\|\theta\|_{2,\omega} + \|F_0\|_{2,\omega} + \|L\| < \frac{1}{c_3} \quad \text{and} \quad 0 < c < \sqrt{\frac{1 - c_3(\|F_0\|_{2,\omega} + \|\theta\|_{2,\omega} + \|L\|)}{2c_0kk_1}},$$

we have

$$0 < c_1 = 2kk_1c^2 + c_3(\|F_0\|_{2,\omega} + \|\theta\|_{2,\omega} + \|L\|) < 1,$$

we then conclude the proof.

Remark 2.2 In the next result, from the mechanical point of view, our weaker assumptions concerning F_0 in $H_0^2(\omega)$ mean that no external stresses are applied to the shell [3]. F_0 is a given function determined by mechanical loads. For some of the results, less regularity on F_0 is required. For example, to prove the uniqueness of weak solution to the dynamic problem with free boundary conditions and, also, to the thermoelastic plates, some authors take F_0 in $H_0^{3+\epsilon}(\omega)$.

3 Iterative Approach: the Main Results

We will study the problem (\mathbb{P}) by considering the following iterative problem.

Let $n \geq 1$, $0 \neq u_0 \in \mathbb{V}$ be given. We first find $\phi_n \in H_0^2(\omega)$ as a solution of the equation $\Delta^2 \phi_n = -[u_{n-1}, u_{n-1} + 2\theta]$ and u_n as a solution of the following problem:

$$(\mathbb{P}_n) \begin{cases} \Delta^2 u_n = F_1(u_{n-1}, \phi_n) + p & \text{in } \omega, \\ u_n = \partial_\nu u_n = 0 & \text{on } \Gamma_0, \\ u_n = 0, \Delta u_n + (1 - \mu)B_1 u_n = 0 & \text{on } \Gamma_1, \\ \Delta u_n + (1 - \mu)B_1 u_n = 0, \partial_\nu(\Delta u_n) + (1 - \mu)B_2 u_n - \vartheta u_n = 0 & \text{on } \Gamma_2, \end{cases}$$

where F_1 is defined by (5).

We are now in a position to state our main result of this section.

Theorem 3.1 *Let $p \in L^2(\omega)$. If $|p|_2, \|\theta\|_{2,\omega}, \|L\|$ and $\|F_0\|_{2,\omega}$ are small, then the problem (\mathbb{P}) has one and only one solution $(u, \phi) \in \mathbb{V} \times H_0^2(\omega)$.*

Proof. We divide it into three steps.

Step 1: Let us consider the problem (\mathbb{P}_n) with $u_0 \neq 0$. We will show that

$$\forall n \in \mathbb{N}, \|u_n\| \leq \|u_0\| \text{ and } \|\phi_{n+1}\| \leq \|u_0\|.$$

For $n = 0$, we have $\|u_0\| \leq \|u_0\|$. Otherwise, for ϕ_1 being the solution of the problem $\Delta^2 \phi_1 = -[u_0, u_0 + 2\theta]$, Proposition 2.1 and Theorem 2.2 ensure that there exists $c_0 > 0$ such that

$$\|\phi_1\| \leq c_0 \|[u_0, u_0 + 2\theta]\|_1,$$

using the proof of Proposition 2.2 with

$$\|u_0\| < c, \quad 0 < c_0 k k_1 c < 1 \text{ and } \|\theta\|_{2,\omega} \leq \frac{1 - c_0 k k_1 c}{8c_0},$$

we can deduce that

$$\|\phi_1\| \leq c_0 k k_1 \|u_0\|^2 + 8c_0 \|\theta\|_{2,\omega} \|u_0\| \leq (c_0 k k_1 c + 8c_0 \|\theta\|_{2,\omega}) \|u_0\| \leq \|u_0\|.$$

The desired inequalities are true for $n = 0$.

Suppose that

$$\forall k = 1, \dots, n, \|u_k\| \leq \|u_0\| \text{ and } \|\phi_{k+1}\| \leq \|u_0\|.$$

Since u_{n+1} is a solution of the problem (\mathbb{P}_{n+1}) , Theorem 2.3 yields that there exists $c_{00} > 0$, and by Proposition 2.2 we have that

$$\begin{aligned} \|u_{n+1}\| &\leq c_{00}(|F_1(u_n, \phi_{n+1})|_1 + |p|_1) \\ &\leq c_{00}(c_1 \|u_n\| + |p|_1) \\ &\leq c_{00}(c_1 \|u_0\| + |p|_1). \end{aligned}$$

If we choose $c > 0$ sufficiently small, such that

$$0 < c_1 < 1, \quad 0 < c_{00}c_1 < 1 \text{ and } \|p\|_1 \leq \frac{(1 - c_{00}c_1)}{c_{00}} \|u_0\|,$$

it follows that

$$\|u_{n+1}\| \leq \|u_0\|.$$

Moreover, for ϕ_{n+2} being the solution of the problem $\Delta^2\phi_{n+2} = -[u_{n+1}, u_{n+1} + 2\theta]$ and after the case $n = 0$, we have

$$\|u_0\| < c, \quad 0 < c_0kk_1c < 1 \text{ and } \|\theta\|_{2,\omega} \leq \frac{1 - c_0kk_1c}{8c_0},$$

moreover, we can deduce that

$$\|\phi_{n+2}\| \leq c_0kk_1 \|u_{n+1}\|^2 + 8c_0 \|\theta\|_{2,\omega} \|u_{n+1}\| \leq (c_0kk_1c + 8c_0 \|\theta\|_{2,\omega}) \|u_{n+1}\| \leq \|u_0\|.$$

Hence,

$$\forall n \in \mathbb{N}, \quad \|u_n\| \leq \|u_0\|, \text{ and } \|\phi_{n+1}\| \leq \|u_0\|.$$

Step 2: Let $m < n$, u_n (resp, u_m) be a solution of the problem (\mathbb{P}_n) (resp, (\mathbb{P}_m)), then $u_n - u_m$ is a solution of the following problem :

$$\left\{ \begin{array}{ll} \Delta^2(u_n - u_m) = F_1(u_{n-1}, \phi_{n-1}) - F_1(u_{m-1}, \phi_{m-1}) & \text{in } \omega, \\ u_n - u_m = 0 \quad \partial_\nu(u_n - u_m) = 0 & \text{on } \Gamma_0, \\ u_n - u_m = 0, \quad \Delta(u_n - u_m) + (1 - \mu)B_1(u_n - u_m) = 0 & \text{on } \Gamma_1, \\ \Delta(u_n - u_m) + (1 - \mu)B_1(u_n - u_m) = 0 & \text{on } \Gamma_2, \\ \partial_\nu(\Delta(u_n - u_m) + (1 - \mu)B_2(u_n - u_m)) - \vartheta(u_n - u_m) = 0 & \text{on } \Gamma_2. \end{array} \right.$$

Using Theorem 2.3 again, we have

$$\begin{aligned} \|u_n - u_m\| &\leq c_{00} \|F_1(u_{n-1}, \phi_{n-1}) - F_1(u_{m-1}, \phi_{m-1})\|_1 \\ &\leq c_{00}c_1 \|u_{n-1} - u_{m-1}\| \\ &\leq (c_{00}c_1)^m \|u_{n-m+1} - u_0\| \\ &\leq (c_{00}c_1)^m \sum_{k=0}^{n-m-1} (c_{00}c_1)^k \|u_1 - u_0\| \\ &\leq 2(c_{00}c_1)^m \sum_{k=0}^{n-m-1} (c_{00}c_1)^k \|u_0\|. \end{aligned}$$

Moreover, for $\phi_n - \phi_m$ being the solution of the problem

$$\Delta^2(\phi_n - \phi_m) = -[u_{n+1}, u_{n+1} + 2\theta] + [u_{m+1}, u_{m+1} + 2\theta],$$

Theorem 2.2 ensures that there exists $c_0 > 0$ such that

$$\begin{aligned} \|\phi_n - \phi_m\| &\leq c_0 \left| [u_{n+1}, u_{n+1} + 2\theta] - [u_{m+1}, u_{m+1} + 2\theta] \right|_1 \\ &\leq c_0 \left(|[u_{n+1}, u_{n+1} - u_{m+1}]|_1 \right. \\ &\quad \left. + |[u_{m+1}, u_{n+1} - u_{m+1}]|_1 + |[2\theta, u_{n+1} - u_{m+1}]|_1 \right) \\ &\leq 8c_0 k k_1 c \|u_{n+1} - u_{m+1}\| + 8c_0 \|\theta\|_{2,\omega} \|u_{n+1} - u_{m+1}\| \\ &\leq (8c_0 k k_1 c + 8c_0 \|\theta\|_{2,\omega}) \|u_{n+1} - u_{m+1}\|. \end{aligned}$$

Using the proof of Proposition 2.2 and Theorem 2.2 with

$$\|u_0\| < c, \quad 0 < 8c_0 k k_1 c < 1 \quad \text{and} \quad \|\theta\|_{2,\omega} \leq \frac{1 - 8c_0 k k_1 c}{8c_0},$$

we can deduce that

$$\|\phi_n - \phi_m\| \leq (8c_0 k k_1 c + 8c_0 \|\theta\|_{2,\omega}) \|u_{n+1} - u_{m+1}\|.$$

This implies that the sequence $(u_n, \phi_n)_{n \geq 0}$ is a Cauchy sequence in $\mathbb{V} \times H_0^2(\omega)$, hence the sequence $(u_n, \phi_n)_{n \geq 0}$ converges to (u, ϕ) in $\mathbb{V} \times H_0^2(\omega)$ and, with Proposition 2.2, we deduce that $F_1(u_n, \phi_{n+1}) + p$ converges to $F_1(u, \phi) + p$ in $L^1(\omega)$.

Since the operator "trace" and the operator " ∂_ν " are continuous, we have that $(u_n)_{|\Gamma_0}, (u_n)_{|\Gamma_1}, (u_n)_{|\Gamma_2}$ and $\partial_\nu(u_n)_{|\Gamma_0}$ converge to $u_{|\Gamma_0}, u_{|\Gamma_1}, u_{|\Gamma_2}$ and $\partial_\nu u_{|\Gamma_0}$ and ϕ_n converges to ϕ on Γ .

Finally, we have that $u_{|\Gamma_0} = u_{|\Gamma_1} = 0, \partial_\nu u_{|\Gamma_0} = 0, \phi_{|\Gamma} = 0$ and $\partial_\nu \phi_{|\Gamma} = 0$.

To conclude that u is a solution of the problem (\mathbb{P}) , we show that u satisfies the following equality:

$$(\Delta u + (1 - \mu)B_1 u)_{|\Gamma_1 \cup \Gamma_2} = 0 \quad \text{and} \quad (\partial_\nu \Delta u + (1 - \mu)B_2 u - \vartheta u)_{|\Gamma_2} = 0.$$

By Lemma 2.1 we have for all $v \in \mathbb{V}$

$$\begin{aligned} \int_\omega \Delta^2(u_n - u)v &= a_0(u_n - u, v) + \int_\Gamma (\partial_\nu \Delta(u_n - u) + (1 - \mu)B_2(u_n - u))v \\ &\quad - \int_\Gamma (\Delta(u_n - u) + (1 - \mu)B_1(u_n - u))\partial_\nu v. \end{aligned}$$

But u_n is a solution of the problem (\mathbb{P}_n) , it follows that

$$(\Delta u_n + (1 - \mu)B_1 u_n)_{|\Gamma_1 \cup \Gamma_2} = 0 \quad \text{and} \quad (\partial_\nu \Delta u_n + (1 - \mu)B_2 u_n)_{|\Gamma_2} - \vartheta(u_n)_{|\Gamma_2} = 0, \quad (6)$$

or $v \in \mathbb{V}$ implies that $v_{|\Gamma_1 \cup \Gamma_2} = 0$ and $\partial_\nu v_{|\Gamma_0} = 0$, then

$$\int_\Gamma (\Delta(u_n - u) + (1 - \mu)B_1(u_n - u))\partial_\nu v = \int_{\Gamma_0 \cup \Gamma_1 \cup \Gamma_2} (\Delta(u_n - u) + (1 - \mu)B_1(u_n - u))\partial_\nu v,$$

$$= \int_{\Gamma_1 \cup \Gamma_2} (\Delta(u_n - u) + (1 - \mu)B_1(u_n - u)) \partial_\nu v.$$

This, together with (6), yield

$$\int_{\Gamma_1 \cup \Gamma_2} (\Delta(u_n - u) + (1 - \mu)B_1(u_n - u)) \partial_\nu v = - \int_{\Gamma_1 \cup \Gamma_2} (\Delta u + (1 - \mu)B_1 u) \partial_\nu v,$$

hence

$$\int_{\Gamma} (\Delta(u_n - u) + (1 - \mu)B_1(u_n - u)) \partial_\nu v = - \int_{\Gamma_1 \cup \Gamma_2} (\Delta u + (1 - \mu)B_1 u) \partial_\nu v.$$

Moreover,

$$\begin{aligned} \int_{\Gamma} (\partial_\nu \Delta(u_n - u) + (1 - \mu)B_2(u_n - u)) v &= \int_{\Gamma_0 \cup \Gamma_1 \cup \Gamma_2} (\partial_\nu \Delta(u_n - u) + (1 - \mu)B_2(u_n - u)) v, \\ &= \int_{\Gamma_2} (\partial_\nu \Delta(u_n - u) + (1 - \mu)B_2(u_n - u)) v. \end{aligned}$$

In view of (6), we deduce that

$$\int_{\Gamma} (\partial_\nu \Delta(u_n - u) + (1 - \mu)B_2(u_n - u)) v = \vartheta \int_{\Gamma_2} u_n v - \int_{\Gamma_2} (\partial_\nu \Delta u + (1 - \mu)B_2 u) v.$$

It follows that

$$\begin{aligned} \int_{\omega} \Delta^2(u_n - u) v &= a_0(u_n - u, v) + \vartheta \int_{\Gamma_2} u_n v - \int_{\Gamma_2} (\partial_\nu \Delta u + (1 - \mu)B_2 u) v \\ &\quad + \int_{\Gamma_1 \cup \Gamma_2} (\Delta u + (1 - \mu)B_1 u) \partial_\nu v. \end{aligned}$$

Now, letting $n \rightarrow +\infty$ in the next equality, we deduce that

$$\forall v \in \mathbb{V}, \quad \vartheta \int_{\Gamma_2} uv - \int_{\Gamma_2} (\partial_\nu \Delta u + (1 - \mu)B_2 u) v + \int_{\Gamma_1 \cup \Gamma_2} (\Delta u + (1 - \mu)B_1 u) \partial_\nu v = 0.$$

This equality implies that

$$\forall v \in H_0^1(\omega) \cap \mathbb{V}, \quad \int_{\Gamma_1 \cup \Gamma_2} (\Delta u + (1 - \mu)B_1 u) \partial_\nu v = 0,$$

it turns out that

$$\Delta u + (1 - \mu)B_1 u = 0, \quad \text{on } \Gamma_1 \cup \Gamma_2.$$

And also, we deduct

$$\forall v \in \mathbb{V}, \quad \vartheta \int_{\Gamma_2} uv - \int_{\Gamma_2} (\partial_\nu \Delta u + (1 - \mu)B_2 u) v = 0,$$

it follows that

$$\partial_\nu \Delta u + (1 - \mu)B_2 u - \vartheta u = 0, \quad \text{on } \Gamma_2.$$

Finally, (u, ϕ) is a solution of the static von Karman equations in $\mathbb{V} \times H_0^2(\omega)$.

Step 3 : For the uniqueness, we suppose that the problem (\mathbb{P}) has two solutions (u_1, ϕ_1) and (u_2, ϕ_2) in $\mathbb{V} \times H_0^2(\omega)$ such that

$$\|u_1\| \leq c \text{ and } \|u_2\| \leq c,$$

where, c is sufficiently small. Since $u_1 - u_2$ is a solution of the following problem:

$$\begin{cases} \Delta^2(u_1 - u_2) = F_1(u_1, \phi_1) - F_1(u_2, \phi_2) & \text{in } \omega, \\ u_1 - u_2 = 0, \quad \partial_\nu(u_1 - u_2) = 0 & \text{on } \Gamma_0, \\ u_1 - u_2 = 0, \quad \Delta(u_1 - u_2) + (1 - \mu)B_1(u_1 - u_2) = 0 & \text{on } \Gamma_1, \\ \Delta(u_1 - u_2) + (1 - \mu)B_1(u_1 - u_2) = 0 & \text{on } \Gamma_2, \\ \partial_\nu(\Delta(u_1 - u_2) + (1 - \mu)B_2(u_1 - u_2)) - \vartheta(u_1 - u_2) = 0 & \text{on } \Gamma_2. \end{cases}$$

Theorem 2.3 implies that there exists $c_{00} > 0$ such that

$$\|u_1 - u_2\| \leq c_{00} |F_1(u_1, \phi_1) - F_1(u_2, \phi_2)|_1 \leq c_{00}c_1 \|u_1 - u_2\|,$$

c is small, thus $0 < c_{00}c_1 < 1$, then $u_1 = u_2$ and $\phi_1 = \phi_2$.

Lastly, the stationary von Karman equations have one and only one solution (u, ϕ) in the space $\mathbb{V} \times H_0^2(\omega)$.

Remark 3.1 In this section we described an iterative method for constructing a unique weak solution, this technique is a good tool for illustrating this weak solution from the numerical point of view.

4 Conclusion

In this paper, we described an iterative method for constructing a unique weak solution to the model with free boundary conditions of buckling and flexible phenomenon of small nonlinear vibrations of the homogenous, isotropic and elastic thin shells of uniform thickness. Our approach is a good tool for justifying the theoretical results under the following weak assumption $F_0 \in H^2(\omega)$. Similar study for the models of dynamic von Karman equations with and without rotational inertia and for free boundary conditions of the shell could be the purpose for future research.

Acknowledgments

The authors would like to thank the anonymous referee for his/her valuable comments and suggestions which improved the final version of the present manuscript.

References

[1] A. Aberqui, J. Bennouna and M. Elmassoudi. Nonlinear Elliptic Equation with Some Measure Data in Musielak-Orlicz Spaces. *Nonlinear Dynamics and Systems Theory* **19**(2) (2019) 227–242.

- [2] A. Yu. Aleksandrov, A. A. Martynyuk and A. A. Tikhonov. Some Problems of Attitude Dynamics and Control of a Rigid Body. *Nonlinear Dynamics and Systems Theory* **20**(2) (2020) 132–143.
- [3] I. Chueshov and I. Lasiecka. *von Karman Evolution, Well-posedness and Long Time Dynamics*. New York, Springer, 2010.
- [4] P.G. Ciarlet and L. Gratie. From the classical to the generalized von Karman and Marguerre von Karman equations. *Journal of Computational and applied Mathematics* **190** (2006) 470–486.
- [5] P.G. Ciarlet. *Mathematical Elasticity. Vol. I. Three Dimensional Elasticity*. Amsterdam, Elsevier Science, 1988.
- [6] P.G. Ciarlet and R. Rabier. *Les Equations de von Karman*. New York, Springer, 1980.
- [7] P.G. Ciarlet. *Mathematical Elasticity. Vol.III, Theory of Shells*. Amsterdam, Elsevier, 2000.
- [8] M. Dilmi, H. Benseridi and Guesmia. Problme de contact sans frottement-Dirichlet pour les quations de Laplace et de Lamé dans un polygone. *Analele Universitatii oradea, Fasc. Matematica, Tom XIV*, 2007 212–236.
- [9] R. Glowinski and O. Pironneau. Numerical methods for the first biharmonic equation and for the two-dimensional stokes problem. *SIAM* **21** (1979) 167–212.
- [10] P. Grisvard. *Singularities in Boundary Value Problems*. Masson, Paris, 1992.
- [11] J.L. Lions and E. Magenes. *Problème aux Limites non Homogènes et Applications*. Vol. 1. Dunod, Paris, 1968.
- [12] J.L. Lions. *Quelques Méthodes de Résolutions des Problèmes aux Limites non Linéaires*. Dunod, Paris, 1969.
- [13] N.F. Morozov. *Selected Two-Dimensional Problems of Theory Elasticity*. LGU, Leningrad, 1978.
- [14] J. Oudaani. Numerical approach to the Uniqueness solution of von Karman evolution. *International Journal of Mathematics in Operational Research* **13**(4) (2018) 450–470.
- [15] S. Stuart Antman. Theodore von Karman. In: *A Panorama of Hungarian Mathematics in the Twentieth Centuray*, pp. 373–382. Springer, Berlin, 2006.
- [16] A. Talha, A. Benkirane and M.S.B. Elemine Vall. Existence of Renormalized Solutions for Some Strongly Parabolic Problems in Musielak-Orlicz-Sobolev Spaces. *Nonlinear Dynamics and Systems Theory* **19**(1) (2019) 97–110.



Stability of the Artificial Equilibrium Points in the Low-Thrust Restricted Three-Body Problem when the Smaller Primary is an Oblate Spheroid

Md. Sanam Suraj¹, Amit Mittal², Krishan Pal^{3*} and Deepak Mittal⁴

¹ *Department of Mathematics, Sri Aurbindo College, University of Delhi, New Delhi, India*

² *Department of Mathematics, A.R.S.D. College, University of Delhi, New Delhi, India*

³ *Department of Mathematics, Maharaja Agrasen College, University of Delhi, New Delhi, India*

⁴ *Department of Computer Science, Deen Dayal Upadhaya College, University of Delhi, New Delhi-110021, India*

Received: December 27, 2019; Revised: October 2, 2020

Abstract: The aim of this paper is to study the existence and stability of the artificial equilibrium points (AEPs) in the low-thrust restricted three-body problem when the smaller primary is an oblate spheroid and the bigger one is a point mass. The AEPs are obtained by cancelling the gravitational and centrifugal forces with continuous low-thrust at a non-equilibrium point. The AEPs are calculated numerically and their movement is shown graphically. The positions of these AEPs will depend on the magnitude and directions of the low-thrust acceleration. Firstly, we have linearized the equations of motion of the spacecraft. The linear stability of the AEPs is studied. We have drawn the stability regions in the $x - y$, $x - z$ and $y - z$ -planes and studied the effect of the oblateness parameter $A \in (0, 1)$ on the motion of the spacecraft. Further, we have determined the zero velocity curves to study the possible boundary regions of motion of the spacecraft. Finally, we have concluded about the effects of the relevant parameters in this problem.

Keywords: *restricted three-body problem; artificial equilibrium points; low-thrust; stability; oblate spheroid; zero velocity curves.*

Mathematics Subject Classification (2010): 70F07, 70F10, 70F15.

* Corresponding author: <mailto:kp11987@gmail.com>

1 Introduction

The classical restricted three-body problem (R3BP) consists of five libration points, three of them are on the straight line joining the primaries, called collinear libration points, and two of them set up equilateral triangle with the primaries. The collinear libration points $L_{1,2,3}$ are always unstable in the linear sense for any value of the mass parameter μ whereas the triangular points $L_{4,5}$ are stable if $\mu < \mu_c = 0.03852\dots$, see Szebehely [1]. In recent times, many perturbing forces such as oblateness, radiation forces of the primaries, Coriolis and centrifugal forces etc., have been included in the study of the R3BP. Subbarao and Sharma [2] have investigated the non-collinear libration points in the circular restricted three-body problem (CR3BP) by taking the bigger primary as an oblate spheroid and found that these libration points form nearly equilateral triangle with the primaries. Sharma et al. [3] have studied the existence and stability of libration points in the R3BP by considering both the primaries as triaxial rigid bodies. In their study, they have found five libration points, in which two are triangular and the remaining three are collinear. Prado [4] has worked on the space trajectories in the circular restricted three-body problem. Further, he assumed that the spacecraft moves under the gravitational forces of two massive bodies which are in circular orbits. He also investigated the orbits which can be used to transfer a spacecraft from one body back to the same body or to transfer a spacecraft from one body to the respective Lagrangian points L_4 and L_5 . Correa et al. [5] introduced two models of the restricted three-body and four-body problems. They have investigated the transfer orbits from a parking orbit around the Earth to the halo orbit in both the dynamical models. Also, they have compared the total velocity increment to both the models.

If continuous low-thrust is used by a spacecraft to balance the gravitational and centrifugal forces, the new equilibrium points appear. These points are usually referred as the Artificial Equilibrium Points (AEPs). The AEP overcomes the position limitation of the classical equilibrium points as it provides a variety of choices for the design of space missions. Therefore, it has been extensively studied by many authors. These studies include the location, stability and periodic orbits of equilibrium points with different types of propulsions such as solar-sail, solar electric propulsion and other low-thrust propulsion.

Farquhar [6] studied the concept of telecommunication systems using the Lagrange points and investigated ballistic periodic orbits about these points in the Earth-Moon system. Dusek [7] and Broschart [8] have studied the stability of equilibrium points with continuous control acceleration. Morimoto et al. [9] have studied the existence and stability of the AEPs in the low-thrust R3BP and found the stable regions. They have used the discriminant of cubic equation and the Descartes sign rule to study the stability of these AEPs. Baig and McInnes [10] have investigated the artificial three-body equilibria for hybrid low-thrust propulsion. In their study, they have introduced a new concept of creating AEPs in the R3BP when the third body uses a hybrid of solar-sail and electric propulsion. Further, Bombardelli and Pelaez [11] have found the locations of AEPs, stability and minimum control acceleration in the CR3BP. Aliasi et al. [12] have proposed a general mathematical model for different propulsion system such as solar-sail, magnetic and electric sail in the CR3BP to study the existence, geometry and stability of AEPs. Furthermore, Ceccaroni and Biggs [13] have investigated the stability conditions and stable regions for the artificial equilibrium points in the low-thrust circular R4BP. In their study, they have obtained eight natural equilibrium points, four of which

are closed to the smaller body. Among the four equilibrium points close to the smaller body, two are stable and two are unstable. Bu et al. [14] have investigated the positions and dynamical characteristic of the AEPs in a binary asteroid system with continuous low-thrust. Recently, Ranjana and Kumar [15] have studied the existence and stability of the AEPs in the circular restricted problem of 2+2 bodies when the shape of a larger mass is taken to be an oblate spheroid. More recently, Sushil et al. [16] have studied the existence and stability of the equilibrium points in the restricted three-body problem with a Geo-Centric satellite including the Earth’s equatorial ellipticity.

In this paper, we have studied the existence and linear stability of the AEPs by considering the smaller primary as an oblate spheroid and the bigger one as a point mass. This paper is organized as follows. In Section 2, we have derived the equations of motion of the spacecraft. In Section 3, we have obtained the locations of AEPs. In Section 4, we have derived the stability conditions and stable regions. In Section 5, we have drawn the zero velocity curves. Finally, in Section 6, we have concluded the results obtained.

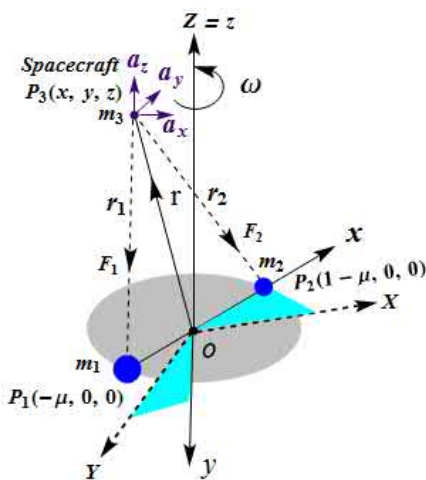


Figure 1: Configuration of the problem.

2 Equations of Motion

Let two celestial bodies of masses m_1 and m_2 ($m_1 > m_2$) be the primaries moving with angular velocity ω in circular orbits about their center of mass O taken as the origin, and let the infinitesimal body (spacecraft) of mass m_3 be moving in the plane of motion of m_1 and m_2 . The motion of the spacecraft is effected by the motion of m_1 and m_2 but not affects them. We shall determine the equations of motion of the infinitesimal body of mass m_3 in dimensionless synodic variables. The line joining the primaries m_1 and m_2 is taken as the X -axis, and the line which passes through the origin O and perpendicular to the OX -axis and is lying in the plane of motion of m_1 and m_2 is considered as the Y -axis, the line which passes through the origin and is perpendicular to the plane of motion of the primaries is taken as the Z -axis. In a synodic frame,

the system of synodic coordinates $O(xyz)$ is initially coincident with the system of inertial coordinates $O(XYZ)$, rotating with the angular velocity ω about the Z -axis (the z axis is coincident with the Z -axis). Let the primaries of masses m_1 and m_2 be located at $P_1(-\mu, 0, 0)$ and $P_2(1-\mu, 0, 0)$, respectively, and the spacecraft be at the point $P_3(x, y, z)$ (see Fig. 1). The angular velocity of the primaries is given by the relation $\omega = \sqrt{\frac{G(m_1+m_2)}{l^3}}$, where l is the distance between the primaries, and G is the Gravitational constant. We scale the units by taking the sum of the masses and the distance between the primaries both equal to unity. Therefore, $m_1 = 1 - \mu$, $m_2 = \mu$ and $\mu = \frac{m_2}{m_1+m_2}$ with $m_1 + m_2 = 1$. Also, the scale of the time is chosen so that the gravitational constant is unity. The equation of motion of the spacecraft in vector form is expressed as

$$\frac{d^2\mathbf{r}}{dt^2} + 2\boldsymbol{\omega} \times \frac{d\mathbf{r}}{dt} = \mathbf{a} - \nabla\Omega = \mathbf{F}, \quad (1)$$

where Ω is the potential (McCuskey [17]) of the system that combines the gravitational potential and the potential from the centripetal acceleration which is defined as

$$\Omega = -\frac{n^2}{2}(x^2 + y^2) - \frac{(1-\mu)}{r_1} - \frac{\mu}{r_2} - \frac{\mu A}{2r_2^3},$$

and

$$\begin{aligned} \mathbf{F} &= \text{total force acting on } m_3, \\ &= \mathbf{F}_1 + \mathbf{F}_2, \\ \mathbf{F}_1 &= \text{gravitational force exerted on } m_3 \text{ due} \\ &\quad \text{to } m_1 \text{ along } \mathbf{P}_3\mathbf{P}_1, \\ \mathbf{F}_2 &= \text{gravitational force exerted on } m_3 \text{ due} \\ &\quad \text{to } m_2 \text{ along } \mathbf{P}_3\mathbf{P}_2. \end{aligned}$$

The vector $\mathbf{a} = (a_x, a_y, a_z)$ is the low-thrust acceleration and $\mathbf{r} = (x, y, z)^T$ is the position vector of the spacecraft from the origin. Thus, the equations of motion of the spacecraft with continuous low-thrust in the dimensionless co-ordinate system can be written as (Morimoto et al. [9])

$$\left. \begin{aligned} \ddot{x} - 2n\dot{y} &= -\Omega_x + a_x = -\Omega_x^*, \\ \ddot{y} + 2n\dot{x} &= -\Omega_y + a_y = -\Omega_y^*, \\ \ddot{z} &= -\Omega_z + a_z = -\Omega_z^*, \end{aligned} \right\} \quad (2)$$

where Ω^* is the effective potential of the system with continuous low-thrust and can be written as

$$\Omega^* = \Omega - a_x x - a_y y - a_z z = -\frac{n^2}{2}(x^2 + y^2) - \frac{(1-\mu)}{r_1} - \frac{\mu}{r_2} - \frac{\mu A}{2r_2^3} - a_x x - a_y y - a_z z,$$

where $r_1 = \sqrt{(x+\mu)^2 + y^2 + z^2}$, $r_2 = \sqrt{(x+\mu-1)^2 + y^2 + z^2}$, $a = \sqrt{a_x^2 + a_y^2 + a_z^2}$, and n is the mean motion of the primaries which is also defined as $n^2 = (1 + \frac{3A}{2})$, where A is the oblateness parameter of m_2 which is defined as $A = \frac{a_1^2 - c_1^2}{5l^2}$, $0 < A < 1$, $a_1 = b_1(a_1 > c_1)$, where a_1, b_1, c_1 are the semi-axes of the rigid-body of mass m_2 , and l is the distance between the primaries.

3 Calculation of the Artificial Equilibrium Points

The AEPs are the solution of the equations $\Omega_x^* = 0, \Omega_y^* = 0, \Omega_z^* = 0$. The AEPs denoted by (x_0, y_0, z_0) are the solution of the equations given by

$$\left. \begin{aligned} -n^2x_0 + \frac{1-\mu}{r_1^3}(x_0 + \mu) + \frac{\mu}{r_2^3}(x_0 - \mu_1 - 1) \left(1 + \frac{3A}{2r_2^2}\right) - a_x &= 0, \\ -n^2y_0 + \frac{1-\mu}{r_1^3}y_0 + \frac{\mu}{r_2^3}y_0 \left(1 + \frac{3A}{2r_2^2}\right) - a_y &= 0, \\ \frac{1-\mu}{r_1^3}z_0 + \frac{\mu}{r_2^3}z_0 \left(1 + \frac{3A}{2r_2^2}\right) - a_z &= 0. \end{aligned} \right\} \quad (3)$$

When $A = 0, \mathbf{a} = (0, 0, 0)$, the above Eqs. (3) reduce to the equations obtained by Szebhely [1]. When $A = 0$, the above Eqs. (3) reduce to the equations obtained by Morimoto et al. [9]. Solve the Eqs. (3) for $z = 0$, then the AEPs are the intersection of $\Omega_x^* = 0$ and $\Omega_y^* = 0$. We have obtained five AEPs for given parameters denoted by L_1, L_2, L_3, L_4 and L_5 . The numerical values of the AEPs are shown in Tables 1, 2. From Table 1, we have observed that there exist three collinear and two non-collinear AEPs when low-thrust acceleration is varying in the x direction. From Table 2, we have observed that there exist five non-collinear AEPs for the fixed values of $\mu = 0.1, \mathbf{a} = (0, 0.0001, 0)$ and for the increasing values of the oblateness parameter A .

We have displayed the movements of AEPs shown graphically in Fig. 2(a, b). In Fig. 2(a), we have plotted the AEPs for the fixed values of $\mu = 0.1, A = 0.01$ and for the increasing values of $\mathbf{a} = (a_x, 0, 0)$. From Fig. 2(a), we have observed that when $\mathbf{a} = (a_x, 0, 0)$ is increasing, the movements of the AEPs L_1, L_2 , and L_3 are almost negligible whereas the AEPs L_4 and L_5 move towards the y -axes. The AEPs L_4 and L_5 are symmetric with respect to the x -axis.

In Fig. 2(b), we have plotted the AEPs for the fixed values of $\mu = 0.1, \mathbf{a} = (0, 0.0001, 0)$ and for the increasing values of the oblateness parameter A . From Fig. 2(b), we have observed that when A is increasing, the AEPs L_1 and L_2 move from right to left towards the primaries m_1 and m_2 , respectively, whereas the AEP L_3 is shifted from left to right towards the bigger primary m_1 and the AEPs L_4 and L_5 move towards the x -axis. Also, we have noticed that the AEPs L_4 and L_5 are not symmetric with respect to the x -axis. We have observed that the AEPs are the new positions of the equilibrium points, with the effect of continuous low-thrust acceleration and oblateness parameters, which are different from the natural equilibrium points.

| $\mu = 0.1$ $A = 0.01$ | | | | |
|---------------------------|---------------|--------------|---------------|------------------------------|
| \mathbf{a} | L_1 | L_2 | L_3 | $L_{4,5}$ |
| (0.0001, 0, 0) | (0.595693, 0) | (1.27013, 0) | (-1.03681, 0) | (0.394700, ± 0.863321) |
| (0.01, 0, 0) | (0.595064, 0) | (1.26863, 0) | (-1.03989, 0) | (0.356034, ± 0.880338) |
| (0.03, 0, 0) | (0.593786, 0) | (1.26563, 0) | (-1.04616, 0) | (0.254245, ± 0.918441) |
| (0.05, 0, 0) | (0.592501, 0) | (1.26267, 0) | (-1.05252, 0) | (0.0946093, ± 0.957963) |

Table 1: The AEPs when the low-thrust acceleration $\mathbf{a} = (a_x, 0, 0)$ is varying in the x -direction.

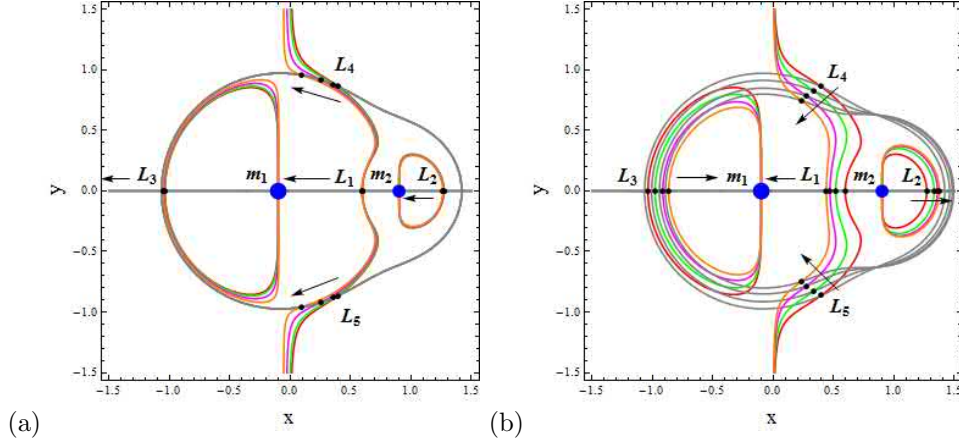


Figure 2: Locations of five AEPs in the low-thrust R3BP for $\mu = 0.1$ under the effect of low-thrust acceleration and oblateness parameters \mathbf{a} , A , respectively, (a) for $A = 0.01$ and for different values of $\mathbf{a} = (0.0001, 0, 0)$ (gray, red), $(0.01, 0, 0)$ (gray, green), $(0.03, 0, 0)$ (gray, magenta), $(0.05, 0, 0)$ (gray, orange), and (b) for $\mathbf{a} = (0, 0.0001, 0)$ and for different values of $A = 0.01$ (gray, red), 0.15 (gray, green), 0.35 (gray, magenta), 0.55 (gray, orange)

| $\mu = 0.1$ | | |
|-------------------------------|--------------------------|-------------------------|
| $\mathbf{a} = (0, 0.0001, 0)$ | | |
| A | L_1 | L_2 |
| $A = 0.01$ | (0.595700, 0.0000172961) | (1.27015, 0.0000656752) |
| $A = 0.15$ | (0.517147, 0.0000140423) | (1.33094, 0.0000541839) |
| $A = 0.35$ | (0.469174, 0.0000122795) | (1.35954, 0.0000424306) |
| $A = 0.55$ | (0.438985, 0.0000112294) | (1.37323, 0.0000347701) |
| L_3 | L_4 | L_5 |
| (-1.036780, 0.001068400) | (0.395227, 0.863036) | (0.394896, -0.863275) |
| (-0.977898, 0.000824811) | (0.336840, 0.826193) | (0.336620, -0.826353) |
| (-0.913935, 0.000611650) | (0.277461, 0.782479) | (0.277319, -0.782585) |
| (-0.864974, 0.000479622) | (0.234858, 0.746633) | (0.234756, -0.746711) |

Table 2: The AEPs in the $x - y$ -plane when the oblateness parameter A is varying.

4 Stability Analysis and Stable Region

For establishing the spacecraft at a non-equilibrium point, a continuous low-thrust is provided to the spacecraft. Now, we give the small displacement to (x_0, y_0, z_0) as $x = x_0 + \delta_x$, $y = y_0 + \delta_y$, $z = z_0 + \delta_z$, ($\delta_x, \delta_y, \delta_z \ll 1$). Using the above displacements, the linearized equations corresponding to Eqs. (2) according to Morimoto et al. [9] are given

by

$$\left. \begin{aligned} \ddot{\delta}_x - 2n\dot{\delta}_y &= (\Omega_{xx}^*)^0 \delta_x + (\Omega_{xy}^*)^0 \delta_y + (\Omega_{xz}^*)^0 \delta_z, \\ \ddot{\delta}_y + 2n\dot{\delta}_x &= (\Omega_{yx}^*)^0 \delta_x + (\Omega_{yy}^*)^0 \delta_y + (\Omega_{yz}^*)^0 \delta_z, \\ \ddot{\delta}_z &= (\Omega_{zx}^*)^0 \delta_x + (\Omega_{zy}^*)^0 \delta_y + (\Omega_{zz}^*)^0 \delta_z, \end{aligned} \right\} \quad (4)$$

where the superscript '0' in Eqs. (4) indicates that the values are to be calculated at the AEP (x_0, y_0, z_0) . Further, the characteristic root λ satisfies

$$\left. \begin{aligned} &\lambda^6 + ((\Omega_{xx}^*)^0 + (\Omega_{yy}^*)^0 + (\Omega_{zz}^*)^0 + 4n^2) \lambda^4 + ((\Omega_{xx}^*)^0 (\Omega_{yy}^*)^0 \\ &+ (\Omega_{xx}^*)^0 (\Omega_{zz}^*)^0 + (\Omega_{yy}^*)^0 (\Omega_{zz}^*)^0 - ((\Omega_{xy}^*)^0)^2 - ((\Omega_{xz}^*)^0)^2 - ((\Omega_{yz}^*)^0)^2 \\ &+ 4n^2 (\Omega_{zz}^*)^0) \lambda^2 + (\Omega_{xx}^*)^0 (\Omega_{yy}^*)^0 (\Omega_{zz}^*)^0 + 2 (\Omega_{xy}^*)^0 (\Omega_{xz}^*)^0 (\Omega_{yz}^*)^0 \\ &- ((\Omega_{xy}^*)^0)^2 (\Omega_{zz}^*)^0 - ((\Omega_{xz}^*)^0)^2 (\Omega_{yy}^*)^0 - ((\Omega_{yz}^*)^0)^2 (\Omega_{xx}^*)^0 = 0. \end{aligned} \right\} \quad (5)$$

Taking $k = \lambda^2$, we have obtained

$$\left. \begin{aligned} &k^3 + ((\Omega_{xx}^*)^0 + (\Omega_{yy}^*)^0 + (\Omega_{zz}^*)^0 + 4n^2) k^2 + ((\Omega_{xx}^*)^0 (\Omega_{yy}^*)^0 \\ &+ (\Omega_{xx}^*)^0 (\Omega_{zz}^*)^0 + (\Omega_{yy}^*)^0 (\Omega_{zz}^*)^0 - ((\Omega_{xy}^*)^0)^2 - ((\Omega_{xz}^*)^0)^2 - ((\Omega_{yz}^*)^0)^2 \\ &+ 4n^2 (\Omega_{zz}^*)^0) k + (\Omega_{xx}^*)^0 (\Omega_{yy}^*)^0 (\Omega_{zz}^*)^0 + 2 (\Omega_{xy}^*)^0 (\Omega_{xz}^*)^0 (\Omega_{yz}^*)^0 \\ &- ((\Omega_{xy}^*)^0)^2 (\Omega_{zz}^*)^0 - ((\Omega_{xz}^*)^0)^2 (\Omega_{yy}^*)^0 - ((\Omega_{yz}^*)^0)^2 (\Omega_{xx}^*)^0 = 0. \end{aligned} \right\} \quad (6)$$

We see that the Eqn. (6) is a cubic equation in k and it can be written as

$$k^3 + d_1 k^2 + d_2 k + d_3 = 0, \quad (7)$$

where

$$\begin{aligned} d_1 &= (\Omega_{xx}^*)^0 + (\Omega_{yy}^*)^0 + (\Omega_{zz}^*)^0 + 4n^2, \\ d_2 &= (\Omega_{xx}^*)^0 (\Omega_{yy}^*)^0 + (\Omega_{xx}^*)^0 (\Omega_{zz}^*)^0 + (\Omega_{yy}^*)^0 (\Omega_{zz}^*)^0 - ((\Omega_{xy}^*)^0)^2 \\ &\quad - ((\Omega_{xz}^*)^0)^2 - ((\Omega_{yz}^*)^0)^2 + 4n^2 (\Omega_{zz}^*)^0, \\ d_3 &= (\Omega_{xx}^*)^0 (\Omega_{yy}^*)^0 (\Omega_{zz}^*)^0 + 2 (\Omega_{xy}^*)^0 (\Omega_{xz}^*)^0 (\Omega_{yz}^*)^0 - ((\Omega_{xy}^*)^0)^2 (\Omega_{zz}^*)^0 \\ &\quad - ((\Omega_{xz}^*)^0)^2 (\Omega_{yy}^*)^0 - ((\Omega_{yz}^*)^0)^2 (\Omega_{xx}^*)^0. \end{aligned}$$

Here, we shall study the linear stability of the AEPs by calculating the characteristic roots of Eqn. (7). As we know that, all the characteristic roots of a cubic equation are either real numbers or one of them is a real number and the other characteristic roots are imaginary numbers. A necessary and sufficient condition for an AEP to be linearly stable is that all the characteristic roots of Eqn. (5) lie in the left-hand side of the λ -plane (i.e., $\lambda \leq 0$). If one or more characteristic roots of Eqn. (5) lie in the right-hand side of the λ -plane, then the AEP is always unstable. If all the characteristic roots of Eqn. (5) lie to the left-hand side of the λ -plane, then Eqn. (7) must have three real and negative roots. The resulting linear stability conditions according to Morimoto et al. [9] and Descartes sign rule are $D \geq 0$, $d_1 > 0$, $d_2 > 0$ and $d_3 > 0$, where D is the

discriminant of the cubic Eqn. (7) and is given by

$$D = \frac{1}{4} \left(d_3 + \frac{2d_1^3 - 9d_1d_2}{27} \right)^2 + \frac{1}{27} \left(d_2 - \frac{d_1^2}{3} \right)^3. \quad (8)$$

Eventually, we have concluded that the system of AEPs is linearly stable when $D \geq 0$, $d_1 > 0$, $d_2 > 0$ and $d_3 > 0$.

Furthermore, we have plotted the stability regions in the $x-y$, $x-z$ and $y-z$ -planes as shown in Fig. 3(a, b, c, d, e, f). From Fig. 3, we have observed that the stability regions reduce around both the primaries for the increasing values of the oblateness parameter $A \in (0, 1)$. According to stability theory, it is concluded that the AEPs located in the stable regions are linearly stable, otherwise unstable. Further, it is concluded that the stable AEPs in these stable regions can be obtained by designing the magnitude and direction of the low-thrust acceleration for space missions.

5 Zero Velocity Curves

The Jacobi integral of the equations of motion is defined as

$$C = 2\Omega + (\dot{x}^2 + \dot{y}^2 + \dot{z}^2). \quad (9)$$

The Jacobi integral of the equations of motion with continuous low-thrust is defined as

$$C' = 2\Omega^* + (\dot{x}^2 + \dot{y}^2 + \dot{z}^2). \quad (10)$$

We have drawn the ZVCs from Eq. (10) by taking $\dot{x} = \dot{y} = \dot{z} = 0$. The white domains correspond to the Hill region, and the cyan color indicates the forbidden regions, while the thick black lines show the ZVCs. In these ZVCs, the black dots indicate the positions of the AEPs, while the blue dots indicate the positions of two primaries m_1 and m_2 . In Fig. 4, we have drawn the ZVCs for $\mu = 0.1$, $A = 0.01$, $\mathbf{a} = (0, 0.0001, 0)$ and for the different values of the Jacobi constant C' . The ZVCs in Fig.4(a, b, c, d) are labeled as $C' = -3.640439$, $C' = -3.415439$, $C' = -3.116439$ and $C' = -2.945439$, respectively.

Fig. 4(a) indicates the ZVC for the value of the Jacobi constant $C' = -3.640439$ and shows that, there exists a circular land (white domains) around both the primaries and the spacecraft trapped in these regions, where the motion is possible and the circular strip (the cyan color) shows the forbidden region where the motion is not possible. Thus, the spacecraft can move around both the primaries and can not move from one primary to other. Fig. 4(b) shows the ZVC for $C' = -3.415439$, it is observed that the spacecraft can freely move in the entire white domain. In Fig. 4(c), there exist a limiting situation for $C' = -3.116439$ and a cusp at L_3 , it is observed that the spacecraft can freely move in the entire white domain. In Fig. 4(d), the curves of zero velocity constitute two branches for $C' = -2.945439$. The first branch contains L_4 and the other branch contains L_5 . Also, the curves split into two parts at L_3 and shrink to the tadpole shaped curves around L_4 and L_5 . Hence, there is only forbidden region around L_4 and L_5 in the tadpole shaped region and the spacecraft is free to move everywhere in the plane. We have observed that for the increasing values of the Jacobi constant C' , the representing possible boundary regions increase in which the spacecraft can freely move from one place to other place.

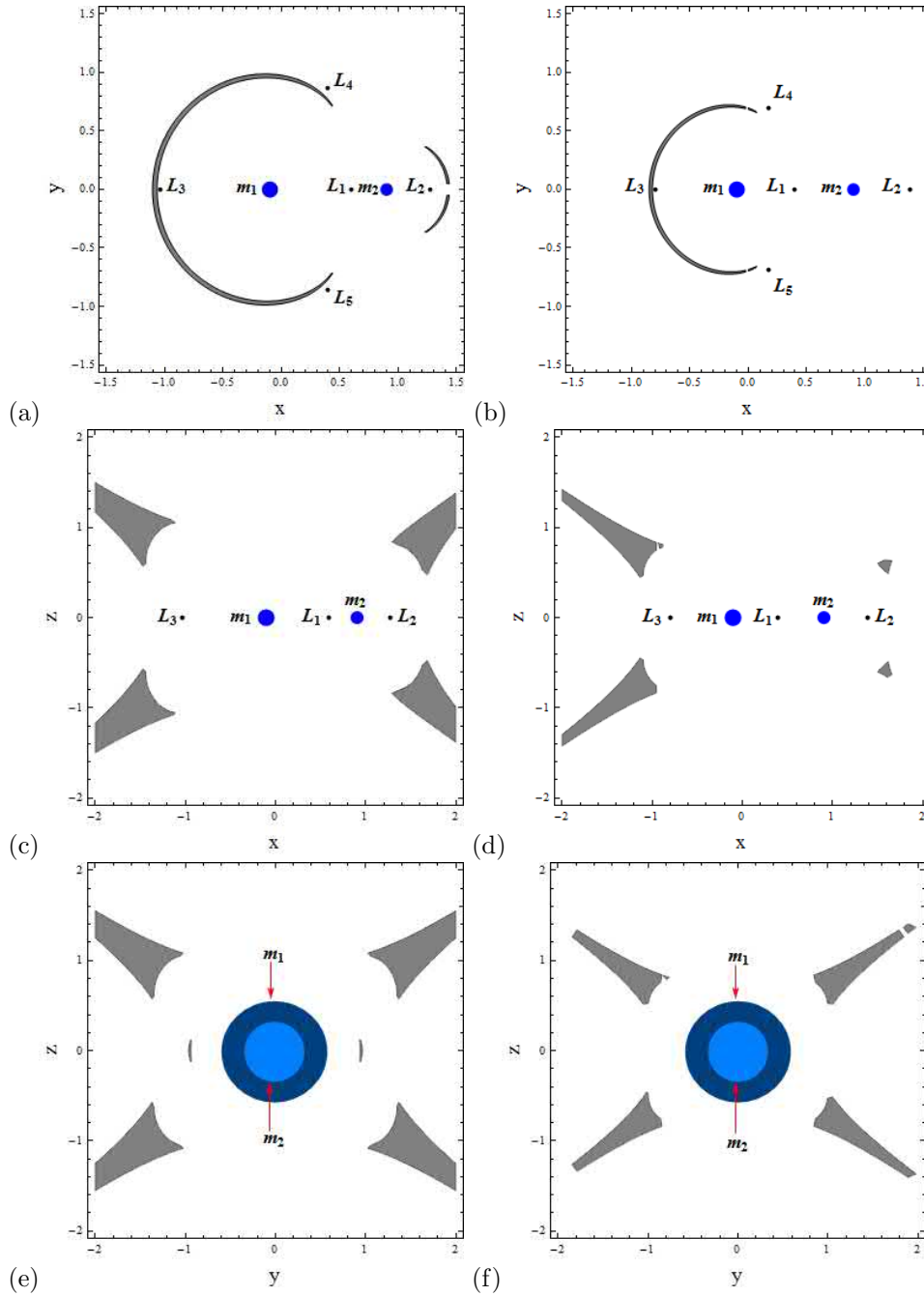


Figure 3: The stable regions (gray area) in the low-thrust R3BP with the effect of oblateness for the mass parameter $\mu = 0.1$, panels-(a, b) in the $x - y$ -plane for $A = 0.01, 0.95$, respectively, panels-(c, d) in the $x - z$ -plane for $A = 0.01, 0.95$, respectively, and panels-(e, f) in the $y - z$ -plane for $A = 0.01, 0.95$, respectively.

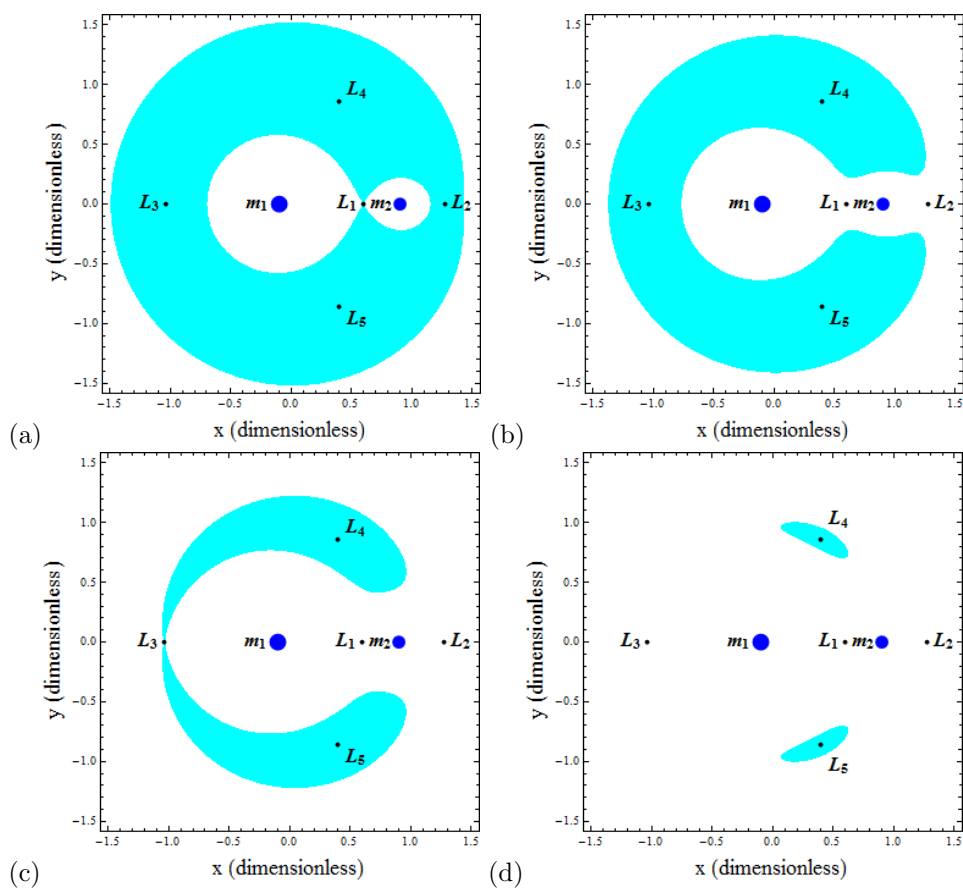


Figure 4: Zero velocity curves for the fixed values of $\mu = 0.1$, $A = 0.01$, $\mathbf{a} = (0, 0.0001, 0)$ and for the different values of the Jacobi constant C' , (a) for $C' = -3.640439$, (b) for $C' = -3.415439$, (c) for $C' = -3.116439$ and (d) for $C' = -2.945439$.

6 Conclusion

In this paper, we have studied the existence and stability of the AEPs in the low-thrust R3BP problem when the smaller primary is an oblate spheroid and the bigger one is a point mass. The AEPs are obtained by introducing the continuous control acceleration at the non-equilibrium points. The numerical values of the AEPs are shown in Tables 1, 2. We have observed that there exist three collinear and two non-collinear AEPs at the low-thrust acceleration varying in the x direction whereas there exist only five non-collinear AEPs at the low-thrust acceleration in the y direction. The movements of AEPs are shown graphically in Fig. 2. We have observed that the non-collinear points L_4 and L_5 are symmetrical about the x -axis at the low-thrust acceleration varying in the x direction. We have derived the equations of motion of the spacecraft in the synodic coordinate system. Further, we have transformed these equations of motion into a six-degree equation. Also, the six-degree equation has been transformed into a cubic equation and we found the conditions for analyzing linear stability. The effect of the oblateness parameter $A \in (0, 1)$ is studied on the motion of the spacecraft. We have plotted the stability regions in the $x - y$, $x - z$ and $y - z$ -planes as shown in Fig. 3. From Fig. 3, we have observed that the stability regions reduce near both the primaries m_1 and m_2 for the increasing values of the oblateness parameter $A \in (0, 1)$.

Our results are different from those by Morimoto et al. [9] in some aspects, namely, (i) they have obtained the AEPs in the low-thrust R3BP, whereas we have obtained the AEPs in the low-thrust R3BP with the effect of the oblateness of the smaller primary. In our case, the AEPs are new positions of natural equilibrium points different from those by Morimoto et al. [9] due to the presence of the oblateness parameter A ($0 < A < 1$). When the oblateness parameter $A = 0$, then the results obtained in this work are in agreement with those by Morimoto et al. [9]. When $\mathbf{a} = (0, 0, 0)$ and $A = 0$, the obtained results are in agreement with the results by Szebehely [1]; (ii) they have found the stability regions in the Sun-Earth system, whereas we have found the stability regions for $\mu = 0.1$ and for different values of the oblateness parameter A ($0 < A < 1$). Finally, we have drawn the ZVCs to determine the possible regions of motion of the spacecraft in which the spacecraft is free to move. We have observed that for the increasing values of the Jacobi constant C' , the possible regions of motion increase, in which the spacecraft can freely move from one place to another. This paper is applicable in the Sun-Earth system for communications of the spacecraft missions.

Acknowledgment

We are very thankful to the **Centre of Fundamental Research in Space Dynamics and Celestial Mechanics (CFRSC)**, New Delhi, India for giving some necessary study materials and other supporting things which are required for the present research work.

References

- [1] V. Szebehely. *Theory of Orbits, the Restricted Problem of Three-Bodies*. Academic press, New York, 1967.
- [2] P. V. Subbarao and R. K. Sharma. A note on the stability of the triangular of equilibrium points in the restricted three-body problem. *Astron. Astrophys.* **43** (1975) 381–383.

- [3] R. K. Sharma, Z. A. Taqvi and K. B. Bhatnagar. Existence of libration points in the restricted three-body problem when both the primaries are triaxial rigid bodies. *Indian J. Pure Appl. Math.* **32**(1) (2001) 125–141.
- [4] A. F. B. A. Prado. A survey on space trajectories in the model of three-bodies. *Nonlinear Dynamics and Systems Theory* **6** (4) (2006) 389–400.
- [5] A. A. Corrêa, A. Prado, T. J. Stuchi and C. Beaugé. Comparison of transfer orbits in the restricted three and four-body problems. *Nonlinear Dynamics and Systems Theory* **7** (3) (2007) 267–277.
- [6] R. W. Farquhar. Lunar communications with libration point satellites. *Spacecraft and Rockets*. **4**(10) (1967) 1383–1384.
- [7] H. M. Dusek. Motion in the vicinity of libration points of a generalized restricted three-body model. *Prog. Astronaut. Rocket*. **17** (1966) 37–54.
- [8] S. B. Broschart and D. J. Sheeres. Control of hovering spacecraft near small bodies: Application to Asteroid 25143 Itokwa. *J. Guid. Control Dyn.* **28**(2) (2005) 343–354.
- [9] M. Y. Morimoto, H. Yamakawa and K. Uesugi. Artificial equilibrium points in the low-thrust restricted three-body problem. *J. Guid. Control Dyn.* **30**(5) (2007) 1563–1567.
- [10] S. Baig and C. R. McInnes. Artificial three-body equilibria for hybrid low-thrust propulsion. *J. Guid. Control Dyn.* **31** (6) (2008) 1644–1655.
- [11] C. Bombardelli and J. Pelaez. On the stability of artificial equilibrium points in the circular restricted three-body problem. *Celest. Mech. Dyn. Astron.* **109**(1) (2011) 13–26. Doi.10.1007/s10569-010-9317.
- [12] G. Alias, G. Mengali and A. Quarta. Artificial equilibrium points for a generalized sail in the circular restricted three-body problem. *Celest. Mech. Dyn. Astron.* **110** (2011) 343–368.
- [13] M. Ceccaroni and J. Biggs. Extension of low-thrust propulsion to the autonomous coplanar circular restricted four-body problem with an application to future Trojan asteroid missions. *Celest. Mech. Dyn. Astron.* **112** (2012) 191–219.
- [14] Shichao Bu, Shuang Li and Hongwei Yang. Artificial equilibrium points in binary asteroid systems with continuous low-thrust. *Astrophys. Space Sci.* **362**(137) (2017). Doi.10.1007/s10509-017-31197-7.
- [15] K. Ranjana and V. Kumar. On the artificial equilibrium points in the circular restricted problem of 2+2 bodies. *Int. J. Astron. Astrophys.* **7**(4) (2017) 239–249.
- [16] S. Yadav, V. Kumar and R. Aggarwal. Existence and stability of equilibrium points in the restricted three-body problem with a Geo-Centric satellite including the Earth’s equatorial ellipticity. *Nonlinear Dynamics and Systems Theory* **19** (4) (2019) 537–550.
- [17] S. W. McCusky. *Introduction to Celestial Mechanics*. Addison-wesley publishing company. Inc. New York, 1963.



General Simplex Method for Fully Fuzzy Linear Programming with the Piecewise Linear Fuzzy Number

M. Z. Tuffaha and M. H. Alrefaei *

Department of Mathematics and Statistics, Jordan University of Science and Technology, Irbid, Jordan

Received: October 25 2019; Revised: September 12, 2020

Abstract: In this paper, we consider the fully fuzzy linear programming problem at which all the attributes and variables of the problem are fuzzy numbers represented by a piecewise linear fuzzy number. This type of fuzzy numbers is used due to its importance as a generalization of some other types of fuzzy numbers. We propose a fuzzy version of the simplex method to solve the problem, which is shown to be a generalization of the conventional simplex method. We represent the simplex method in a tabulated form and discuss whether a final solution exists, the problem is infeasible or it is unbounded. Finally, it is shown that the proposed method is more realistic than some of the existing methods.

Keywords: *piecewise linear fuzzy number; linear programming; fully fuzzy linear programming; polygonal fuzzy number.*

Mathematics Subject Classification (2010): 90C70.

1 Introduction

Linear programming has been an important mathematical tool to solve real life problems for a long time. If some of the data in a linear programming problem are vague, i.e., not precise due to unclear boundaries, then these data are usually represented by fuzzy numbers. This fuzzy representation of the data gives a more realistic manipulation of the problem under consideration since many real life problems contain fuzzy expressions such as “approximately”, “almost” or “about”. Ignoring such expressions and representing the data as crisp (unfuzzy) numbers cost losing some information about the resources, costs or variables. Many applications of fuzziness can be found in different mathematical fields [1, 9]. The literature is rich of applications of fuzzy linear programming problems see, for example, [2, 4, 6]. A more general case is to have a fully fuzzy linear programming

* Corresponding author: <mailto:alrefaei@just.edu.jo>

(FFLP) problem, where all the attributes and the variables in the problem are fuzzy [5, 14].

Different solution approaches for FFLP problems can be found in the literature. For instance, some authors convert the problem into one or more crisp linear programming (CLP) problems with one or more objectives using some ranking method to get rid of the fuzziness, then solve the new problems using the known methods for solving conventional single or multi-objective linear programming problems [7, 14]. On the other hand, some researchers prefer to solve the problem directly without converting it into another type of problem. This is usually done using a fuzzy version of the simplex method [5, 11].

Many types of fuzzy numbers were used in the literature to represent this fuzziness, namely, the triangular fuzzy number which was used by Ozkok et al. [14], the trapezoidal fuzzy number which was considered by Das et al. [7] and by Kumar & Kaur [12], and other types of fuzzy numbers used widely in the literature. A more general type of fuzzy numbers is the n -polygonal fuzzy number, which generalizes the triangular and the trapezoidal fuzzy numbers. It has been gaining a great interest recently, especially in neural networks [13, 17].

In a previous work [15], Tuffaha and Alrefaie studied the piecewise linear fuzzy number of order n (PLFN- n), which is an n -polygonal fuzzy number with equidistant knots. Convenient arithmetic operations were proposed on the PLFN- n in [15] and shown to satisfy the most important properties such as commutativity, associativity, having an identity and preserving the ranking value. Moreover, the operations were shown to give a generalization of the conventional binary operations on the real numbers. Later on, Tuffaha and Alrefaie [16] showed extra properties for the arithmetic operations. These new definitions were used for solving a fully fuzzy transportation problem (FFTP) [3]. In this paper, we consider a fully fuzzy linear programming problem and represent the fuzziness by the PLFN- n for the first time. A generalization of the known simplex method is proposed using the arithmetic operations given in [15].

The paper is organized as follows. In Section 2, we give some preliminaries needed throughout the paper. After that, in Section 3, the fully fuzzy linear programming problem is constructed and the solution method is proposed. The advantages of the proposed method are shown in Section 4, and some concluding remarks are given in Section 5.

2 Preliminaries

In this section, we present the definition of PLFN- n and the binary operations on PLFN- n 's. We also give some definitions to clarify some concepts related to the PLFN- n 's, such as the fuzzy matrices and the maximum and minimum of a set of fuzzy values or fuzzy-valued functions.

The following definitions are about the piecewise linear fuzzy number that is presented in [15].

Definition 2.1 A fuzzy set \tilde{A} is called a **Piecewise Linear Fuzzy Number of Order n** (PLFN- n) if its membership function is given by

$$f_{\tilde{A}}(x) = \begin{cases} \frac{1}{n} \left[\frac{x-p_i}{p_{i+1}-p_i} \right] + \frac{i}{n} & ; p_i \leq x \leq p_{i+1}, \quad i = 0, \dots, n-1 \\ 1 & ; p_n \leq x \leq q_0 \\ \frac{-1}{n} \left[\frac{x-q_i}{q_{i+1}-q_i} \right] + \frac{n-i}{n} & ; q_i \leq x \leq q_{i+1}, \quad i = 0, \dots, n-1 \\ 0 & otherwise. \end{cases}$$

PLFN- n is represented by its knots: $(p_0, p_1, \dots, p_n; q_0, q_1, \dots, q_n)$. The family of all PLFN- n 's is denoted by \mathcal{PL}_n . Moreover, a crisp (unfuzzy) real number c can be represented in the PLFN- n form as $c = (c, c, \dots, c; c, c, \dots, c)$.

Definition 2.2 Let $(p_0, p_1, \dots, p_n; q_0, q_1, \dots, q_n)$ be a PLFN- n . Then its ranking value is given by

$$\mathfrak{R}(\tilde{P}) = \frac{1}{4n} [p_0 + 2p_1 + 2p_2 + \dots + 2p_{n-1} + p_n + q_0 + 2q_1 + 2q_2 + \dots + 2q_{n-1} + q_n].$$

Definition 2.3 Let $\tilde{P} = (p_0, p_1, \dots, p_n; q_0, q_1, \dots, q_n), \tilde{Q} = (r_0, r_1, \dots, r_n; s_0, s_1, \dots, s_n) \in \mathcal{PL}_n$. The **addition** of \tilde{P} and \tilde{Q} is defined as follows:

$$\tilde{P} \oplus \tilde{Q} = (p_0 + r_0, p_1 + r_1, \dots, p_n + r_n; q_0 + s_0, q_1 + s_1, \dots, q_n + s_n).$$

Moreover, the **multiplication** of \tilde{P} and \tilde{Q} is $\tilde{P} \otimes \tilde{Q} = (t_0, t_1, \dots, t_n; u_0, u_1, \dots, u_n)$, where

$$\begin{aligned} u_n &= \frac{1}{4n} [I + \sum_{i=1}^n (2i - 1)X_i + 2nX_{n+1} + \sum_{i=1}^n (2(n + i) - 1)X_{n+1+i}] \\ u_{i-1} &= u_i - X_{n+1+i}, \text{ for } i = n, n - 1, \dots, 1 \\ t_n &= u_0 - X_{n+1} \\ t_{i-1} &= t_i - X_i, \text{ for } i = n, n - 1, \dots, 1, \\ \text{and } I &= \frac{1}{4n} [(p_0 + 2p_1 + \dots + 2p_{n-1} + p_n + q_0 + 2q_1 + \dots + 2q_{n-1} + q_n) * \\ &\quad (r_0 + 2r_1 + \dots + 2r_{n-1} + r_n + s_0 + 2s_1 + \dots + 2s_{n-1} + s_n)] \\ X_i &= (p_i - p_{i-1}) + (r_i - r_{i-1}), \text{ for } i = n, n - 1, \dots, 1 \\ X_{n+1} &= (q_0 - p_n) + (s_0 - r_n) \\ X_{n+1+i} &= (q_i - q_{i-1}) + (s_i - s_{i-1}), \text{ for } i = n, n - 1, \dots, 1. \end{aligned}$$

This definition guarantees the preservation of the most common properties of PLFN- n 's.

Definition 2.4 Let $\tilde{P} = (p_0, p_1, \dots, p_n; q_0, q_1, \dots, q_n) \in \mathcal{PL}_n$. If $\mathfrak{R}(\tilde{P}) \neq 0$, then the **multiplicative inverse** of \tilde{P} , in the sense that $\mathfrak{R}(\tilde{P} \otimes \tilde{P}^{-1}) = 1$, is defined to be $\tilde{P}^{-1} = (t_0, t_1, \dots, t_n; u_0, u_1, \dots, u_n)$, where

$$\begin{aligned} t_0 &= \frac{1}{\mathfrak{R}(\tilde{P})} + \frac{1}{4n} (p_0 + 2p_1 + \dots + 2p_{n-1} + p_n + q_0 + 2q_1 + \dots + 2q_{n-1} - (4n - 1)q_n) \\ t_i &= t_{i-1} + (q_{n-i+1} - q_{n-i}) \text{ for all } i = 1, \dots, n \\ u_0 &= t_n + (q_0 - p_n) \\ u_i &= u_{i-1} + (p_{n-i+1} - p_{n-i}) \text{ for all } i = 1, \dots, n. \end{aligned}$$

The following definitions are about the equalities, inequalities and matrices with PLFN- n from [16].

Definition 2.5 Let \tilde{a} and \tilde{b} be two PLFN- n 's. Then

- \tilde{a} and \tilde{b} are **equivalent**, denoted $\tilde{a} \approx \tilde{b}$, if $\mathfrak{R}(\tilde{a}) = \mathfrak{R}(\tilde{b})$.

- \tilde{a} is **greater** than \tilde{b} , denoted $\tilde{a} \succeq \tilde{b}$, if $\mathfrak{R}(\tilde{a}) \geq \mathfrak{R}(\tilde{b})$.
- \tilde{a} is **smaller** than \tilde{b} , denoted $\tilde{a} \preceq \tilde{b}$, if $\mathfrak{R}(\tilde{a}) \leq \mathfrak{R}(\tilde{b})$.

Definition 2.6

- A matrix whose entries are PLFN- n 's is called a *piecewise linear fuzzy matrix* $\tilde{\mathbf{M}}$.
- The set of all piecewise linear fuzzy matrices is denoted by $\mathcal{M}(\mathcal{PL}_n)$.
- The addition and multiplication of piecewise linear fuzzy matrices are similar to those of real matrices, but using the binary operations given in Definition 2.3 on \mathcal{PL}_n .

Definition 2.7 Let $\tilde{\mathbf{A}} = [\tilde{a}_{ij}]_{m \times k}$, $\tilde{\mathbf{B}} = [\tilde{b}_{ij}]_{m \times k} \in \mathcal{M}(\mathcal{PL}_n)$. Then

1. $\tilde{\mathbf{A}}$ and $\tilde{\mathbf{B}}$ are *equal* or *equivalent*, written $\tilde{\mathbf{A}} = \tilde{\mathbf{B}}$ or $\tilde{\mathbf{A}} \approx \tilde{\mathbf{B}}$, if their corresponding entries are equal or equivalent, respectively.
2. A set of rows of $\tilde{\mathbf{A}}$, $\{\tilde{\mathbf{a}}_{i_1}, \tilde{\mathbf{a}}_{i_2}, \dots, \tilde{\mathbf{a}}_{i_p}\}$, are *linearly independent* if the equation $(c_1 \otimes \tilde{\mathbf{a}}_{i_1}) \oplus (c_2 \otimes \tilde{\mathbf{a}}_{i_2}) \oplus \dots \oplus (c_p \otimes \tilde{\mathbf{a}}_{i_p}) \approx \tilde{\mathbf{0}}$ with $c_1, c_2, \dots, c_p \in \mathbb{R}$ can only be satisfied by $c_i = 0$ for all $i = 1, \dots, p$.
3. The *rank* of $\tilde{\mathbf{A}}$ is the maximal number of linearly independent rows of $\tilde{\mathbf{A}}$.
4. If $m = k$, then $\tilde{\mathbf{A}}$ is a *square fuzzy matrix*, and we define the *determinant* of $\tilde{\mathbf{A}}$, denoted $\det(\tilde{\mathbf{A}})$, to be a PLFN- n computed in a similar way to how we compute the determinant of a real square matrix, but using the binary operations given in Definition 2.3 on \mathcal{PL}_n . Furthermore, if $\det(\tilde{\mathbf{A}}) \not\approx 0$, then the *inverse matrix* $\tilde{\mathbf{A}}^{-1}$ can also be found by similar techniques to finding the inverse matrix of a real matrix, but here $\tilde{\mathbf{A}} \otimes \tilde{\mathbf{A}}^{-1} \approx \tilde{\mathbf{I}}$, where the square matrix $\tilde{\mathbf{I}}$ is a *fuzzy identity matrix* in $\mathcal{M}(\mathcal{PL}_n)$ whose entries are equivalent to zero, except for the entries in the main diagonal which are equivalent to one.

It is known that a linear programming problem seeks the maximum or minimum of a function subject to given constraints. The following definitions present the definition of maximum or minimum of a set of fuzzy values or fuzzy-valued functions.

Definition 2.8 Let I be an arbitrary index set, and let $\tilde{S} = \{\tilde{a}_i : i \in I\}$ be a set of PLFN- n 's. We define the *maximum* and *minimum fuzzy value* of the elements of \tilde{S} , denoted $\max(\tilde{S})$ and $\min(\tilde{S})$, to be the elements of \tilde{S} with the maximum and minimum ranking values, respectively. In other words, if $h_1 = \max\{\mathfrak{R}(\tilde{a}_k) : \tilde{a}_k \in \tilde{S}\}$ and $h_2 = \min\{\mathfrak{R}(\tilde{a}_k) : \tilde{a}_k \in \tilde{S}\}$, then

$$\max(\tilde{S}) = \{\tilde{a}_i \in \tilde{S} : \mathfrak{R}(\tilde{a}_i) = h_1\}, \quad \min(\tilde{S}) = \{\tilde{a}_i \in \tilde{S} : \mathfrak{R}(\tilde{a}_i) = h_2\}.$$

Note that $\max(\tilde{S})$ and $\min(\tilde{S})$ may have more than one element of \tilde{S} if it contains more than one PLFN- n with the maximum or minimum ranking value.

Definition 2.9 Let $\tilde{f} : (\mathcal{PL}_n)^k \rightarrow \mathcal{PL}_n$, where $k \in \mathbb{N}$, be a fuzzy-valued function. Then the *maximum* and *minimum* of \tilde{f} are defined by

$$\max(\tilde{f}) = \max\{\tilde{f}(\tilde{\mathbf{x}}) : \tilde{\mathbf{x}} \in (\mathcal{PL}_n)^k\}, \quad \min(\tilde{f}) = \min\{\tilde{f}(\tilde{\mathbf{x}}) : \tilde{\mathbf{x}} \in (\mathcal{PL}_n)^k\}.$$

Remark 2.1 Note that $\max(\tilde{f}) = -\min(-\tilde{f})$.

3 Fully Fuzzy Linear Programming with the Piecewise Linear Fuzzy Number

In this section, we construct the FFLP problem with PLFN- n and propose a solution method. We generalize the simplex algorithm in order to solve a FFLP problem with PLFN- n 's of the form

$$\begin{aligned} \min \quad & \tilde{z} = \tilde{\mathbf{c}}\tilde{\mathbf{x}} \\ \text{s.t.} \quad & \tilde{\mathbf{A}}\tilde{\mathbf{x}} \approx \tilde{\mathbf{b}} \\ & \tilde{\mathbf{x}} \succeq \tilde{\mathbf{0}}, \end{aligned} \tag{1}$$

where $\tilde{\mathbf{c}} = [\tilde{c}_j]_{1 \times l}$, $\tilde{\mathbf{x}} = [\tilde{x}_j]_{l \times 1}$, $\tilde{\mathbf{A}} = [\tilde{a}_{ij}]_{m \times l}$, $\tilde{\mathbf{b}} = [\tilde{b}_i]_{m \times 1}$ are fuzzy matrices with PLFN- n 's. Moreover, $\tilde{b}_i \succeq \tilde{0}$ for all $i = 1, \dots, m$, and the matrix $\tilde{\mathbf{A}}$ is with rank m .

3.1 Basic feasible solutions

After possibly rearranging the columns $\tilde{\mathbf{a}}_j$ of $\tilde{\mathbf{A}}$, let $\tilde{\mathbf{A}} = [\tilde{\mathbf{B}}\tilde{\mathbf{N}}]$, where $\tilde{\mathbf{B}}$ is an $m \times m$ invertible matrix consisting of m columns of $\tilde{\mathbf{a}}_j$, and $\tilde{\mathbf{N}}$ is an $m \times (l - m)$ matrix with the rest of the columns. Then the constrains can be written as $[\tilde{\mathbf{B}} \ \tilde{\mathbf{N}}]\tilde{\mathbf{x}} \approx \tilde{\mathbf{b}}$. The variables vector can then be split as follows: $[\tilde{\mathbf{B}} \ \tilde{\mathbf{N}}] \begin{bmatrix} \tilde{\mathbf{x}}_B \\ \tilde{\mathbf{x}}_N \end{bmatrix} \approx \tilde{\mathbf{b}}$, which gives $\tilde{\mathbf{B}}\tilde{\mathbf{x}}_B \oplus \tilde{\mathbf{N}}\tilde{\mathbf{x}}_N \approx \tilde{\mathbf{b}}$ or

$$\tilde{\mathbf{x}}_B \oplus \tilde{\mathbf{B}}^{-1}\tilde{\mathbf{N}}\tilde{\mathbf{x}}_N \approx \tilde{\mathbf{B}}^{-1}\tilde{\mathbf{b}}. \tag{2}$$

One solution is $\tilde{\mathbf{x}} = \begin{bmatrix} \tilde{\mathbf{x}}_B \\ \tilde{\mathbf{x}}_N \end{bmatrix} = \begin{bmatrix} \tilde{\mathbf{B}}^{-1}\tilde{\mathbf{b}} \\ \tilde{\mathbf{0}} \end{bmatrix}$, which is called a *basic solution*. $\tilde{\mathbf{B}}$ is called the *basis*, and the components of $\tilde{\mathbf{x}}_B$ are called the *basic variables*. If $\tilde{\mathbf{x}}_B \succeq \tilde{\mathbf{0}}$, then $\tilde{\mathbf{x}}$ is called a *basic feasible solution (b.f.s.)*.

3.2 The fuzzy simplex method

Assume problem (1) has a basic feasible solution $\tilde{\mathbf{x}}' = \begin{bmatrix} \tilde{\mathbf{x}}_B \\ \tilde{\mathbf{x}}_N \end{bmatrix} = \begin{bmatrix} \tilde{\mathbf{B}}^{-1}\tilde{\mathbf{b}} \\ \tilde{\mathbf{0}} \end{bmatrix}$, whose objective value is given by

$$\tilde{z}_0 = \tilde{\mathbf{c}} \begin{bmatrix} \tilde{\mathbf{B}}^{-1}\tilde{\mathbf{b}} \\ \tilde{\mathbf{0}} \end{bmatrix} = [\tilde{\mathbf{c}}_B \ \tilde{\mathbf{c}}_N] \begin{bmatrix} \tilde{\mathbf{B}}^{-1}\tilde{\mathbf{b}} \\ \tilde{\mathbf{0}} \end{bmatrix} = \tilde{\mathbf{c}}_B\tilde{\mathbf{B}}^{-1}\tilde{\mathbf{b}}. \tag{3}$$

The objective function in augmented form is

$$\tilde{z} = [\tilde{\mathbf{c}}_B \ \tilde{\mathbf{c}}_N] \begin{bmatrix} \tilde{\mathbf{x}}_B \\ \tilde{\mathbf{x}}_N \end{bmatrix} = \tilde{\mathbf{c}}_B\tilde{\mathbf{x}}_B \oplus \tilde{\mathbf{c}}_N\tilde{\mathbf{x}}_N. \tag{4}$$

From (2), we have

$$\tilde{\mathbf{x}}_B \approx \tilde{\mathbf{B}}^{-1}\tilde{\mathbf{b}} \ominus \tilde{\mathbf{B}}^{-1}\tilde{\mathbf{N}}\tilde{\mathbf{x}}_N. \tag{5}$$

Substituting (5) in (4) and simplifying give

$$\tilde{z} \oplus (\tilde{\mathbf{c}}_B\tilde{\mathbf{B}}^{-1}\tilde{\mathbf{N}} \ominus \tilde{\mathbf{c}}_N)\tilde{\mathbf{x}}_N \approx \tilde{\mathbf{c}}_B\tilde{\mathbf{B}}^{-1}\tilde{\mathbf{b}}.$$

Denote $\tilde{\mathbf{z}}_N = \tilde{\mathbf{c}}_B\tilde{\mathbf{B}}^{-1}\tilde{\mathbf{N}}$, then

$$\tilde{z} \oplus (\tilde{\mathbf{z}}_N \ominus \tilde{\mathbf{c}}_N)\tilde{\mathbf{x}}_N \approx \tilde{\mathbf{c}}_B\tilde{\mathbf{B}}^{-1}\tilde{\mathbf{b}}. \tag{6}$$

From equations (6) and (2), and putting $\tilde{\mathbf{b}} = \tilde{\mathbf{B}}^{-1}\tilde{\mathbf{b}}$, the current b.f.s. can be represented in tabular form as

| | $\tilde{\mathbf{x}}_B$ | $\tilde{\mathbf{x}}_N$ | RHS |
|------------------------|------------------------|---|---|
| \tilde{z} | $\tilde{\mathbf{0}}$ | $\tilde{\mathbf{z}}_N \ominus \tilde{\mathbf{c}}_N$ | $\tilde{\mathbf{c}}_B \tilde{\mathbf{B}}^{-1} \tilde{\mathbf{b}}$ |
| $\tilde{\mathbf{x}}_B$ | $\tilde{\mathbf{I}}$ | $\tilde{\mathbf{B}}^{-1} \tilde{\mathbf{N}}$ | $\tilde{\mathbf{b}}$ |

We assume the absence of *degeneracy*, i.e., we consider that $\tilde{\mathbf{b}} \succ 0$. The case of degeneracy, where $\tilde{\mathbf{b}}$ has zero values, is known to cause some problems and needs a special discussion that will be cited later.

Let J be the current set of indices of the non-basic variables, then $\tilde{z}_j \ominus \tilde{c}_j$, where $j \in J$ are the elements of $\tilde{\mathbf{z}}_N \ominus \tilde{\mathbf{c}}_N$. Now, from equation (6) we have

$$\tilde{z} \approx \tilde{z}_0 \ominus \sum_{j \in J} (\tilde{z}_j \ominus \tilde{c}_j) \tilde{x}_j. \tag{7}$$

If $\tilde{z}_j \ominus \tilde{c}_j < 0$ for all $j \in J$, then the current solution cannot be improved anymore, and it is optimal. On the other hand, if $\tilde{z}_j \ominus \tilde{c}_j \leq 0$ for all $j \in J$, and $\tilde{z}_k \ominus \tilde{c}_k \approx 0$ for some $k \in J$, then increasing the value of \tilde{x}_k does not affect the objective value, which means that we have alternative optimal solutions with the same objective value. However, such case is not treated differently than the previous case in this paper. In other words, even if we have alternative optimal solutions, we will take only one of them into consideration.

Finally, if there exists $\tilde{z}_k \ominus \tilde{c}_k \succ 0$ for some $k \in J$, then \tilde{x}_k enters the basis because this improves the objective value and one basic solution leaves the basis. To determine the leaving variable, we use the ratio test in order to maintain feasibility, i.e., keep all basic variables non negative. In order to maintain the nonnegativity of the variables, \tilde{x}_k is increased until the first point at which some basic variable \tilde{x}_{B_r} drops to zero. In fact, we can increase \tilde{x}_k until

$$\tilde{x}_k = \frac{\tilde{b}_r}{\tilde{y}_{rk}} = \min \left\{ \frac{\tilde{b}_i}{\tilde{y}_{ik}}; \tilde{y}_{ik} \succ 0, i = 1, \dots, m \right\}, \tag{8}$$

and then \tilde{x}_{B_r} leaves the basis and we call it the *blocking variable*, and (8) is called the *minimum ratio*. In fact, the only purpose of finding the minimum ratio is to determine the blocking variable. However, we can use the ranking function to facilitate the calculations, and the following *ranked minimum ratio* is enough to achieve the purpose:

$$\frac{\mathfrak{R}[\tilde{b}_r]}{\mathfrak{R}[\tilde{y}_{rk}]} = \min \left\{ \frac{\mathfrak{R}[\tilde{b}_i]}{\mathfrak{R}[\tilde{y}_{ik}]}; \tilde{y}_{ik} \succ 0, i = 1, \dots, m \right\}. \tag{9}$$

In tabular format, we can change the basis using the elementary row operations, which are known to maintain an equivalent problem, such that \tilde{x}_k enters the basis and \tilde{x}_{B_r} leaves it.

If $\tilde{y}_k \leq 0$, i.e., the ranking values of all its elements are less than or equal to zero. Then there is no blocking variable, and the value of \tilde{x}_k can be increased indefinitely giving always a better objective value without violating any of the constraints. Thus, the problem is *unbounded* and the vector $\tilde{\mathbf{d}} = \begin{bmatrix} -\tilde{y}_k \\ \tilde{\mathbf{e}}_k \end{bmatrix}$ is the *direction of unboundedness*. To illustrate, we give two examples, one has optimal solution and the other is unbounded.

Example 3.1 Consider the following FFLP problem:

$$\begin{aligned}
 \min \quad & (1, 2, 3; 3, 4, 5) \otimes \tilde{x}_1 \oplus (-7, -4.5, -3; -1, 1, 2) \otimes \tilde{x}_2 \\
 \text{s.t.} \quad & (-4, -2, -1; 2, 3, 5) \otimes \tilde{x}_1 \oplus (2, 3, 5; 6, 6.5, 8) \otimes \tilde{x}_2 \preceq (-1, 0, 1; 1, 3.5, 4) \\
 & (1, 3, 4; 4, 5, 7) \otimes \tilde{x}_1 \oplus (-3, -2.5, -2; -1, 0, 3) \otimes \tilde{x}_2 \preceq (5, 6, 7; 9, 10, 11) \\
 & \tilde{x}_1, \tilde{x}_2 \succeq \tilde{0}.
 \end{aligned} \tag{10}$$

Adding the slack variables gives the following first simplex table:

| | \tilde{x}_1 | \tilde{x}_2 | \tilde{y}_1 | \tilde{y}_2 | RHS |
|---------------------|----------------------------------|--|---------------|---------------|--------------------------------|
| \tilde{z} RV | $(-5, -4, -3; -3, -2, -1)$ -3 | $(-2, -1, 1; 3, 4.5, 7)$ 2 | 0 | 0 | 0 |
| \tilde{y}_1 RV | $(-4, -2, -1; 2, 3, 5)$ 0.5 | $(2, 3, 5; 6, 6.5, 8)$ $\triangleright 5 \triangleleft$ | 1 | 0 | $(-1, 0, 1; 1, 3.5, 4)$ 1.5 |
| \tilde{y}_2 RV | $(1, 3, 4; 4, 5, 7)$ 4 | $(-3, -2.5, -2; -1, 0, 3)$ -1 | 0 | 1 | $(5, 6, 7; 9, 10, 11)$ 8 |

where the ranking value (RV) of each fuzzy number is written below it.

$$\tilde{z}_k \ominus \tilde{c}_k = \max\{(-5, -4, -3; -3, -2, -1), (-2, -1, 1; 3, 4.5, 7), 0\} = (-2, -1, 1; 3, 4.5, 7) \succ 0,$$

thus the current solution is not optimal. From the ranked minimum ratio test (9), we find

$$\frac{\mathfrak{R}[\tilde{b}_r]}{\mathfrak{R}[\tilde{y}_{rk}]} = \mathfrak{R}[(-1, 0, 1; 1, 3.5, 4)] \otimes \mathfrak{R}[(2, 3, 5; 6, 6.5, 8)^{-1}] = 1.5 * 0.2 = 0.3,$$

so we pivot at $(2, 3, 5; 6, 6.5, 8)$ by performing the elementary row operations

$$\begin{aligned}
 R_1 &\leftarrow (2, 3, 5; 6, 6.5, 8)^{-1} \otimes R_1 \\
 R_0 &\leftarrow -(-2, -1, 1; 3, 4.5, 7) \otimes R_1 \oplus R_0 \\
 R_2 &\leftarrow -(-3, -2.5, -2; -1, 0, 3) \otimes R_1 \oplus R_2.
 \end{aligned}$$

This gives the second simplex table:

| | \tilde{x}_1 | \tilde{x}_2 | \tilde{y}_1 | \tilde{y}_2 | RHS |
|---------------------|---|---------------------------------|---|---------------|---|
| \tilde{z} RV | $(-17.7, -10.7, -6.7; -0.7, 5.3, 10.3)$ -3.2 | $(-15, -9, -3; 3, 9, 15)$ 0 | $(-8.4, -4.4, -2.4; 0.6, 4.6, 6.6)$ -0.4 | 0 | $(-11.1, -6.1, -3.1; -0.1, 6.4, 8.9)$ -0.6 |
| \tilde{x}_2 RV | $(-7.4, -3.9, -2.4; 1.6, 4.6, 7.6)$ 0.1 | $(-5, -2.5, 0; 2, 4.5, 7)$ 1 | $(-2.8, -1.3, -0.8; 0.2, 2.2, 3.2)$ 0.2 | 0 | $(-5.2, -2.7, -1.2; -0.2, 4.3, 5.8)$ 0.3 |
| \tilde{y}_2 RV | $(-10.4, -1.9, 1.6; 6.6, 11.1, 16.6)$ 4.1 | $(-12, -6, -2; 2, 6, 12)$ 0 | $(-6.8, -2.3, -0.8; 1.2, 3.7, 5.2)$ 0.2 | 1 | $(-4.2, 2.3, 5.8; 9.8, 15.8, 18.8)$ 8.3 |

$\tilde{z}_k \ominus \tilde{c}_k = \max\{(-17.7, -10.7, -6.7; -0.7, 5.3, 10.3), (-15, -9, -3; 3, 9, 15), (-8.4, -4.4, -2.4; 0.6, 4.6, 6.6), 0\} = 0,$ thus the solution is optimal. The optimal solution for the problem is $\tilde{x}_1 = 0, \tilde{x}_2 = (-5.2, -2.7, -1.2; -0.2, 4.3, 5.8)$ with the fuzzy objective value $\tilde{z}^* = (-8.9, -6.4, 0.1, 3.1, 6.1, 11.1)$. Now, we solve the RLP problem for problem (10), which is

$$\begin{aligned}
 \min \quad & 3x_1 - 2x_2 \\
 \text{s.t.} \quad & 0.5x_1 + 5x_2 \leq 1.5 \\
 & 4x_1 - x_2 \leq 8 \\
 & x_1, x_2 \geq 0.
 \end{aligned}$$

Its optimal solution is $x_1 = 0$, $x_2 = 0.3$ with the optimal objective value $z^* = -0.6$. As expected, we have $x_1 = \mathfrak{R}(\tilde{x}_1)$, $x_2 = \mathfrak{R}(\tilde{x}_2)$ and $z^* = \mathfrak{R}(\tilde{z}^*)$.

Here is another example for an unbounded FFLP with PLFN- n 's.

Example 3.2 Suppose we have the following simplex table that represents some step in the fuzzy simplex algorithm to solve some FFLP with PLFN- n 's:

| | \tilde{x}_1 | \tilde{x}_2 | \tilde{x}_3 | \tilde{x}_4 | RHS |
|---------------|---------------------------------|---------------------------------|----------------------------------|------------------------------------|-------------------------------|
| \tilde{z} | $(-13, -8, -3, 0; 0, 3, 8, 13)$ | $(-13, -9, -3, 0; 0, 4, 8, 13)$ | $(-16, -9, -4, 0; 2, 6, 11, 18)$ | $(-17, -12, -7, -3; -1, 3, 8, 13)$ | $(-4, -1, 1, 4; 4, 7, 9, 12)$ |
| RV | 0 | 0 | 1 | -2 | -10 |
| \tilde{x}_2 | $(-8, -6, -3, -1; 1, 3, 6, 8)$ | $(-6, -4, -2, 0; 2, 4, 6, 8)$ | $(-11, -8, -4, -2; 0, 2, 6, 9)$ | $(-13, -6, -2, 1; 1, 6, 8, 11)$ | $(-4, -1, 1, 4; 4, 7, 9, 12)$ |
| RV | 0 | 1 | -1 | 1 | 4 |
| \tilde{x}_1 | $(-2, -1, 0, 1; 1, 2, 3, 4)$ | $(-3, -2, -1, 0; 0, 1, 2, 3)$ | $(-7, -5, -3, -2; -2, -1, 1, 3)$ | $(-3, -1, 0, 1; 1, 2, 3, 5)$ | $(-2, -1, 0, 2; 2, 4, 5, 6)$ |
| RV | 1 | 0 | -2 | 1 | 2 |

It is clear that the variable \tilde{x}_3 needs to enter the basis. However,

$$\tilde{\mathbf{y}}_3 = \begin{bmatrix} \tilde{y}_{23} \\ \tilde{y}_{13} \end{bmatrix} = \begin{bmatrix} (-11, -8, -4, -2; 0, 2, 6, 9) \\ (-7, -5, -3, -2; -2, -1, 1, 3) \end{bmatrix} \preceq \tilde{\mathbf{0}}.$$

Therefore, the problem is unbounded with the direction of unboundedness:

$$\tilde{\mathbf{d}} = \begin{bmatrix} -\tilde{y}_{13} \\ -\tilde{y}_{23} \\ 1 \\ 0 \end{bmatrix} = \begin{bmatrix} (-3, -1, 1, 2; 2, 3, 5, 7) \\ (-9, -6, -2, 0; 2, 4, 8, 11) \\ (1, 1, 1, 1; 1, 1, 1, 1) \\ (0, 0, 0, 0; 0, 0, 0, 0) \end{bmatrix}.$$

4 Advantages of the Proposed Method

Applying the proposed method to a FFLP problem with PLFN- n 's preserves the ranking values in each step of every iteration, which gives a fuzzy solution with ranking values equal to the solution of the corresponding RLP problem. This property makes the proposed method more realistic than the other methods existing in the literature that do not guarantee the ranking values are preserved throughout the solution. To illustrate, we implement the proposed method using the following example that was solved by Das et al. [7]. The results are compared to the results obtained via the Das method. The problem is a special case of the PLFN- n which is a trapezoidal fuzzy number that is considered as a flat PLFN-1.

Example 4.1

$$\begin{aligned} \max \quad & \tilde{z} = (7, 10; 14, 17) \otimes \tilde{x}_1 \oplus (8, 13; 15, 20) \otimes \tilde{x}_2 \\ \text{s.t.} \quad & (11, 13; 15, 17) \otimes \tilde{x}_1 \oplus (7, 11; 13, 17) \otimes \tilde{x}_2 \preceq (94, 100; 102, 108) \\ & (12, 14; 16, 18) \otimes \tilde{x}_1 \oplus (8, 12; 14, 18) \otimes \tilde{x}_2 \preceq (104, 112; 114, 122) \\ & \tilde{x}_1, \tilde{x}_2 \succeq \tilde{\mathbf{0}}. \end{aligned} \tag{11}$$

| | Solution by Das | Solution by the proposed method | RS of Das | RS of the proposed method | Solution of the corresponding RLP |
|---------------|-----------------------------|--|-----------|---------------------------|-----------------------------------|
| \tilde{x}_1 | (0, 3; 3, 6) | (0, 0; 0, 0) | 3 | 0 | 0 |
| \tilde{x}_2 | (4.38, 4.38; 4.38, 4.38) | $(\frac{-43}{12}, \frac{77}{12}, \frac{125}{12}, \frac{245}{12})$ | 4.38 | $\frac{101}{12}$ | $\frac{101}{12}$ |
| \tilde{z}^* | (71.94, 86.94; 95.7, 110.7) | $(\frac{-815}{6}, \frac{-723}{6}, \frac{-689}{6}, \frac{-599}{6})$ | 91.32 | 117.8 | 117.8 |

It is clear that the solution by the proposed method coincide with the solution of the RLP problem, while the solution in [7] does not.

Similarly, if the problem is solved by some existing methods, the solution does not coincide with the solution of the RLP. For instance, Das et al. [7] have solved the previous problem using two methods proposed by Kumar & Kaur [12] and Ganesan & Veeramani [8]. The ranking values of the optimal objective values are 70.3 and 94, respectively. Both of these values do not coincide with the optimal objective value for the RLP problem.

Another advantage is that the proposed method is a generalization of the conventional simplex method. Suppose we have a crisp linear programming problem (P). Since every crisp real number “a” can be written in the form of a PLFN-*n* as $(a, a, \dots, a; a, a, \dots, a)$, then we can replace every crisp number in problem (P) by its PLFN-*n* form. This results in a FFLP problem, call it the *fuzzified problem*, that can be solved by the proposed method. However, the proposed method preserves the ranking values in each step and the arithmetic operations on the piecewise linear fuzzy number generalize the known operations on the crisp numbers. This means that the solution of the fuzzified problem by the proposed method is identical to the solution of the original crisp problem using the known simplex method. This means that the simplex method is generalized by the proposed fuzzy simplex method.

5 Conclusion

In this paper, a fully fuzzy linear programming problem with piecewise linear fuzzy numbers is constructed. A solution method depending on extending the simplex method is then proposed. The considered technique results in a generalization of the conventional simplex algorithm. When the proposed method is applied to crisp linear programming problems, it gives the same results as those obtained by using the classical simplex method.

Considering the PLFN-*n* to represent the fuzziness in the problem gives a wider range of problems that can be solved by the proposed method. The mostly used types of fuzzy numbers in the literature are the triangular, the trapezoidal and the hexagonal fuzzy numbers which are special cases of the PLFN-*n*.

Many applications of the constructed problem and the proposed solution method can be done, such as transportation or supply chain problems with fuzzy data.

Finding the initial basic feasible solution in the case of having constraints of the type “ \approx ” or “ \succeq ” is under study and will be presented in a future paper.

Acknowledgments

This work is supported by Jordan University of Science and Technology under Research Grant Number: 20170376.

References

- [1] A. Abbadi, F. Hamidia, A. Morsli and A. Tlemcani. Optimal Voltage Controller using T-S Fuzzy Model for Multimachine Power Systems. *Nonlinear Dynamics and Systems Theory* **19** (2) (2019) 217–226.
- [2] M. Alrefaei, A. Alawneh and M. Hassan. Fuzzy linear programming for supply chain management in steel industry. *Applied Mathematical Sciences* **8** (103) (2014) 5105–5114.
- [3] M. Alrefaei, N. Ibrahim and M. Tuffaha. Solving Fully Fuzzy Transportation Problem with n-Polygonal Fuzzy Numbers. 1st International Conference on Mechanical, Aeronautical and Industrial Engineering Technologies (MechaniTek 2020) **1** (1) (2020) 69–74.
- [4] A. Baykasoğlu and K. Subulan. An analysis of fully fuzzy linear programming with fuzzy decision variables through logistics network design problem. *Knowledge-Based Systems* **90** (2015) 165–184.
- [5] T. Beaula and S. Rajalakshmi. Solving fully fuzzy linear programming problem using breaking points. *International Journal of Applied Operational Research* **2** (3) (2012) 11–20.
- [6] B. Bilgen. Supply chain network modeling in a golf club industry via fuzzy linear programming approach. *Journal of Intelligent & Fuzzy Systems* **21** (4) (2010) 243–253.
- [7] S. K. Das, T. Mandal and S. Edalatpanah. A mathematical model for solving fully fuzzy linear programming problem with trapezoidal fuzzy numbers. *Applied Intelligence* **46** (3) (2017) 509–519.
- [8] K. Ganesan and P. Veeramani. Fuzzy linear programs with trapezoidal fuzzy numbers. *Annals of Operations Research* **143** (1) (2006) 305–315.
- [9] F. Hamidia and A. Abbadi, A. Tlemcani and M.S. Boucherit. Dual Star Induction Motor Supplied with Double Photovoltaic Panels Based on Fuzzy Logic Type-2. *Nonlinear Dynamics and Systems Theory* **18** (4) (2018) 359–371.
- [10] J. Kaur and A. Kumar. Mehar’s method for solving fully fuzzy linear programming problems with l-r fuzzy parameters. *Applied Mathematical Modelling* **37** (12) (2013) 7142–7153.
- [11] I. U. Khan, T. Ahmad and N. Maan. A simplified novel technique for solving fully fuzzy linear programming problems. *Journal of Optimization Theory and Applications* **159** (2) (2012) 536–546.
- [12] A. Kumar and J. Kaur. A new method for solving fuzzy linear programs with trapezoidal fuzzy numbers. *Journal of fuzzy set valued analysis* **2011** (2011) 12 pages.
- [13] X. Li and D. Li. The structure and realization of a polygonal fuzzy neural network. *International Journal of Machine Learning and Cybernetics* **7** (3) (2016) 373–389.
- [14] B. A. Ozkok, I. Albayrak, H. G. Kocken and M. Ahlatcioglu. An approach for finding fuzzy optimal and approximate fuzzy optimal solution of fully fuzzy linear programming problems with mixed constraints. *Journal of Intelligent & Fuzzy Systems* **31** (1) (2016) 623–632.
- [15] M. Z. Tuffaha and M. H. Alrefaei. Arithmetic operations on piecewise linear fuzzy number. *AIP Conference Proceedings* **1991** (1) (2018) 020024.
- [16] M. Z. Tuffaha and M. H. Alrefaei. Properties of Binary Operations of n-Polygonal Fuzzy Numbers. *Advances in Intelligent Systems and Computing* **1111 AISC** (2020) 256–265.
- [17] G. Wang and X. Li. Universal approximation of polygonal fuzzy neural networks in sense of k-integral norms. *Science China Information Sciences* **54** (11) (2011) 2307–2323.
- [18] L. A. Zadeh. Fuzzy sets. *Information and control* **8**(3) (1965) 338–353.



Contents of Volume 20, 2020

| | | |
|---|----------|------|
| Volume 20 | Number 1 | 2020 |
| PERSONAGE IN SCIENCE | | |
| Professor V.M. Starzhinskii. To the 100th Birthday Anniversary | 1 | |
| <i>A.A. Martynyuk, N.A. Izobov, A.G. Mazko and V.I. Zhukovskii</i> | | |
| Generalized Monotone Method for Nonlinear Caputo Fractional Impulsive Differential Equations | 3 | |
| <i>Y. Bai and A.S. Vatsala</i> | | |
| Control Design for Non-Linear Uncertain Systems via Coefficient Diagram Method: Application to Solar Thermal Cylindrical Parabolic Trough Concentrators | 21 | |
| <i>Z. Fenchouche, M. Chakir, O. Benzineb, M.S. Boucherit and M. Tadjine</i> | | |
| Adaptive Sliding Mode Control Synchronization of a Novel, Highly Chaotic 3-D System with Two Exponential Nonlinearities | 38 | |
| <i>F. Hannachi</i> | | |
| Motion Control Design of UNUSAITS AUV Using Sliding PID | 51 | |
| <i>T. Herlambang, S. Subchan, H. Nurhadi and D. Adzkiya</i> | | |
| Alternative Legendre Functions for Solving Nonlinear Fractional Fredholm Integro-Differential Equations | 61 | |
| <i>Khawlah H. Hussain</i> | | |
| On the Boundedness of a Novel Four-Dimensional Hyperchaotic System | 72 | |
| <i>S. Rezzag</i> | | |
| Periodic Solutions in Non-Homogeneous Hill Equation | 78 | |
| <i>A. Rodriguez and J. Collado</i> | | |
| Estimates of Accuracy for Asymptotic Soliton-Like Solutions to the Singularly Perturbed Benjamin-Bona-Mahony Equation | 92 | |
| <i>V. H. Samoilenko, Yu. I. Samoilenko and L. V. Vovk</i> | | |
| Oscillation Criteria for Delay Equations with Several Non-Monotone Arguments | 107 | |
| <i>I. P. Stavroulakis, Zh. Kh. Zhunussova, L. Kh. Zhunussova and K. Dosmagulova</i> | | |
| Volume 20 | Number 2 | 2020 |
| Solving a System of Nonlinear Fractional Partial Differential Equations Using the Sinc-Muntz Collocation Method | 119 | |
| <i>Mahmood Shareef Ajeel, Morteza Gachpazan and Ali Reza Soheili</i> | | |
| Some Problems of Attitude Dynamics and Control of a Rigid Body | 132 | |
| <i>A. Yu. Aleksandrov, A. A. Martynyuk and A. A. Tikhonov</i> | | |
| Chaos in New 2-d Discrete Mapping and Its Application in Optimization | 144 | |
| <i>R. Bououden, M. S. Abdelouahab and F. Jarad</i> | | |
| Sensorless Two Series Connected Quasi Six-Phase IM Based Direct Torque Control for Torque Ripples Minimization | 153 | |
| <i>Y. Chedni, DJ. Boudana, A. Mouldia, L. Nezli and P. Wira</i> | | |

| | |
|---|-----|
| Analysis of the Dynamics of a Two-Degree-of-Freedom Nonlinear Mechanical System under Harmonic Excitation | 168 |
| <i>Akram Khalil Cheib, V. E. Puzyrov and N. V. Savchenko</i> | |
| Numerical Approximation of the Exact Control for the Vibrating Rod with Improvement of the Final Error by Particle Swarm Optimization | 179 |
| <i>A. Khernane</i> | |
| The Finite Element Method for Nonlinear Nonstandard Volterra Integral Equations | 191 |
| <i>M. Khumalo and A. Dlamini</i> | |
| Control of a Novel Class of Uncertain Fractional-Order Hyperchaotic Systems with External Disturbances via Sliding Mode Controller | 203 |
| <i>B. Labeled, S. Kaouache and M. S. Abdelouahab</i> | |
| Stochastic Dengue Mathematical Model in the Presence of Wolbachia: Exploring the Disease Extinction | 214 |
| <i>M. Z. Ndiu and A. K. Supriatna</i> | |

Volume 20

Number 3

2020

| | |
|--|-----|
| Existence of Weak Solutions for Nonlinear p -Elliptic Problem by Topological Degree Method | 229 |
| <i>A. Abbassi, C. Allalou and A. Kassidi</i> | |
| Unified Continuous and Discrete Lur'e Systems Stability Analysis Based on Augmented Model Description | 242 |
| <i>A. Ayadi, K. Dchich, B. Sfaihi and M. Benrejeb</i> | |
| Dynamical Analysis, Stabilization and Discretization of a Chaotic Financial Model with Fractional Order | 253 |
| <i>R.R. Barkat and T. Menacer</i> | |
| Sinc-Galerkin Method for Solving Higher Order Fractional Boundary Value Problems | 267 |
| <i>A. Darweesh and K. Al-Khaled</i> | |
| Optimization of Linear Quadratic Regulator with Tracking Applied to Autonomous Underwater Vehicle (AUV) Using Cuckoo Search | 282 |
| <i>T. Herlambang, D. Rahmalia, H. Nurhadi, D. Adzkiya and S. Subchan</i> | |
| Natural Daftardar-Jafari Method for Solving Fractional Partial Differential Equations | 299 |
| <i>H. Jafari, M.N. Ncube, S.P. Moshokoa and L. Makhubela</i> | |
| Increased Order Generalized Combination Synchronization of Non-Identical Dimensional Fractional-Order Systems by Introducing Different Observable Variable Functions | 307 |
| <i>S. Kaouache, N.E. Hamri, A.S. Hacimliyan, E. Kandiran, B. Deruni and A.C. Keles</i> | |
| Gradient Optimal Control Problems for a Class of Infinite Dimensional Systems | 316 |
| <i>M.O. Sidi and S. A. Beinane</i> | |
| Absolutely Unstable Differential Equations with Aftereffect | 327 |
| <i>V.Yu. Slyusarchuk</i> | |
| Stability of the Artificial Equilibrium Points in the Low-Thrust Restricted Three-Body Problem when the Bigger Primary is a Source of Radiation | 333 |
| <i>Md. Sanam Suraj, Amit Mittal and Krishan Pal</i> | |
| Obituary for Nelly Nikitina (1939 – 2020) | 345 |

Volume 20

Number 4

2020

| | |
|---|-----|
| Fixed Point Regions, Unified Construction of Fixed Point Mappings for Integral, Quadratic, and Fractional Equations | 347 |
| <i>T. A. Burton and I. K. Purnaras</i> | |
| An Enhanced Bi-Directional Chaotic Optimization Algorithm | 365 |
| <i>F. Derouiche and T. Hamaizia</i> | |
| Speed Sensorless Direct Torque Control Strategy of a Doubly Fed Induction Motor Using an ANN and an EKF | 374 |
| <i>T. Djellouli, S. Moulahoum, A. Mouldia, M.S. Bouchrit and P. Wira</i> | |
| Solving Laplace Equation within Local Fractional Operators by Using Local Fractional Differential Transform and Laplace Variational Iteration Methods | 388 |
| <i>H. K. Jassim, J. Vahidi and V. M. Ariyan</i> | |
| Solution to the Critical Burgers Equation for Small Data in a Bounded Domain | 397 |
| <i>M. B. Kania</i> | |
| Application of the Direct Power Control Strategy in a Shunt Active Filter by Exploiting the Solar Photovoltaic Energy as a Continuous Source | 410 |
| <i>A. Morsli, A. Tlemçani, A. Krama, A. Abbadi, L. Zellouma and H. Nouri</i> | |
| Uniqueness of Solution to the von Karman Equations with Free Boundary Conditions | 425 |
| <i>J. Oudaani, A. El Mouatasim and B. El-Aqqad</i> | |
| Stability of the Artificial Equilibrium Points in the Low-Thrust Restricted Three-Body Problem when the Smaller Primary is an Oblate Spheroid | 439 |
| <i>Md. Sanam Suraj, Amit Mittal, Krishan Pal and Deepak Mittal</i> | |
| General Simplex Method for Fully Fuzzy Linear Programming with the Piecewise Linear Fuzzy Number | 451 |
| <i>M. Z. Tuffaha and M. H. Alrefaei</i> | |
| Contents of Volume 20, 2020 | 461 |

BIRKHÄUSER

Book Series : Systems & Control: Foundations & Applications

Stability Theory for Dynamic Equations on Time Scales

Book Series: Systems & Control: Foundations & Applications: 223 pp., 2016

ISBN 978-3-319-42212-1, DOI 10.1007/978-3-319-42213-8,

A.A. Martynyuk

Institute of Mechanics, National Academy of Sciences of Ukraine, Kyiv, Ukraine

This monograph is a first in the world to present three approaches for stability analysis of solutions of dynamic equations. The first approach is based on the application of dynamic integral inequalities and the fundamental matrix of solutions of linear approximation of dynamic equations. The second is based on the generalization of the direct Lyapunov method for equations on time scales, using scalar, vector and matrix-valued auxiliary functions. The third approach is the application of auxiliary functions (scalar, vector, or matrix-valued ones) in combination with differential dynamic inequalities. This is an alternative comparison method, developed for time continuous and time discrete systems. In recent decades, automatic control theory in the study of air- and spacecraft dynamics and in other areas of modern applied mathematics has encountered problems in the analysis of the behavior of solutions of time continuous-discrete linear and/or nonlinear equations of perturbed motion. In the book "Men of Mathematics," 1937, E.T.Bell wrote: "A major task of mathematics today is to harmonize the continuous and the discrete, to include them in one comprehensive mathematics, and to eliminate obscurity from both." Mathematical analysis on time scales accomplishes exactly this.

CONTENTS (5 chapters)

Preface • Elements of Time Scales Analysis • Method of Dynamic Integral Inequalities • Lyapunov Theory for Dynamic Equations • Comparison Method • Applications • Index

The Stability Theory for Dynamic Equations on Time Scales fulfills the reference needs of pure and applied mathematicians, applied physicist, industrial engineerings, operations researchers, and upper-level undergraduate and graduate students studying ordinary differential, difference and dynamic equations on time scales. This research has potential applications in such areas as theoretical and applied mechanics, neurodynamics, mathematical biology and finance among others.

For more information and how to order please check:
<http://www.springer.com/de/book/9783319422121>
